ΕΛΛΗΝΙΚΗ ΔΗΜΟΚΡΑΤΙΑ

ΠΑΝΕΠΙΣΤΗΜΙΟ ΙΩΑΝΝΙΝΩΝ

ΠΟΛΥΤΕΧΝΙΚΗ ΣΧΟΛΗ

ΤΜΗΜΑ ΜΗΧΑΝΙΚΩΝ ΕΠΙΣΤΗΜΗΣ ΥΛΙΚΩΝ

ΔΙΑΤΜΗΜΑΤΙΚΟ ΠΡΟΓΡΑΜΜΑ ΜΕΤΑΠΤΥΧΙΑΚΩΝ ΣΠΟΥΔΩΝ

«ΧΗΜΕΙΑ ΚΑΙ ΤΕΧΝΟΛΟΓΙΑ ΥΛΙΚΩΝ»

ΜΕΤΑΠΤΥΧΙΑΚΗ ΔΙΑΤΡΙΒΗ

ΑΓΓΕΛΙΚΗ ΙΩΣΗΦ

ΥΠΟΛΟΓΙΣΤΙΚΗ ΜΕΛΕΤΗ ΤΗΣ ΛΕΙΤΟΥΡΓΙΚΟΤΗΤΑΣ ΤΟΥ ΕΓΚΕΦΑΛΟΥ

ΙΩΑΝΝΙΝΑ, 2021

Εσώφυλλο:

Η παρούσα Μεταπτυχιακή Διατριβή εκπονήθηκε στο πλαίσιο των σπουδών για την απόκτηση του Μεταπτυχιακού Διπλώματος Ειδίκευσης στη Χημεία και Τεχνολογία των Υλικών που απονέμει το Τμήμα Μηχανικών Επιστήμης Υλικών του Πανεπιστημίου Ιωαννίνων.

Εγκρίθηκε την …….. από την εξεταστική επιτροπή:

ΟΝΟΜΑΤΕΠΩΝΥΜΟ	ΒΑΘΜΙΔΑ
1. Λεωνίδας Γεργίδης(Επιβλέπων)	Αναπληρωτής Καθηγητής ΤΜΕΥ της Πολυτεχνικής Σχολής του Πανεπιστημίου Ιωαννίνων.
2. Δημήτριος Ι. Φωτιάδης	Καθηγητής ΤΜΕΥ της Πολυτεχνικής Σχολής του Πανεπιστημίου Ιωαννίνων.
3. Αλκιβιάδης Παϊπέτης	Καθηγητής ΤΜΕΥ της Πολυτεχνικής Σχολής του Πανεπιστημίου Ιωαννίνων.

ΥΠΕΥΘΥΝΗ ΔΗΛΩΣΗ

‘’Δηλώνω υπεύθυνα ότι η παρούσα διατριβή εκπονήθηκε κάτω από διεθνείς ηθικούς και ακαδημαϊκούς κανόνες δεοντολογίας και προστασίας της πνευματικής ιδιοκτησίας. Σύμφωνα με τους κανόνες αυτούς, δεν έχω προβεί σε ιδιοποίηση ξένου επιστημονικού έργου και έχω πλήρως αναφέρει τις πηγές που χρησιμοποίησα στην εργασία αυτή.’’

(Υπογραφή υποψηφίου)

ΠΡΟΛΟΓΟΣ

Η παρούσα μεταπτυχιακή διπλωματική εργασία έχει ως στόχο την υπολογιστική μελέτη της συνεκτικότητας, τόσο την λειτουργική όσο και την αποτελεσματική, του εγκεφάλου. Αυτή η μελέτη πραγματοποιήθηκε χρησιμοποιώντας δεδομένα λειτουργικής απεικόνισης μαγνητικού συντονισμού (fMRI) ασθενών με τη νόσο Πάρκινσον, τα οποία συγκρίθηκαν με αντίστοιχα λειτουργικά δεδομένα υγιών υποκειμένων. Αξίζει να αναφερθεί ότι οι ασθενείς, που συμμετέχουν, βρίσκονται στα πρώτα στάδια της νόσου και δεν έχουν λάβει κάποια φαρμακευτική αγωγή, ενώ το σύνολο των δεδομένων προέρχεται από πείραμα σε κατάσταση ηρεμίας.

Η δομή της παρούσας διατριβής διαρθρώνεται σε έξι ξεχωριστά κεφάλαια, όπου στα τέσσερα πρώτα γίνεται μία αναλυτική θεωρητική προσέγγιση της νόσου του Πάρκινσον, της λειτουργικής απεικόνισης μαγνητικού συντονισμού, της μεθοδολογίας που ακολουθείται προκειμένου να εξεταστεί το συγκεκριμένο θέμα και επίσης της μέχρι τώρα εξέλιξης που έχει πραγματοποιηθεί μέσω βιβλιογραφικής ανασκόπησης. Στα τελευταία δύο κεφάλαια παρουσιάζεται η πειραματική πορεία που ακολουθήθηκε καθώς επίσης και τα συμπεράσματα που εξήχθησαν.

Πιο συγκεκριμένα, στο πρώτο κεφάλαιο γίνεται η περιγραφή της νόσου του Πάρκινσον, δηλαδή του βασικού φαινομένου που προκαλεί την νόσο αφού αποτελεί την μοναδική ασθένεια του κλάδου των νευροεκφυλιστικών διαταραχών που έχει διευκρινιστεί η παθοφυσιολογία της. Επίσης παρουσιάζονται οι κλίμακες κλινικής αξιολόγησης της ασθένειας που έχουν αναπτυχθεί μαζί με τα κλινικά χαρακτηριστικά της. Ενώ γίνεται σημαντική αναφορά στις υπάρχουσες θεραπείες, που θεραπεύουν κυρίως συμπτώματα της νόσου, και στα επιδημιολογικά στοιχεία και στοιχεία που σχετίζονται με την εμφάνισή της.
Στο επόμενο κεφάλαιο παρουσιάζεται μία εκτενής αναφορά στην λειτουργική απεικόνιση μαγνητικού συντονισμού ξεκινώντας με ιστορικά στοιχεία και τις βασικές αρχές λειτουργίας της ευρέως διαδεδομένης διαγνωστικής τεχνικής. Παρουσιάζονται δηλαδή στοιχεία για την αντίδραση BOLD, τους τύπους πειραματικού σχεδιασμού, την διαδικασία λήψης των λειτουργικών εικόνων, τις χρονοσειρές fMRI, τις κλινικές εφαρμογές και τέλος τα πλεονεκτήματα και μειονεκτήματα χρήσης της συγκεκριμένης τεχνικής.

Η βιβλιογραφική ανασκόπηση των πρόσφατων μελετών σε σχέση με τη νόσο του Πάρκινσον και την εφαρμογή της τεχνικής fMRI για την εξέταση αυτής, αποτελεί το βασικό περιεχόμενο του τρίτου κεφαλαίου. Οι μελέτες που παρουσιάζονται έχουν χωριστεί σε δύο κατηγορίες ανάλογα με τον πειραματικό σχεδιασμό. Δηλαδή αναφέρονται τόσο μελέτες που η λήψη των εικόνων σχετίζεται με κάποιο ερέθισμα (ηχητικό, οπτικό) όσο και μελέτες

όπου η απόκτηση των εικόνων δε βασίζεται σε κάποιο ερέθισμα, πραγματοποιείται απουσία ερεθίσματος και καλείται κατάσταση ηρεμίας.

Στο τέταρτο κεφάλαιο πραγματοποιείται μία εκτενής παρουσίαση των τριών τύπων συνεκτικότητας του εγκεφάλου, δηλαδή της δομικής, λειτουργικής και αποτελεσματικής. Ενώ επίσης παρουσιάζονται οι μέθοδοι που υπάρχουν για την μελέτη και ανίχνευση των διαφόρων τύπων συνεκτικότητας του εγκεφάλου.

Η αναλυτική περιγραφή της μεθοδολογίας που ακολουθήθηκε στο πειραματικό μέρος της παρούσας εργασίας και τα αποτελέσματα που προέκυψαν παρουσιάζονται στο πέμπτο κεφάλαιο. Συγκεκριμένα παρουσιάζονται οι τρεις ξεχωριστές μελέτες με τις τρεις ξεχωριστές μεθόδους ανάλυσης που εφαρμόστηκαν. Οι δύο πρώτες μελέτες στόχευαν στην ανίχνευση της λειτουργικής συνεκτικότητας ενώ η τελευταία στην ανίχνευση της αποτελεσματικής συνεκτικότητας.

Στο έκτο και τελευταίο κεφάλαιο της εργασίας γίνεται η συζήτηση των αποτελεσμάτων που προέκυψαν, βάσει των μεθοδολογιών που εφαρμόστηκαν ενώ προτείνεται η συνέχιση της έρευνας σε ασθενείς που βρίσκονται στα πρώτα στάδια της νόσου του Πάρκινσον.

ΠΕΡΙΛΗΨΗ

Η μελέτη της λειτουργικότητας του εγκεφάλου βοηθά στην κατανόηση της εγκεφαλικής δραστηριότητας και στο πως αυτή μεταβάλλεται σε σχέση με τις διάφορες παθήσεις. Η παρούσα μεταπτυχιακή διπλωματική εργασία ασχολείται με την υπολογιστική μελέτη της συνεκτικότητας του εγκεφάλου, τόσο την λειτουργική όσο και την αποτελεσματική ή αιτιώδη, σε ασθενείς με τη νόσο Πάρκινσον που βρίσκονται στα πρώτα στάδια. Για το σκοπό αυτό χρησιμοποιήθηκαν δεδομένα λειτουργικής απεικόνισης μαγνητικού συντονισμού (functional Magnetic Resonance Imaging- fMRI) δεκατεσσάρων ασθενών με Πάρκινσον τα οποία συγκρίθηκαν με αντίστοιχα δεδομένα δεκατεσσάρων υγιών υποκειμένων, όταν αυτοί βρίσκονταν σε κατάσταση ηρεμίας. Η μελέτη της λειτουργικής συνεκτικότητας μπορεί να πραγματοποιηθεί με την επιλογή κατάλληλων υπολογιστικών μεθόδων, οι οποίες είτε βασίζονται σε δεδομένα που δεν χρειάζονται προηγούμενη γνώση είτε βασίζονται σε μοντέλα όπου απαιτείται προηγούμενη γνώση. Στη συγκεκριμένη εργασία εφαρμόστηκε η ανάλυση ανεξάρτητων συνιστωσών (ICA) η οποία ανήκει στην πρώτη κατηγορία, καθώς επίσης και μία μέθοδος που βασίζεται σε μοντέλα μέσω του εργαλείου CONN. Για τη μελέτη της αποτελεσματικής συνεκτικότητας εφαρμόστηκε η μέθοδος των φασματικών αιτιοκρατικών μοντέλων (spDCM). Τα αποτελέσματα έδειξαν ότι υπάρχει σημαντική αλλοίωση της λειτουργικής συνεκτικότητας των εγκεφαλικών δικτύων των ασθενών ακόμα και στα πολύ πρώιμα στάδια της νόσου. Ενώ όλες οι αλλαγές που παρατηρούνται, οδηγούν σε μη κινητικά συμπτώματα των ασθενών.

Λέξεις κλειδιά: *Νόσος του Πάρκινσον, fMRI, συνεκτικότητα εγκεφάλου, κατάσταση ηρεμίας.*

HELLENIC REPUBLIC

UNIVERSITY OF IOANNINA

TECHNICAL SCHOOL

DEPARTMENT OF MATERIALS SCIENCE AND ENGINEERING

MASTER SCIENCE

«CHEMISTRY AND TECNOLOGY OF MATERIALS»

MSc THESIS

AGGELIKI IOSIF

COMPUTATIONAL MODELING OF BRAIN FUNCTIONAL CONNECTIVITY

IOANNINA, 2021

Dedication

To My Family and Friends

PREFACE

The main aim of the current master thesis is the computational modeling of brain connectivity, both the functional and the effective connectivity. This computational study was conducted with the use of fMRI data of patients with Parkinson's disease (PD) that compared with individual functional data of controls subjects. It is worth noticing that the participating patients are in the early stages of the disease and they have not taken any kind of medication, while the dataset derive from an experiment in resting-state.

The structure of the current thesis is consisted of six separate chapters. In the first four chapters there is a detailed theoretical approach of Parkinson's disease (PD), the functional magnetic resonance imaging (fMRI), the methodology that applied so as to study the current issue and also the progress that has been made so far through a state of the art. In the last two chapters the experimental course that is followed as well as the conclusions that resulted are presented.

More specifically, the first chapter refers to Parkinson's disease. In particular, the chapter describes the basic phenomenon that causes the disease since it is the only disease in the field of neurodegenerative disorders that its pathophysiology has been classified. Moreover, the clinical rating scales of the disease that have been developed along with the clinical features are reported. Additionally, the existing treatments, which mainly treat the symptoms of the disease, the epidemiology and the risk factors are significantly addressed.
In the following chapter an extensive report of functional magnetic resonance imaging (fMRI), starting with historical information and the principles of the popular diagnostic technique is presented. Furthermore, the BOLD mechanism, the types of experimental design, the image acquisition, the fMRI time-series, the clinical applications and finally the advantages and disadvantages of the specific technique are also discussed.

The state of the art of the recent studies relatively to PD with the application of fMRI, is the main content of the third chapter. The presented studies are separated in two categories depending on the experimental design. There is a report both for task-based studies and resting-state studies.

In the fourth chapter there is an extensive presentation of the three types of brain connectivity, namely structural, functional and effective, while the methods used in the particular study as well as the detection of these three types of brain connectivity is also reported.

The detailed description of the methodology that is followed in the experimental part of the thesis and the results that were extracted, are presented in the fifth chapter. Precisely, three different studies associated with the three separate methods that have been applied are shown. Two of them aimed in the detection of the functional connectivity while the last one in the detection of effective connectivity.

In the sixth and last chapter of the thesis a brief discussion of the obtained results, based on the methodologies that applied is made. A kind recommendation for the continuation of research in patients being in the early stages of Parkinson's disease is also included.

ABSTRACT

The study of brain connectivity helps to understand the activation of the brain and the alterations that may be occurred, due to the presence of different diseases. The current master thesis is focused on the computational modeling of brain connectivity, both the functional and effective connectivity, in de-novo Parkinson's disease (PD) patients in the early stages of the disease. For that reason resting-state fMRI data of fourteen PD patients and fourteen healthy controls respectively were used, so as to make a comparison. The study of functional connectivity can be carried out with the selection of appropriate computational techniques, where they could be data-driven with no need of prior knowledge or model-based with the need of prior knowledge. In the current thesis the ICA method which is a data-driven method was used, while also a model-based method via CONN toolbox was implemented. For the study of effective connectivity spectral DCM was used. The results showed that there is significant alteration in functional connectivity of brain networks, even in such early stages of the disease. All the observed alterations contribute to non-motor symptoms of PD patients.

Key words: *Parkinson's disease, fMRI, brain connectivity, resting-state condition.*

List of Abbreviations

PD	*Parkinson's disease*
DAT	*Dopamine transporter*
SPECT	*Single-photon emission computed tomography*
PSP	*Progressive supranuclear palsy*
MSA	*Multiple system atrophy*
CBD	*Corticobasal degeneration*
DLP	*Dynamin-like protein*
MRI	*Magnetic resonance imaging*
MPTP	*1-methyl-4-phenyl -1,2,3,6-tetrahydropyridine*
CT	*Computed tomography*
HY	*Hoehn & Yahr scale*
UPDRS	*Unified Parkinson's disease rating scale*
MDS	*Movements disorders society*
PET	*Position emission tomography*
fMRI	*functional Magnetic resonance imaging*
REM	*Rapid eye movement*
PDRP	*Parkinson's disease related pattern*
DCM	*Dynamic causal modelling*
EEG	*Electroencephalography*
MEG	*Magnetoencephalography*
NMR	*Nuclear magnetic resonance*
BOLD	*Blood oxygen level dependent*
CBF	*Cerebral blood flow*
ASL	*Anterial spin labeling*
EPI	*Echo planar imaging*
ERPs	*Event-related potentials*
SNR	*Signal to noise ratio*
ATL	*Adult T-cell leukemia / lymphoma*
AD	*Alzheimer's disease*
ANCOVA	*Analysis of covariance*
SPM	*Statistical parametric mapping*
GenA	*Generation of action words*
ON	*Object naming*
MMO	*Man-made objects*
MBO	*Manipulable biological objects*
L-DOPA	*Levodopa*
MNI	*Montreal neurological institute space*
AFNI	*Analysis of functional neuroimages*
STN	*Subthalamic nucleus*
GPe	*External pallidum*
GPi	*Internal pallidum*
SNr	*Substantia nigra pars reticularis*
FOG	*Freezing of gait*

ICA	*Independent component analysis*
NMSS	*Non-motor symptoms scale*
FSL	*FMRIB software library*
VBM	*Voxel-based morphometry*
dFC	*dynamic functional connectivity*
DMN	*Default mode network*
FPN	*Frontoparietal network*
NRS	*Numeric rating scale*
DCP	*Dorsal caudal putamen*
PSC	*Primary sensorimotor cortex*
LPC	*Lateral premotor cortex*
IPC	*Inferior parietal cortex*
ACC	*Anterior cingulate cortex*
BSPL	*Bilateral superior parietal lobes*
LIC	*Left insular cortex*
PMC	*Primary motor cortex*
FPN	*Frontoparietal cortex*
MPRAGE	*Magnetization prepared rapid gradient echo*
CSA	*Cortical sensorimotor areas*
FC	*Functional connectivity*
fSNR	*functional signal to noise ratio*
TR	*Repetition time*
TA	*Acquisition time*
DCT	*Discrete cosine transform*
MAP	*Maximum a posterior approach*
FWHM	*Full width half maximum*
GM	*Gray matter*
WM	*White matter*
CST	*Cortico-spinal tract*
DTI	*Diffusion tensor imaging*
MD	*Mean diffusivity*
FA	*Franctional anisotropy*
CSF	*Cerebrospinal fluid*
LPF	*Local field potentials*
CCA	*Cross-correlation analysis*
CA	*Coherence analysis*
pICA	*probabilistic independent component analysis*
sICA	*spatial independent component analysis*
tICA	*temporal independent component analysis*
PCA	*Prinsipal component analysis*
SVD	*Singular value decomposition*
FCA	*Fuzzy clustering analysis*
HCA	*Hierarchical clustering analysis*
ROI	*Region of interest*
HRF	*Hemodynamic response function*

GLM	*General linear model*
GRF	*Gaussian random field*
CNR	*Contrast to noise ratios*
fcMRI	*functional connectivity Magnetic resonance imaging*
SEM	*Structural equation modelling*
sLDSf	*switching Linear dynamic systems*
PPI	*Psychophysiological interactions*
GCM	*Granger causality mapping*
MAR	*Multivariate autoregressive*
VAR	*Vector autoregressive*
AR	*Autoregression*
spDCM	*spectral Dynamic causal modelling*
hIRF	*hemodynamic Impulse response function*
EC	*Effective connectivity*
TE	*Echo time*
TI	*Inversion time*
FOV	*Field of view*
NEX	*Number of excitations*
FLAIR	*Fluid attenuated inversion recovery*
MPFC	*Medial prefrontal cortex*
lLPC	*left Lateral parietal cortex*
rLPC	*right Lateral parietal cortex*
PCC	*Posterior cingulate cortex*
p-FWE	*Family-wise error corrected p-value*
p-FDR	*False discovery rate corrected p-value*
p-unc	*Uncorrected p-value*
ICs	*Independent components*
FFX	*Fixed effects inference method*

List of Symbols

$x = [x_1, x_2, x_3, 1]^T$	Position
$y = [y_1, y_2, y_3, 1]^T$	Position
f	Image
g	Image template
M	Transformation matrix
M_t	Translations matrix
M_θ	Rotation matrix about the x axon
M_φ	Rotation matrix about the y axon
M_ω	Rotation matrix about the z axes
M_f	Transformation matrix into Euclidian space for image f
M_g	Transformation matrix into Euclidian space for image g
x_{mm}, y_{mm}, z_{mm}	Voxel's dimensions
a, b, c	Dimensions of images
p	Parameter vector
v	Voxel
s	Parameter that is used to offset the differences in voxel intensity
x_t	Translation about the x axon
y_t	Translation about the y axon
z_t	Translation about the z axon
θ	Rotation about the x axon
φ	Rotation about the y axon
ω	Rotation about the z axon
q	Slices
m	Number of rows
n	Number of columns
k	Time points
a_{ij}	Intensity value of the voxel that is localized in slice q
M_z	Focus matrix
M_s	Shearing matrix
t_j	Translation for each three dimensions
$b_j(x_j)$	jth basic function at spatial position x_i
d	Length of kernel
h	Kernel
A_u	Kernel amplitude
u	Units away from the center
$F_x(k)$, $F_y(k)$	Timecourses
μ	lag
$Var(x), Var(y)$	Variances of $F_x(k)$, $F_y(k)$
$Cov_{x,y}(u)$	Cross variance of $F_x(k)$, $F_y(k)$
E	Expected value
$E(F_x)$,$E(F_y)$	Expectation or the mean of $F_x(k)$ and $F_y(k)$ respectively
$F_{x,y}(\lambda)$	Cross spectrum

$F_{x,x}(\lambda)$, $F_{y,y}(\lambda)$	Power spectrum
X	Timecourses
T	Time points
N	Voxels
S_i	Singular value of X
U_i	ith principal component
V_i	Corresponding eigen map
p	Number of the collected components
C_i	ith underlying signal source
A	Mixing matrix
$P(C_i)$	Probability of the ith underlying signal source
W	Independent components
q	Statistically independent non-Gaussian sources
p	Dimensional time-series
$\eta_{(t)}$	Additive Gaussian noise
X_i	p-dimensional column vector
S_i	q-dimensional column vector
μ	Constant part
M_{ij}	Metric that measures the probability of a voxel i relates to j
D_{ij}	Distance within voxel i and the centroid C_j of a cluster j
K	Number of the primary clusters
φ	Weighting component
X_i	Vector which includes the coordinates of a cluster centroid i
D_{cc}^1 , D_{cc}^2	Distance metrics
$CC_{x,y}$	Cross-correlation of $F_x(k)$ and $F_y(k)$ at lag zero
ω_f , φ_f	Complex frequency components of $F_x(k)$ and $F_y(k)$ respectively
$Re^{(*)}, Im^{(*)}$	Real and imaginary component of signal *
Y	Data matrix
M	Path coefficients matrix
ε	Independent and identically distributed Gaussian noise
I	Identify matrix
$x[n]$, $y[n]$	Time courses of two brain areas
$u[n]$	White noise
$A[i]$	Autoregression (AR) coefficients
$F_{x,y}$	Linear dependence
t	Time
$\frac{dz}{dt}$	Derivative of neuronal activity in time
$u_t(j)$	jth of J extrinsic inputs at time t
A, $B^{(j)}$, C	Connectivity matrices
θ	Joint parameter vector
$h(u,\theta)$	Predicted BOLD response
λ	Output nonlinearity
e	Observation error
X	Confounding effects

$\dot{z}$	Rate in change of the neural states z
θ	Unknown parameters of the evolution equation
φ	Unknown parameters of the observation equation
v	*S*tochastic process (state noise)
A	Jacobian
α, β	Parameters that controls the amplitudes and exponents
z_t	Variable
y_t	Observation equation
v_t	Observation level input
ζ_t	Noise
$\boldsymbol{R^{ij}}$	Diagonal covariance matrix
$\boldsymbol{\Phi}$	Matrix
β	Matrix
V	Nodes
E	Edges

Table of contents

List of Figures

Chapter 1

Chapter 2

Chapter 4

Chapter 5

List of Tables

Chapter 1

Chapter 3

Chapter 5

Chapter 7

1.1 Pathophysiology, Diagnosis

Parkinson's disease (PD) is a progressive neurodegenerative disease characterized typically by motor features of tremor, rigidity and bradykinesia, due to depletion of dopaminergic nigrostriatal neurons [1]. It can also been characterized as a chronic degenerative disorder of the Central Nervous System, which is slowly evolving and affecting movement, muscle control and balance. It is the second most common neurodegenerative disease, after Alzheimer's disease, and its prevalence will increase as the population ages. Parkinson's disease was first described by James Parkinson in 1817 under the term '' shaking palsy'' and later named to his honor. Nearly two hundred years after the first description of the disease, its aetiology is still unknown and the cure is only symptomatic. Parkinson's disease has made significant progress in the last decades, as it is unique from the neurodegenerative diseases that has been elucidated its pathophysiology [2].

The basic phenomenon that describes the neural pathophysiology of PD is a dopaminergic neuronal loss in the substantia nigra in the basal gaglia of the cerebra. Inside the degenerating neurons can be observed specific inclusion bodies (Lewy bodies). In

healthy people, the function of the extrapyramidal system that processes the movement information from the cortex to the striatum and returns it through the thalamus back to the cortex, has been controlled by the dopaminergic neurons. Although in PD's patients, the control of the extrapyramidal system is disturbed and the feedback from the striatum to the cortex is modified. All these abnormalities in the function of basal ganglia lead to the motor symptoms of PD [3]. In Figure 1.1 it can be observed the difference in dopamine levels between a healthy individual and a patient with PD.

As it has been already mentioned, PD has long been characterized by the classical motor features of parkinsonism associated with Lewy bodies and loss of dopaminergic neurons in the substantia nigra. However, the symptomatology of PD is now recognized as heterogeneous, with clinically significant non-motor features. Similarly its pathology involves extensive regions of the nervous system, various neurotransmitters and protein aggregates other than just Lewy bodies [1].

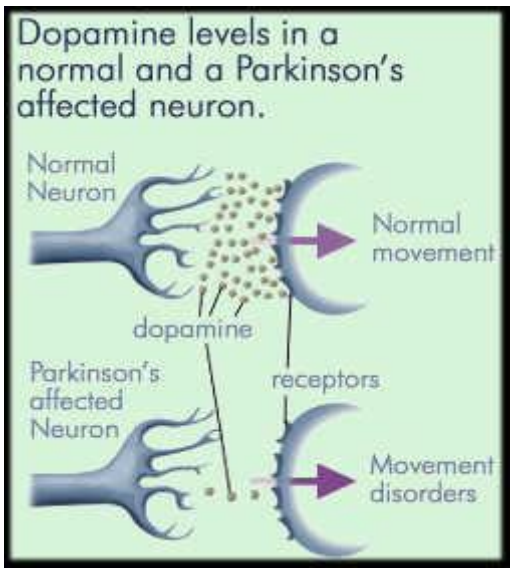

Figure 1.1: Dopamine levels in a normal and a Parkinson's affected nerve fiber [4].

The standard way that a physician follows for a definite diagnosis of PD, relies on the typical clinical presentation with a combination of a post-mortem histopathologic confirmation of characteristic neuronal loss together with the presence of Lewy bodies [5, 6]. Functional brain imaging (e.g. dopamine transporter (DAT) imaging combined with single-photon emission computed tomography (SPECT)) does not have the ability to distinguish PD from other degenerative causes of parkinsonism (PSP, MSA, CBD, DLB) but is of value to differentiate against for example tremor, drug induced tremor and psychogenic

symptoms. From the other hand, structural brain imaging methods (MRI) have the ability to rule out differential diagnoses, for example vascular parkinsonism. Due to the lack of specific biomarkers, PD is still in practice a clinical diagnosis [1, 7]. According to the UK Brain Bank Criteria (Table 1.1), the clinical diagnosis of PD relies on the presence of bradykinesia together with at least one more of the cardinal motor symptoms and the exclusion underlying causes of secondary parkinsonism [8].

Table 1. 1: UK Brain Bank Criteria for PD [1, 8].

Step1: Diagnosis of Parkinsonian syndrome
Bradykinesia At least one of the following : Muscular rigidity 4-6 Hz rest tremor Postural instability not caused by primary visual, vestibular cerebellar, or proprioceptive dysfunction.
Step 2: Exclusion criteria for PD
History of repeated strokes with stepwise progression of parkinsonian features. History of repeated head injury and definite encephalitis. Neuroleptic treatment at onset symptoms. Negative response to large doses of levodopa (if malabsorption excluded). Sustained remission. Strictly unilateral features after 3 years. Early severe autonomic involvement. Early severe dementia with disturbances of memory, language and praxis. Oculogyric crisis. Supranuclear gaze palsy. Babinski sign. Cerebellar signs. MPTP exposure. Presence of a cerebral tumor or communicating hydrocephalus on CT scan or MRI. More than one affected relative.
Step 3: Supportive prospective criteria for PD
Three or more of the following features are required for diagnosis of definite Parkinson's disease: Unilateral onset. Rest tremor present. Progressive disorder. Persistent asymmetry affecting the side on onset most. Excellent response (70-100%) to levodopa. Severe levodopa-induced chorea. Levodopa response for 5 years or more. Clinical course of 10 years or more.

A more recent insight in the diagnosis of PD is the recognition of non-motors symptoms as a primary part of the disease. Such symptoms are currently not included in the

diagnostic criteria for PD [7]. A debatable feature of PD is impairment of muscle strength. In modern time that symptom has received little attention and clinically apparent reduction of that has generally not been considered as primary symptom of PD [9, 10]. However when James Parkinson first described '' the shaking palsy'' he held it as a key feature of the disease and self-perceived muscle weakness to be a common complaint in PD patients. Clinical assessment of muscle strength can only provide rough estimations [11].

1.2 Clinical Rating Scales

Although Parkinson's disease (PD) is progressive and worsens over time, it is highly individual and affects people differently. The symptoms may vary in their severity between patients, so not all people who have PD will experience all the symptoms. Also the progression of the disease differs in each case. However, physicians have established several clinical scales that describe how the disease progresses as well as the severity of the disease. The most traditional example is the Hoehn and Yahr (HY) that has first introduced in the 1960's and since then used worldwide. A modified version has later been introduced with the addition of intermediate stages between the original five. The original version includes the following five stages (Table 1.2) [12].

Stage 1 of PD

That is the earliest stage of the disease where the symptoms are mild and only seen on one side of the body (unilateral involvement). Usually there is minimal or no functional impairment. In this stage it is very difficult to make a diagnosis so the physician must wait to see if the symptoms get worse over time. Symptoms at stage one may include tremor, such as intermittent tremor of one hand, rigidity, one hand or leg may feel more clumsy than another, or one side of the face may be affected, impacting the expression.

Stage 2 of PD

Stage two is also considered as an early stage of the disease and it is characterized by symptoms on both sides of the body (bilateral involvement) or at the midline without impairment to balance. Stage two may develop months or years after the first stage. Although the patient can still be able to perform tasks of daily living at this stage the symptoms that experiences are different from the previous stage. The symptoms of that stage may include the loss of facial expression on both sides of the face, decreased blinking, abnormalities of the speech, soft or monotone voice, fading volume after starting to speak loudly, slurring speech, stiffness or rigidity of the muscles in the trunk that may result in neck or back pain, stooped posture and general slowness in all daily activities. The diagnosis is much easier at this stage except from the case that the stage one was missed and the only

symptoms that experienced the patient were lack of spontaneous movement or slowness, so PD may be misinterpreted as only advancing age.

Stage 3 of PD

In the category of mid-stage is considered the stage three and is characterized by loss of balance and slowness of movement. The patient faced the inability to make the rapid, automatic and involuntary adjustments that are necessary to prevent falling and falls are common at this stage. In general all other symptoms of PD are also present at this stage. An important clarifying factor is that the patient is still fully independent in their daily living activities. It is worth to be mentioned that the diagnosis is not in doubt at this stage and the physician will diagnose impairments in reflexes at this stage.

Stage 4 of PD

Parkinson's disease in that stage has progressed as a severely disabling disease. Patients may be able to walk and stand without help, but they are noticeably incapacitated. Also are unable to live an independent life and need assistance with some activities of daily living. The necessity of help define that stage.

Stage 5 of PD

That stage is the most advanced and is characterized by the inability to rise from a chair or get out of bed without help. Also they may have the tendency to fall when standing or turning and they may freeze or stumble when walking. Hallucinations or delusions are symptoms that may be experienced by the patient at that stage.

It is worth noting that some patients with PD never reach the stage five, while the symptoms are worsen over time. Also the length of time to progress through the different stages varies from individual to individual. The treatments that are available in every stage of the disease can help to manage the progression. However, the earlier physician makes the diagnosis and the earlier the stage at which the disease is diagnosed, the more effective is the treatment at alleviating symptoms [13].

Table 1. 2: Stages of Parkinson's disease from Hoehn and Yahr scale [13].

	Early PD		**Mid-stage PD**	**Advanced PD**	
Stage of PD	1	2	3	4	5
Severity of symptoms	MILD	MILD	MODERATE	SEVERE	SEVERE

Another rating scale that has been developed was the Unified Parkinson's Disease Rating Scale (UPDRS). The Unified Parkinson's Disease Rating Scale (UPDRS), which was designed in the 1980's and later revised by the Movements Disorders Society (MDS), is the most widely used clinical rating scale the past few years. The new version is named as MDS-UPDRS. The UPDRS is a multidimensional tool and includes both questionnaire parts (I, II, IV) as well as a clinical examination (part III). Specifically part I-II address experiences of daily living (non- motor and motor), part III address clinical motor signs and part IV address therapy complications (dyskinesias and motor fluctuations). In the UPDRS, evolvement of symptoms and/or disabilities is reflected by declined scores [14]. Clinical rating scales, such as Schwab and England functional assessment scale and a set of validated tests have been developed and used but the most widely used are the aforementioned [15].

1.3 Epidemiology and risk factors

As it has already been mentioned, Parkinson's disease is recognized as the most common neurodegenerative disease after Alzheimer's disease. Higher levels of prevalence of PD are observed in Europe, North America and South America compared with African, Asian and Arabic countries. The incidence of PD ranges from 10-18 per 100000 person-years. The risk of developing PD is clearly multifactorial but the elaborate interplay between various factors is just beginning to be deciphered. For example gender is an established risk factor with the ratio between male and female is 3:2. Another risk factor for that disease is ethnicity. People of Hispanic ethnic origin, non-Hispanic Whites, Asians and Blacks have highest incidence in contrast with the USA. Nevertheless age is a great risk factor for developing Parkinson's disease. The prevalence and incidence increase exponentially with age and peak after 80 years of age. Due to the increase of life expectancy worldwide this result has important public health implications. The conclusion of all these will be the rise of the number of people with PD by more than 50% by 2030 [16].

Environmental exposures are included in the list of risk factors that cause PD. Results of an analysis that examine 30 different potential risk factors identified 11 environmental factors that altered the risk of PD. Some examples of factors that increase risk were pesticide exposure, prior head injury, rural living, β- blocker use, agricultural occupation and well-water drinking. Environmental factors that found to be associated with a decreased risk were tobacco smoking, coffee drinking, non-steroidal anti-inflammatory drug use, calcium channel blocker use and alcohol consumption. While there is growing evidence that smoking and alcohol drinking both reduce the risk of PD, their dose-related associations remain controversial and are less well-defined in women. A recent nationwide

cohort study showed that the risk of PD in relation to smoking and alcohol differed within men and women. They found sex-related differences in both individual and joint impacts of smoking and alcohol drinking on the risk incident PD. More specifically risk lowering effect of current smoking tended to be stronger in men, whereas that of alcohol drinking tended to be stronger in women. These sex-related differences in smoking and alcohol may be explained by different effects of nicotine and multiple mechanisms, due to alcohol, in the brain [116]. However another more recent case-control study showed that PD patients can quit from smoking much easier than healthy people, suggesting that the negative association with smoking could instead be due to a decreased responsiveness to nicotine during the prodromal phase of PD.

The participation of genetics to PD is suggested by the increased risk of disease associated with a family history of PD or tremor. The most convincing evidence came with the discovery of monogenic forms of PD· the first gene was the SNCA which encodes the protein α- synuclein and was associated with inherited PD. In the past decade, almost 900 genetic association studies have implicated dozens of potential gene loci in PD. A further understanding of PD risk factors and their interactions is needed so as to broad the information about the elucidation of pathogenic mechanisms, identification of biomarkers and individualization of treatment [10].

1.4 Clinical Features

The triad of motor symptoms (tremor, bradykinesia, rigidity) is the clinical features that are associated with Parkinson's disease. However PD is also associated with many non-motor symptoms that are often appeared years or even decades before the motor symptoms and the diagnosis of PD.

That pre-motor or else prodromal phase of PD start, most of the times, 12-14 years before diagnosis. There is evidence that the disease begin in the peripheral autonomic nervous system and/or the olfactory bulb and then spreading through central nervous system affecting the lower brainstem structures before involving the substantia nigra. Symptoms such as hyposmia, constipation and rapid eye movement sleep disorders may appear in PD patients before motor symptoms begin. Patients that have faced tremor, balance problems, depression, constipation, fatigue and urinary dysfunction 5 years before diagnosis were more likely to develop PD than those without symptoms. Additionally, individuals with constipation or tremor have a higher risk of developing PD over 10 years of follow-up. Early non-motor symptoms include impaired olfactory ability, autonomic dysfunction, pain, fatigue, sleep disorders and cognitive and psychiatric disturbances. These

symptoms affect the quality of patient's life. Also autonomic symptoms are difficult to treat with orthostatic hypotension causing significant problems for patients. Dementia occurs in 83% of patients with PD after 20 years of diagnosis. Research in that prodromal state of PD was very interesting because that time point may be ideal and a very significant step for therapeutic intervention. Many case-studies that have included patients with early PD, those within 2 years of diagnosis, have observed dopaminergic neuronal loss. So it would be optimal for future studies in disease-modifying treatments to participate patients in prodromal state.

The severity of motor and non-motor symptoms worsens as the disease progresses. As it is known PD is a very heterogeneous disease and there has been attempt to subclassify it further. One subclassification that is based on clinical characteristics suggests two subtypes: a tremor dominant PD and a non-tremor dominant PD. A patient with the first type lacks of any other motor symptoms and responds better to dopamine replacement therapy. On the other hand, a patient with the second type may develop an akinetic-rigid syndrome and a postural instability disorder, as well as an increased incidence of non-motor features. In an advanced stage of the disease, all kind of symptoms may become resistant to current medications. Postural instability and freezing of gait may lead to falls and fractures, while dementia and hallucinations can develop in some patients which lead to home placement [17].

1.5 Treatment

Initiation of symptomatic therapy

Available therapies for PD only treat symptoms of the disease. The basic treatment for motor symptoms that physician follow, includes drugs that enhance intracerebral dopamine concentrations or those that stimulate dopamine receptors. Levodopa, dopamine agonists, monoamine oxidase type B inhibitors and amantadine (less used) are included in that list of drugs. The initiation of the treatment must happen when symptoms are worsening and affect patient's life. Since none of the aforementioned drugs have proven to be neuroprotective or disease-modifying therapy, physician does not have to start the therapy at the time of diagnosis for all patients. From the other hand, there is justification for delay. Dopaminergic treatments for symptoms such as bradykinesia and rigidity respond at the early stages of the disease. Inversely dopamine replacement therapy is not effective for tremor, especially in lower doses· anti-cholinergic drugs (trihexyphenidyl, clozapine) can treat tremor. Also monoamine oxidase type B inhibitors are the best only moderately beneficial.

Something else that is has to be taken into account is the adverse reactions that drugs can cause at patients. For example, dopamine agonists and levodopa are both associated with nausea, daytime somnolence and oedema. These side- effects tend to be more frequent with dopamine agonists. Also dopamine agonists should be avoided in patients with a history of addiction, obsessive- compulsive disorder or impulsive personality, because there is a probability to develop impulse control disorders at that kind of patients. Last but not least, dopamine agonists are not prescribed for elderly patients because can cause hallucinations. Long term use of levodopa is associated with motor complications, although can treat effectively symptoms. So as to delay the appearance of these complications, an initial therapy of levodopa sparing with a monoamine oxidase type B inhibitor or else dopamine agonist can be considered [18].

Management of symptoms and complications

Complications of long-term therapy, usually describe the advance stage of the disease. Motor and non-motor fluctuations, dyskinesia and psychosis are included and affect the quality of patient's life. Fluctuations and dyskinesia are probably results from pulsatile stimulation of striatal dopamine receptors, which appear later on the disease and more specifically, when intracerebral levodopa concentrations become more closely linked to plasma levodopa concentrations. Motor complications can reduced with non-dopaminergic treatments. For example drugs with serotonergic or nicotinic properties and drugs that inhibit glutamatergic signalling or adenosine A2A receptors are being tested as potential treatments. Psychosis in PD is treated via clozapine, but because it can be associated with potentially life-threatening agranulocytosis (an idiosyncratic adverse drug reaction), it is necessary to monitor regular the haematological status.

Relating to the non-motor symptoms, these have limited options of treatment as well as response to that. For example, depression - which is a significant non-motor symptom - is typically treated with antidepressants. In patients without PD but with depression, non-pharmacological therapies such as electroconvulsive therapy and repetitive trans-cranial magnetic stimulation are used effectively. Such therapy has not been tested in patients with PD.

Surgical treatment

At the stage of moderate to severe PD only deep brain stimulation- of either the subthalamic nucleus or globus pallidus internus- is a well established treatment for motor symptoms. In general surgical treatment is an option when motor fluctuations and dyskinesia are not existed but the parkinsonian motor features continue to respond to levodopa. Certainly

further study is needed to establish the contributions of the stimulation versus the effect of improvement in motor function and reduction in dopaminergic drugs that accompany deep brain stimulation. Usually the surgical treatment is recommended 10-13 years after diagnosis of PD. The development of disease modifying drugs that will help to slow down or even stop the underlying neurodegenerative process is very ambitious for the progress of PD. Multiple cellular processes are involved in neurodegeneration in PD and thus the underlying causes of the disease are heterogeneous [1].

1.6 Problems and future aspects

The major standard in the diagnostics of PD and the observation of disease's progression are the clinical diagnostic criteria along with the clinical rating scales. However, problems are observed both in the diagnostics and the treatment of the disease. The result from these problems is the loss of 50-60% of the dopaminergic neurons by the time of the diagnosis. It is quite understandable that the diagnostic accuracy is low and also there are no objectively measured characteristics and methods (e.g. biomarkers) for describing the progress of the disease and for quantifying the efficacy of treatment in PD. In these objective methods are included, motor performance and olfaction tests, oculomotor and neurophysiological measurements, imaging techniques (e.g. MRI, SPECT, PET, fMRI), biochemical measurements (e.g. blood tests), evaluation of rapid eye movement (REM), sleep behavior disorder and genetic tests. Advantages and disadvantages have been observed from every single method, regarding the sensitivity, usability and the cost-effectiveness. The identification and evaluation of biomarkers has started but none of them is widely available or clinically used for PD. Maybe a combination of biomarkers will be effective for treated PD [15, 16].

Regarding to the imaging methods that have been used with the rise of neuroscience a plethora of new approaches and methods have become available. Future developments in functional imaging, structural imaging and nuclear imaging can be very helpful so as to understand and diagnose or even treat PD.

In this thesis will be refer only about functional imaging because it is the method of interest. More specifically fMRI is an approach that has made significant progress in understanding the pathophysiology of PD. The field has grown from focusing on abnormal task related activity in isolated brain regions (such as putamen) to demonstrating abnormal interactions between intrinsic, large scale networks in patients with PD such as the cortico-striatal circuit. An existing approach that has been used for a long time is the Parkinson's Disease Related Pattern (PDRP). That approach is specific for PD and it is a metabolic

covariance pattern that can be calculated with PET and fMRI data. Although it has proven its validity, has not been translated into standard clinical practice.

Another more recent approach, which deals with multi-dimensional data, is the use of generative models. Those are computational models that estimate how observed fMRI data were generated, given a set of priors and hypotheses regarding the configuration of the network. Dynamic Causal Modelling (DCM) is used in this approach because it can compare different models of brain function within a group or between two groups. Also DCM has been used in PD so as to test how networks interactions give rise to tremor and to abnormal voluntary actions. A third approach is the extraction of biologically meaningful features from multi-dimensional imaging data. For example using resting-state fMRI data, parameters can be calculated that reflect gradient of corticostriatal connectivity across striatal subregions. Finally another development could lie in improved functional MRI sequences, enabling brain imaging at a high temporal and/or spatial resolution. If clinically validated such approaches may be helpful for diagnosis and disease monitoring [19]. More details about fMRI are presented in the following chapter (Chapter 2).

Chapter 2: Functional Magnetic Resonance Imaging

2.1 History

The activity of human brain was first recorded in the 1920s by the German psychiatrist Hans Berger while he was practising on electroencephalographic methods. Since then, a variety of methods that aim to map brain activity have been developed. Two basic classes of mapping technique have evolved: those that map (or localise) the underlying electrical activity of the brain; and those that map local physiological or metabolic consequences of alterations in brain electrical activity. Among the former are the non-invasive neural electromagnetic techniques of electroencephalography (EEG) and magnetoencephalography (MEG). These methods allow high temporal resolution of neuronal processes (typically over a 10-100ms time scale) while the spatial resolution is poor (between 1 and several centimetres). Methods such as magnetic resonance imaging (MRI), positron emission tomography (PET) and functional magnetic resonance imaging (fMRI) -in vivo imaging techniques- belong in the second category. These methods present sensitivity to the changes in regional blood perfusion, blood volume or blood oxygenation in accompany

neuronal activity. Especially the fMRI- the technique that is on focus on this study- allow good spatial resolution with limited temporal resolution [21, 22].

Human functional brain mapping as it is presently know it began when the experimental strategies of cognitive psychology were combined with modern brain imaging techniques (first PET and then fMRI) to examine how brain function supports mental activities. This combination of disciplines and techniques galvanized the field of cognitive neuroscience, which has rapidly expanded to include a broad range of the social sciences in addition to basic scientists interested in the neurophysiology, cell biology and genetics of the imaging signals. Although much of this work has transpired over the past couple of decades, its roots can be traced back more than a century.

The scientific developments which have led to modern fMRI are described through the following phases. The idea that local blood flow within the brain is intimately related to brain function is surprisingly old. Angelo Mosso, a prominent Italian physiologist of the 19th century, had carefully monitored the pulsations of the brain in adults through neurosurgically created bony defects in the skulls of patients. He noted that when his subjects engaged tasks such as mathematical calculations the pulsations of the brain increased locally. Such observations led him to conclude, that blood flow to the brain followed function. The actual physiological relationship between brain function and blood flow was first explored in 1890 by Charles Roy and Charles Sherrington. Despite the promising beginning there was no progress during the first quarter of the 20th century. Until a remarkable clinical study of a patient that was reported by John Fulton in the 1928. During the course of his evaluation and treatment for a vascular malformation lying over his visual cortex, the patient remarked that a noise that he perceived in the back of his head increased in intensity when he was using his eyes. The conclusion drawn from this remarkable case was that blood flow to visual cortices was sensitive to the attention paid to objects in the environment. Seymour Kety (1955) et al developed the first quantitative method for measuring whole brain blood flow and metabolism in humans. Because their measurements were confined to the whole brain they were not suitable for 'brain mapping'. However, their introduction of an in vivo tissue autoradiographic measurement of regional blood flow in laboratory animals provided the first glimpse of quantitative regional changes in blood flow in the brain related directly to brain function.

David Ingvar, Neils Lassen and their Scandinavian colleagues following the work by Seymour Kety, introduced methods applicable to humans that permitted regional blood-flow measurements to be made using scintillation detectors arrayed like a helmet over the head.

They demonstrated conclusively that brain blood flow changed regionally in normal human subjects during task performance. Until 1986 it was thought that behaviourally induced increases in local blood flow were the direct consequence of an increase in the brain's need for oxygen to metabolize glucose to carbon dioxide and water for the production of energy. Based on this hypothesis, functionally induced increases in blood flow should be accompanied by quantitatively similar changes in oxygen consumption with no change in the ratio of oxy- to deoxyhemoglobin. Cooper recorded oxygen availability in the human cortex in patients undergoing evaluation for epilepsy while their subjects performed various cognitive and motor tasks. They clearly showed task-induced focal increases in oxygen availability signifying that blood flow had increased more than oxygen consumption.

In 1971 Godfrey Hounsfield introduced X-ray computed tomography (or CT as it is now called). In creating CT, Hounsfield had arrived at a practical solution to the problem of creating 3D transaxial tomographic images of an intact object from data obtained by passing highly focused X-ray beams through the object and recording their attenuation. Hounsfield's invention received enormous attention and quite literally changed the whole idea about the observation of human brain. Also, were difficult to interpret, unpleasant and sometimes dangerous clinical techniques such as pneumoencephalography. CT, however, was an anatomical tool. Function was to be the province of PET and MRI. After the invention of CT, the use of radiopharmaceuticals labelled with positron emitting radionuclides for biomedical research and clinical application had been the objective of several research groups. The first medical cyclotron was installed in Hammersmith Hospital in London in 1955 and was followed by installations at the Massachusetts General Hospital and Washington University's Mallinckrodt Institute of Radiology in 1965. By 1974 there were 15 such installations worldwide. Work among these groups provided much important background knowledge for the introduction of PET.

Finally, another technology emerged contemporaneously with PET and CT named MRI. Magnetic Resonance Imaging is based upon yet another set of physical principles associated with the behaviour of atoms in water in a magnetic field. The physical principles associated with MRI were discovered independently by Felix Bloch and Edward Purcell et al. in 1946. Many years of research followed, in which the technique was used for basic research in chemistry. During that time it was known as nuclear magnetic resonance (NMR). The first important step in the development of fMRI was the work of a group of researchers at the Massachusetts General Hospital working on the use of exogenously administered MRI contrast agents designed to produce transient changes in the MRI image as the agent passed

through the brain after its intravenous administration. Experiments in rodents and dogs using contrast agents confined to the vascular compartment and novel rapid data acquisition strategies demonstrated for the first time with MRI that it was possible to measure changes in brain blood volume produced by physiological manipulations of brain blood flow. This approach was extended to normal human volunteers for task activation brain mapping by the same group in 1991. Remarkably 91 years after, Michael Faraday studied the magnetic susceptibilities of oxygenated and deoxygenated haemoglobin differed significantly.

In 1982, Keith Thulborn took the story one step further while seeking to exploit the difference in magnetic susceptibility of oxy- and deoxyhemoglobin for the measurement of brain oxygen consumption with MRI. He clearly demonstrated the feasibility of measuring the state of oxygenation of blood in vivo with MRI, another crucial step on the road to fMRI BOLD imaging as it is known. The potential of BOLD fMRI was soon realised with publications from three groups in 1992. However the success of the human brain imaging was the product not only of relevant physiology, that could be imaged, and the scanning devices, that could accomplish this, but also of the behavioural paradigms that approached human behaviour in a principled and quantitative manner, while accommodating the constraints of the imaging environment and strategies to process the resulting data.

Since the 19th century, and possibly longer, two perspectives on brain functions have existed. One view posits that the brain is primarily driven by external inputs; the other holds that the brain operates on its own, intrinsically, with sensory information interacting with rather than determining its operation. Although neither view is today dominant, the former clearly has motivated the majority of research at all levels of neuroscience including that in cognitive neuroscience. This is not entirely surprising given the enormous success of experiments measuring brain responses to controlled stimuli [23].

Functional Magnetic Resonance Imaging (fMRI) is a neuroimaging tool that employs MRI to image dynamic changes in brain tissue that are caused by alterations in neural metabolism. These alterations may be caused by asking the subject to perform a task designed to target a specific cognitive process or may be happened spontaneously while the subject is in resting-state (absence of conscious mentation). In every case a dynamic series of T2* weighted scans is acquired, resulting in time-series of signals for every brain voxel. These time-series are submitted to various levels of denoising (preprocessing steps) before model or data driven analyses are applied to obtain maps of activity. Due to condition that BOLD signals are tiny, such analyses use statistical methods to discern false from true

activation [24]. Every functional imaging technique is studying about brain activation, blood flow in microscopic level and diffusion.

2.2 Brain activation

There are two primary consequences when the neuronal activity is increased, and both of them can be detected by MRI. These are the alterations in local cerebral blood flow (CBF) and in oxygen concentration (BOLD contrast: Blood Oxygen Level Dependent). These changes in CBF can be detected either by using an injected contrast agent and perfusion weighted MRI or non-invasively by arterial spin labelling (ASL). In the case of ASL there are some disadvantages such as sensitivity reduction, increase of acquisition time and increase in sensitivity to motion compared with the BOLD contrast. Its use is focusing on acquiring quantitative measurements of baseline cerebral blood flow (CBF) so as to model neurobiological mechanisms of activation, calibration of vasoreactivity; rather than mapping the brain function [25].

The most common method of fMRI takes advantage of the fact that when neurons in the brain become active, the amount of blood flowing through that area is increased. The interesting thing in that case is that the amount of blood that reaches at the area is more than is needed to replenish the oxygen that is used by the activity of the cells. Thus the activity related increase in blood flow caused by neuronal activity leads to a relative surplus in local blood oxygen. The signal measured in fMRI depends on this change in oxygenation and is referring as the blood oxygen level dependent signal (BOLD) [26].

2.2.1 The fMRI BOLD signal

The blood oxygen level dependent (BOLD) signal of functional magnetic resonance imaging arises from the magnetic properties of haemoglobin and the manner in which the brain metabolism and blood flow are related to changes in neuronal activity. It is worth noting that under normal conditions the concentrations of local oxygen are relatively low, so blood contains a high concentration of paramagnetic deoxyhaemoglobin, whereas the brain tissue is diamagnetic [27]. Little effect on the magnetic field of an MRI scanner has the fully oxygenated haemoglobin in arteries. However when haemoglobin loses oxygen to the tissue as it passes through the capillaries of the brain the resulting de-oxygenated haemoglobin disrupts the MRI magnetic field in proportion to the amount of oxygen lost. With the increase of brain activity, blood flow and glucose consumption increase much more than oxygen consumption. Due to the increasing magnetic susceptibility of the oxygenated blood, the activation area is characterized by great T2* constant in comparison to the non-

activated brain regions. As a result the amount of de-oxygenated haemoglobin decreases in the area of increased activity and the BOLD signal is enhanced. When brain activity decreases, the reverse happens. All the aforementioned are shown in Figure 2.1 [28].

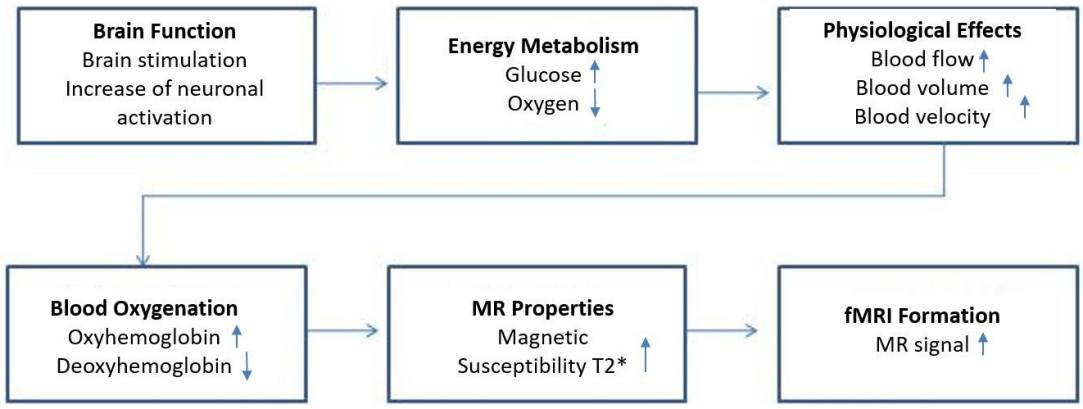

Figure 2. 1: Schematic representation of the fMRI formation [29].

As it is known, the hemodynamic response is the increase in blood flow that follows a brief period of neuronal activity. There are two details about that response that underlie the basic features of BOLD fMRI and determine how the data must be analyzed. At first, while neuronal activity last less than milliseconds, the hemodynamic response is slow. Thus the increase in blood flow that follows this activity takes about 5 seconds to reach its maximum. This peak is followed by a long undershoot that does not fully return to baseline for at least 15-20 seconds. The second detail is that the hemodynamic response can be treated as a linear time-invariant system. This linearity makes it possible to create a straight forward statistical model that describes the time course of hemodynamic signals that would be expected given some particular time course of neuronal activity, using the mathematical operation of convolution [26].

In Figure 2.2, the common features of the fMRI BOLD response in a period of neuronal stimulation are a) the initial dip, b) positive BOLD response and c) post stimulus undershoot. When there is an activation of a voxel in BOLD fMRI, it has been noted that the signal increases above the baseline at about 2 seconds following the onset of neuronal activity. After that, is growing to a maximum value (peak) of about 5 seconds from a shot duration stimulus. Provided that the neuronal activity is extended across a block of time, the peak could be similarly extended in a plateau. After reaching its peak, the BOLD signal

decreases in amplitude to a blow-baseline level and remains below baseline for an extended interval. Such event is named as post stimulus undershoot [30, 29].

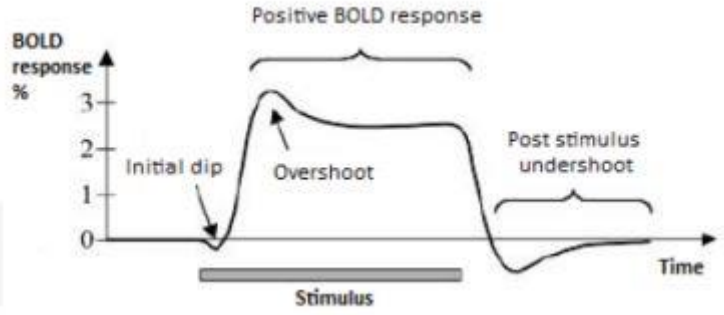

Figure 2. 2: Schematic representation of the BOLD response [29].

2.3 Image acquisition process-Types of fMRI experimental design

The primary approach to fMRI and diffusion imaging for connectivity studies involves single shot imaging using EPI (Echo Planar Imaging). Since its initial application, EPI scan times for whole brain coverage have not substantially decreased. Progress in shortening the EPI acquisition time for spatial encoding only modestly reduces acquisition time for whole brain coverage. This modest reduction is because each slice incorporates a physiological contrast preparation period that can equal or exceed the time employed for collecting the EPI echo train [31].

The data acquisition consists of the following stages. At the beginning the subject is positioned in the scanner so as to start the process of fMRI experiment. After that the subject is asked to perform several tasks or is stimulated so that different processes or emotions are triggered. It is worth to be mentioned that the stimuli is usually audio or visual and stimulations involve the motor cortex, as well as, more cognitive demand functions such as the function of memory and thought. All these experimental conditions are repeated at different period of time and can be alternated by inactive and relaxing periods [29]. The necessary equipment for an fMRI experiment is shown in Figure 2.3.

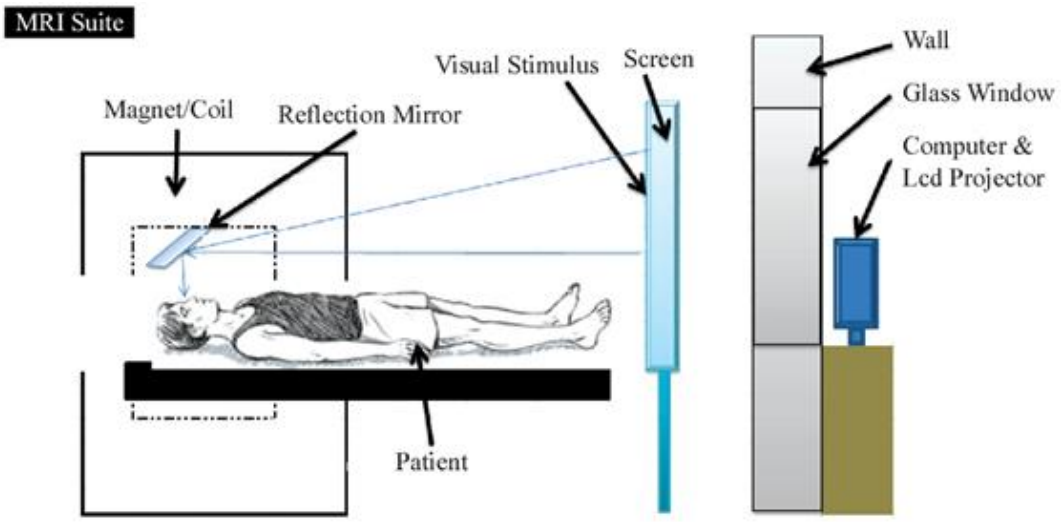

Figure 2. 3: The necessary equipment for an fMRI experiment [42].

Much of what is currently known about brain function comes from studies in which a task or stimulus is administered and the resulting changes in neuronal activity and behaviour are measured. However, the brain is very active even as there is no input or output of stimuli or task [28]. Due to that reason the experimental design for fMRI includes task-based designs and resting-state designs. Of course the combination of both methods is very important, due to the findings that are derived.

2.3.1 Task- based fMRI

In a typical experiment, a low resolution image of the brain is acquired every few seconds and over the course of the experiment, 100 images or more are usually recorded. The stimulus can either be presented in a "block design", "event- related design'' and ''mixed design''. The first type alternates relatively long periods of rest and stimulation, whereas the second type presents short events at varying intervals. The third type is actually a combination of the previous types, but it is not preferable type because it is much more complicated to design and analyze. In each type of design the effect size is inferred from the difference in BOLD contrast between the two states [22, 24].

The ''block design'' constitute the most efficient type of design for comparing brain responses in different states during the imaging experiment. This design uses long alternating periods (30seconds), during each of which a discrete cognitive state is maintained. Only two states will be, in the simplest case, which are alternated throughout the experiment in order to ensure that variations arising from fluctuations in scanner

sensitivity, patient movement or changes in attention. All these have the same effect on the signal responses associated with both states. It is worth to be mentioned that it is difficult to control precisely a cognitive state for a long period of time of each block [21].

The design of ''event-related'' experiments requires careful consideration of numerous issues of measurement, modelling and inference. ''Event-related'' or trial-based measurement, as it is called, is already standard in the field of electrophysiology, namely stimulus-locked, event-related potentials (ERPs) [32]. In instances where tasks are inappropriate for ''block design'', for example as in an ''oddball'' paradigm, an event-related design can be used in which data acquired while discrete stimuli or responses are repeated. So as to acquire a measurable response, the results from many trials are averaged.

Comparing of two types of design, event-related design demands longer acquisition times than block design, so as to achieve a sufficient signal to noise ratio. It has been shown that block designs are optimum for detecting activation. Whereas event-related designs are most efficient for the characterization of the activation of the time course (mixed designs lie in between them). Also when there is need to take a decision whether a hypothesized activation occurs in a brain region, the most effective from the types is block design. It is preferable to use the event-related design when more details are needed about the characteristics of the neural response to the cognitive manipulation [21, 24].

2.3.2 Resting-state fMRI

The knowledge that has been gained the past decades about brain functions focused on task state studies, when the presence of stimuli evokes the brain activity. As it has already been mentioned, the brain remains active even in the absence of stimuli. For that reason, recent studies involve investigation of brain fluctuations at resting conditions and their results demonstrate that spontaneous modulation of the BOLD does not produce randomly [33].
In other words, resting-state fMRI measures spontaneous, low frequency fluctuations in the BOLD signal, so as to investigate the functional architecture of the brain [34]. The participants are not required to perform any kind of cognitive task, motor or even to pay attention to any particular stimulus. Instead they have to clear their minds and not to engage in specific thoughts or visual images [35, 123].

The most common purpose for using resting-state fMRI is the use of a larger sample of patients which are contracted from different diseases. In contrast to task state fMRI, most of the patients could not do the experiment correctly in fMRI scanner. Also the resting-state uses the same data for every study is up to do, for example language and motor studies; however in task state every experiment is unique and needs different data.

The energy consumption in resting-state is one-fifth of the total energy of the body and it is used to support ongoing neuronal signals. In case of task state fMRI the same variable (energy consumption) is usually very small, less than 5%. Another thing that is needed to take into account is that the most signals from the ongoing spontaneous BOLD modulations are desired signals, because they are focused on resting-state fMRI. But only a small percentage of signals (less than 20%), that came from task state approaches are considered as desired. The expected outcome is that the signal to noise ratio is better in resting-state studies than task-based approaches. Last but not least, an important advantage of resting-state is that it can ignore the parameters that may cause problems to the study; something like that is very difficult to achieve in task state approaches.

It is understandable that resting-state approach has not have only advantages and it is not the preferable type for every fMRI study, between the two. Every approach has advantages and disadvantages and each of them can be used on many studies. For example, some disadvantages of resting-state are the following:

- It is difficult to control whether the subject is awake or is in sleep state, because there are not individual differences in brain activity between the two states.
- The poor acknowledge about the neural interactions and their relation to individual skill leads to the conclusion that, so as to define the structural network the task-based approach is required.
- Brain default energy, in multi tasking analyses, is related to the subject mental state (tired, excited, etc.) so it is impossible to control that parameter without using task related experiments.
- The memory of every subject is cannot be tested during resting-state experiment because subjects are not thinking of something specific [33].

2.4 Advantages and disadvantages of fMRI

Functional Magnetic Resonance Imaging is a technique that provides high quality in vivo brain images. At least three features of MR images rendered them valuable for providing improved anatomical definition of cerebral lesions. Those are a) the high resolution of images, b) the ability to obtain clear views of every corner of the brain, c) the well defined demarcation of abnormal signals that reflected underlying pathology. Also functional MRI does not involve ionizing radiation, so it can be used repeatedly in subjects; even in children. Technical improvements that must be done, will lead to the increase of spatial and temporal resolution. Something that has to be improved is firstly the high cost and secondly the position of patient's body during the experiment [36, 37].

2.5 Spatial and temporal resolution

The notion of spatial resolution describes the ability to separate the alterations in an image (or map) across different spatial locations; while the term temporal resolution describes the ability to separate alterations in a single location over time [30]. Although fMRI combines relatively high spatial and temporal resolution, it is far from being an ideal reflection of the neuronal response. Spatially, the signal is permitted in the whole brain area, not only to areas of increased neuronal activity, as changes in oxygen extraction and changes in blood flow [22]. Although it is restricted by signal to noise ratio (SNR). Smaller voxels recommend smaller SNR but also enhance spatial resolution by detect smaller structures and smaller activated areas [29]. It provides special information about grey and white matter in the order of millimetres for spatial resolution whereas a few seconds for temporal resolution. The typical fMRI pixel size is 3-4mm, although with higher field magnets (7T) a pixel size of 500 microns or less may be readily achieved. The resolution of PET is limited by the size of the gamma ray detectors as well as the positron annihilation range, is typically larger than 5-10mm. In the case of NIRS resolution, it is low approximately 10-20mm and is limited predominantly by the strong scatter and attenuation of IR photons. The resolution in EEG and MEG is similarly limited to larger than 10-20mm by the fact that a unique reconstruction of dipoles is not possible from scalp based measurements of electrical or magnetic distributions and models and regularization must be employed for model estimation. In contrast with MEG, in EEG the scalp measurements may be spatially distorted by heterogeneous electrical conduction paths within the brain/skull [25].

Temporally, the haemodynamic response and the signal to noise ratio (SNR) are factors that restrict that type of resolution of the fMRI signal. The BOLD response has a width of approximately three seconds and typically peaks after four to six seconds after onset of a neuronal stimulus. However the variability of the BOLD response limits the temporal resolution more than the lag itself, in brain regions, subjects and tasks. Temporal resolution in a real fMRI experiment is further governed by T1 relaxation processes and hardware characteristics, along with the limits imposed by the BOLD response [22]. PET scans requires minutes to complete due to the low count rates of injected radio nuclides, so changes in neuronal processes can only be studied by repeated scanning. Due to the fact that NIRS reports changes in blood oxygenation, just like BOLD, exhibits similar temporal limitations with fMRI. On the other hand EEG and MEG have millisecond temporal resolution and can easily capture the dynamics of evoked responses that last from a few milliseconds to several hundred milliseconds. In the case of combine two approaches, fMRI

and EEG, it is preferable to use fMRI maps as spatial priors to reconstruct high temporal resolution electrophysiology, thereby gaining resolution in both dimensions [25]. There are some ways for enhancing the fMRI spatial and temporal resolution. These are: 1) by optimizing the MRI pulse sequences, 2) by improving resonators, 3) by using higher magnetic fields, 4) by developing intelligent strategies for parallel imaging.

2.5.1 Source of noise in fMRI

The noise that has been reported probably comes from the activity that evoked from the experiment. The sources that cause the noise are the following: 1) systematic noise due to tissue pulsation related to cardiac and respiratory cycles, 2) noise due to the movement of the subject, 3) noise due to the slow fluctuations of blood oxygenation and 4) thermal noise due to the subject, the receiver coil and the amplifiers [29].

2.5.2 fMRI time-series

It is important to order fMRI scans as a function of time or as it is known, treat them as a time-series (Figure 2.4). This is necessary because the BOLD signal will tend to be correlated across successive scans and that means that can no longer be treated as independent samples. The main reason for this correlation is the fast acquisition time (T_R) for fMRI relative to the duration of the BOLD response. Managing fMRI data as time-series also allows us to view statistical analyses in signal processing terms [38].

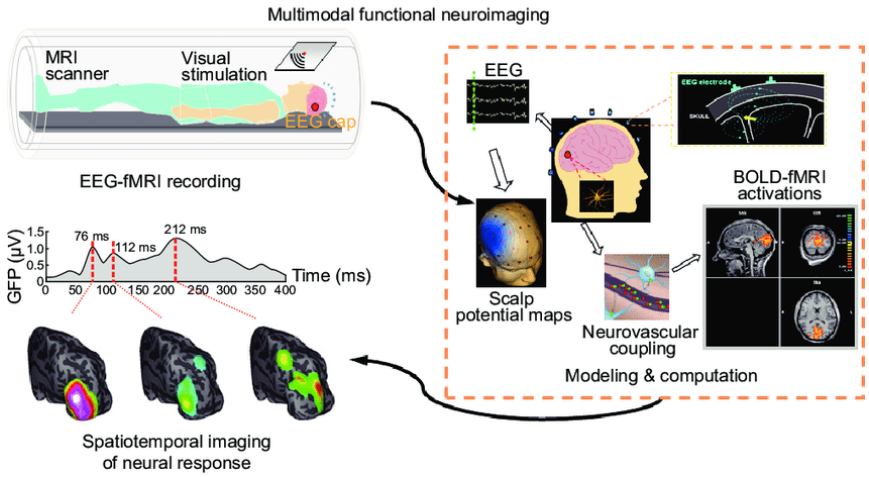

Figure 2. 4: Functional MRI time-series [41].

2.6 Applications of fMRI

The rise in availability of magnetic resonance imaging for detecting disorders in the living brain has made it a very attractive technology for defining neural structure and function in a

large amount of prominent diseases. Neuroimaging has become a major focus for multi-institutional research in progressive alterations in brain architecture, proxy biomarkers of treatment response as well as the outcome of disease from cognitive activation and connectivity. In general the variety of applications of fMRI is classified in two categories, cognitive neuroscience and clinical applications [39].

2.6.1 Cognitive neuroscience

An interdisciplinary area of research that combines measurement of brain activity with simultaneous performance of cognitive tasks by human subjects is called cognitive neuroscience. Mainly this area of research connects the science of human brain (Neuroscience) and the science of mind (Cognitive Sciences) [43]. The use of fMRI focuses on understanding the way in which an area of interest (activated area) affects another one. For instance, as it is already known a visual stimulus can have an impact on the brain response at the touch of an object or a face. Demonstrating and learning the plasticity of brain systems it is a field of research where applications of cognitive neuroscience have already been used [22].

2.6.2 Clinical applications

The functional MRI can localize brain functions well, allowing eloquent brain areas to be defined, characterizing the reorganization of patterns of brain activation as a consequence of disease or injury. Also this technique can indentify differences in brain function between subjects associated with disease susceptibility or other factors causing variation [21]. In clinical applications there are several aspects of fMRI that should be taken into account so as to receive important information from clinical studies. These aspects are: safety and preparation of the patient, necessity of effective patient cooperation, scanner capability, analysis and presentation of data, correct organization of paradigms, quantitative and qualitative sufficiency of the staff.

This technique is preferable because it is available to use before the operation, thus allows more informed decision between the surgeon and the patient. Also it is non-invasive, repeatable and can be overlaid with anatomy. The visualization is in 3D [122]. In case, for example, of a brain tumor surgery its use is very important. fMRI can define the relationship of lesions to eloquent areas prior to surgery. Also it can determine the need for intra-operative electrocortical mapping. The definition of a surgical plan for resection and the determination of language lateralization are other two usages of fMRI. There are some limitations that have to be mentioned. At first fMRI is better at demonstrating motor areas

rather than language areas. The BOLD signal, which is based on this technique, can be affected by biological aspects of brain tumors. Moreover in patients with profound neurologic deficits may be difficult to acquire a clear perception about the tumor. Last but not least, fMRI does not demonstrate essential cortex.

As in brain tumor surgery like so in planning surgical interventions for epilepsy, fMRI has become the central technique of mapping eloquent regions responsible for motor, somatosensory, language and memory functions [122]. So as to manage and treat epilepsy, fMRI determine lateralization of language dominance and also predict the risk for declining the language function. Furthermore, it is used as an adjunct to direct cortical stimulation in order to map the relationship between lesions to language, motor and somatosensory areas. Another use is to predict memory deficits following ATL (Adult T-cell leukemia/ lymphoma). Functional MRI can also be used in conjunction with EEG to indentify seizure foci. Specifically this conjunction may help to localize lesions where EEG and imaging data and EEG are discordant.

Functional MRI has been shown in many studies to be capable of demonstrating impairment of the activation of the hippocampus and parahippocampal gyrus during memory encoding tasks in patients with Alzheimer's disease (AD). The discovery of the presence of an fMRI- based biomarker in patients at risk for Alzheimer's disease has also been an attractive and active area of research. Its use is related with the understanding of the pathophysiology basis that causes the memory loss in patients with AD. Also fMRI can predict the decline in cognitive function and can test transitions in brain physiology in response to pharmacologic agents.

In conclusion, fMRI has shown great utility identifying the anatomic location corresponding with specific motor, somatosensory, language and cognitive processes. It is helpful to understand the neuroanatomic and pathophysiologic alterations that occur in response to brain tumors, epilepsy, movement disorders, dementia and trauma. A very promising area for fMRI is the creation of biomarkers that will be useful for monitoring diseases of the central nervous system and for testing the utility of already existing and experimental treatments [40]. Scientists have used fMRI to identify abnormal functional brain activity during task performance in a variety of patient populations, including those with neurodegenerative, demyelinating and other neurological disorders that emphasize the potential benefit of fMRI in both basic and clinical fields of research [39]. The importance of fMRI lays not only in its usage for diagnosis of diseases such as Dementia, Parkinson's disease, Autism, Alzheimer's disease etc., but also in its ability to differentiate the

characteristics of each disease in healthy and pathological subjects. In chapter 3 there is an extensive description about the use of fMRI in Parkinson's disease.

Chapter 3: State of the art

3.1 Brain imaging in Parkinson's Disease

After the clarification of the pathophysiology of PD, several studies have been established so as to better understand the way that this neurogenerative disease works. Except from the pathophysiology, brain imaging techniques are helpful tools that have been used for a better understanding of PD. The combination of these (imaging techniques & pathophysiology) can lead all scientists that are involved, in new unknown pathways that will help to treat PD.

In this chapter, some of the recent and of interest studies (for this thesis) are referenced and described below. There is a classification of the studies in two subcategories according to presence (Task-based studies) or absence (Resting-state studies) of a particular task. fMRI is the imaging technique that will be referenced in most of the cases, because that is the tool that is used to acquisition all the data for this thesis.

3.1.1 Task-based studies

Sabatini et al. studied about the cortical reorganization in akinetic patients with PD. In that functional MRI study has been participated six akinetic patients and six normal subjects that were all right handed. The selected patients had mild to moderate symptoms so as to ensure that they can perform the task in their off state. The type of motor task had not been chosen by chance but because it induces a clear activation signal in areas that are involved in both motor programming and motor execution. The performance of imaging

was done on a Siemens Magneton Vision scanner operating at 1.5T and equipped with EPI (echoplanar imanging) hardware. During the performance the subjects were resting for 30 s and activating for 30 s four times. Also T1-weighted images were acquired so as to obtain structural three-dimensional volume. One statistical analysis on a pixel by pixel basis was done, using SPM96, for all the participants (patients & healthy controls) and the parametric maps that were acquired were then generated using an ANCOVA (analysis of covariance) model. Comparing the results of activation in patients with those of controls, increased fMRI signals were observed in the right and left primary cortex, in the right and left premotor cortex, in the right and left inferior parietal cortex, in the caudal part of SMA and in the cingulated cortex. On the other hand increased fMRI signals in controls were obtained in small areas of left lateral premotor cortex, in the rostral part of the SMA, in the left inferior parietal cortex and in the right dorsolateral prefrontal cortex. In summary that study presents that the cortical motor pathways are being disorganized in a complicated way, by the subcortical putaminal dopamine deficit [44].

Another interesting fMRI study was about the automatic movements by underlying neural mechanisms in patients with PD, by *Wu et al.*. Twelve patients with PD were included in that research and were compared with fourteen age-matched healthy controls. The tasks that have to be accomplished so as to take some significant results were four. Two of them were self-initiated, self-paced sequences of finger movements with different complexity until the automatic performance of them. The other two were dual tasks where subjects were asked to perform visual letter-counting that was similar with sequential movements. Subjects were asked to lie down in the MR scanner with response device on their right hand. For that reason the whole group was right handed. According to the fMRI procedure, T2*-sensitive functional images were obtained using a whole-body 1.5 T scanner and a standard head coil. Also so as to obtain the functional images, an EPI gradient echo sequence was used. The images were acquired before and after the achievement of automaticity from the subjects and each scanning session lasted four minutes. For the imaging analysis SPM 99 software was used. A fixed effect boxcar design was used in order to model the data which convolved with a heamodynamic response function. The results showed that the left primary sensorimotor cortex, bilateral premotor areas, bilateral parietal cortex, bilateral dorsal lateral prefrontal cortex, bilateral SMA, bilateral anterior cingulated motor cortex, bilateral basal ganglia, bilateral insular cortex and bilateral cerebellum were the activated areas for the patient's group before training. After training the behavior pattern of the activation was similar except from areas, bilateral superior parietal lobes and left insular

cortex, that were less activated than the before training process. As for healthy controls, before training the brain activations were matched with those for patients. Although after training, less activation was obtained in the bilateral premotor area, bilateral superior and inferior parietal lobes and pre-SMA. Comparing healthy controls with patients before training, patients showed greater activation in the bilateral cerebellum, bilateral parietal cortex, bilateral premotor area, bilateral precuneus and bilateral dorsal lateral prefrontal cortex while performing the sequence-4. Healthy controls had greater activity in the pre-SMA than in patients. After the training, patients had still greater activations in the aforementioned areas and also the results showed that there was no area in healthy controls with greater activation than in patient's group. As a conclusion, automaticity is an ability that a patient with PD can achieve after a proper training but with more difficulty than a healthy subject. That study was the first one that suggests that a PD patient needs more brain activity to balance out for basal ganglia dysfunction so as to perform automatic movements [45].

The next study was all about of exploring the cerebral substrates of action- related word production in non-demented PD patients. That study of *Péran et al.* was affected from previous studies that have resulted in, that for non-demented PD patients is a little hard to produce verbs in a word generation situation. An event-related fMRI task was used so as to explore the brain regions that are involved in generation of action-words (GenA) and in object naming (ON) in an amount of fourteen PD patients. For the two tasks was used a standard set of object drawings that were either man-made objects (MMO) or manipulable biological objects (MBO). In object naming, subjects must name aloud the objects drawings that they were seeing while in GenA must produce orally a verb pointing an action that could be performed with the pictured object. Only for the task of GenA, a study of twelve young Italian healthy controls was performed. For that study was used a 3T magnetic resonance imaging scanner while the acquisition of fMRI data happened using a gradient echo imaging (EPI). So as to remove the noise from the data, the Cool Edit Pro software was used. After the acquisition the data were analyzed using SPM2 implemented in MATLAB. As for the statistical analysis, is consisted of two steps. The first comprised individual analyses performed on each of the 12 subjects. The second step consisted of a group analysis in which contrast images that were obtained previously, were combined in a second level random effect analysis yielding main contrasts. The main brain activations, for the ON task, were observed bilaterally in the frontal cortex, superior temporal cortex, supplementary motor area (SMA), inferior occipital cortex, fusiform gyrus, lingual gyrus and cerebellum. For

the GenA task, the observed brain activations were similar with the ON task except from the regions of the frontal and temporal cortices that were activated to a greater degree. Also there was an extra activation in the left inferior and superior parietal cortex. Comparing the two tasks the following results were observed: 1)GenA $_{MBO}$> ON $_{MBO}$ in the left occipital cortex, left supramarginal gyrus and ACC, 2) GenA $_{MMO}$> ON $_{MMO}$ in the left prefrontal cortex and right insula, 3) GenA $_{MBO}$> ON $_{MMO}$ occipital cortex bilaterally, ACC, left prefrontal cortex, left frontal operculum, left supramarginal gyrus and right superior frontal cortex. As for the results from the correlation analyses the main activations where in the left pre-central gyrus in all conditions. Those results lead to the outcome that there is a relationship between the motor system dysfunction in PD patients and the extent of activation in verb generation, which is a task that process in depth of semantic representation of actions [46].

The last study of the category of task-based studies that will be referenced in this thesis, is a little different from the aforementioned because included except from the Parkinson's disease and some atypical parkinsonian syndromes. Also is a longitudinal study that lasted one year. More specifically *Burciu et al.* investigated changes in brain activity in patients with Parkinson's disease, Multiple system atrophy (MSA) and Progressive supranuclear palsy (PSP) using task-based functional MRI. The regions of interest that they focus were the putamen, primary motor cortex (M1), supplementary motor area (SMA) and superior motor regions of the cerebellum (lobules V-V1) using a unimanual grip force fMRI protocol. Also they hypothesized that the basal ganglia and motor cortex would have reduced fMRI signal in PD, MSA, PSP comparing with the healthy controls which both MSA and PSP would have extensive and more pronounced cortical changes than PD. In this cohort study the amount of participants was one-hundred and twelve (112) with forty six PD patients, thirteen MSA patients, nineteen PSP patients and thirty four healthy controls. Most of the patients were taking medication but the performance of the test happened 12-14 hours after the overnight dose of antiparkinsonian medication. All the participants were produced force against a custom-designed MRI compatible fiber optic transducer with a resolution of 0.025N. The protocol consisted of a block design with shifting force and rest blocks. After the acquisition of data with a 3T Philips system along with a T2*- weighted, single shot, echoplanar pulse sequence and an anatomical 3D T1-weighted sequence, the processing steps carried out. The last ones were based in previous studies of grip force in parkinsonian disorders. Then they examined group differences at baseline using analysis of covariance (ANOVA). The results demonstrated group differences at baseline in age and gender. Also patients with PD showed a decline in functional connectivity after the one year

follow up in the putamen and M1 compared to controls. As for MSA patients the changes of functional activity were exclusively extrastriatal and included a reduction in the areas of M1, SMA and superior cerebellum. At last, in PSP patients all the regions of interest had less activation after one-year of study compared to baseline. The functional activity of these regions did not change in the healthy controls. Overall that study provided evidence for distinct patterns of motor-related changes across the basal ganglia and cerebello-thalamo-cortical loops in PD, MSA and PSP. These findings could provide a platform to test therapeutic strategies that aim to slow the progression of parkinsonian disorders [53].

3.1.2 Resting-state studies

Resting-state functional connectivity MRI is a technique that permits the investigation of large scale functional networks at whole brain level based on the temporal correlation of spontaneous fluctuations in a very low frequency range. That technique has been discovered by *Biswal et al*. (1995) and has successfully been used to identify a variety of intrinsic cortical and cortico-subcortical networks with a homogenous resolution in the millimeter range [120].

The first resting-state study that will be referenced in this thesis is from *Kwak et al.* where they investigated alterations in cortico-striatal functional connectivity networks within PD patients and age matched controls using six different striatal seed regions. They tested twenty- five mild to moderate stage PD patients where thirteen of them had taken levodopa (L-DOPA ON) and twelve had received placebo medications (L-DOPA OFF). The controls group was consisted of twenty-four individuals where none of them had taken any medication. The participants underwent of the fMRI scanner, as usual, so as to collect the fMRI data which were preprocessed as part of a standard processing stream at the University of Michigan. After the preprocessing, was followed the normalization to MNI space using SPM5. Except from the usual analysis a frequency content analysis of the fMRI BOLD signal was performed, using ANOVA. The results were presented with the left side of the images because that was the more affected brain hemisphere. They observed an overall increase in the strength of cortico-striatal functional connectivity within PD patients of L-DOPA OFF and controls. That connectivity was decreased within motor cortical regions in the case of L-DOPA ON patients. More specifically for the caudate seed, the ventromedial prefrontal and orbitofrontal regions for inferior ventral striatum, the dorsolateral prefrontal and frontal eye field regions for superior ventral striatum and dorsal caudate. As for putamen seed, the primary and secondary motor areas were affected. Also between PD-ON and PD-OFF they did not find any areas more correlated with putamen and caudate

themselves than the putamen and caudate seed regions; except from the dorsal prefrontal cortex in PD-OFF and the dorsolateral prefrontal cortex in PD-ON which exhibited more correlated activity with the caudate. From the frequency content analysis the results showed an overall elevation of cortico-striatal functional connectivity in PD patients and that Levodopa decreased the heightened connectivity. From the results they concluded that PD and L-DOPA are variables that affect striatal resting state BOLD signal oscillations and cortico-striatal network coherence [47].

Skidmore et al. focused his fMRI study in connectivity brain networks based on wavelet correlation analysis in Parkinson data. In fourteen subjects with idiopathic PD and fifteen age-matched healthy controls they investigated the efficiency of human brain functional networks. That type of correlation analysis can show the functional similarity between brain regions that were activated in a defined frequency interval or wavelet scale. This is important in the case of a resting-state study where the greatest frequencies are below 0.1 Hz and non neural sources of correlations belong to higher frequency ranges. Functional images were acquired using a Philips Acheiva 3T scanner while also three dimensional structural images were acquired. For every dataset the geometric displacement, and more specifically the head motion, was accurate and the co-registration step was performed using the Montreal Neurologic Institute gradient-echo echoplanar imaging (EPI) template with the AFNI package. Also data were not spatially smoothed but the regional parcellation was performed in base of the anatomical labeling template. That parcellation leaded to a separation of each hemisphere into 116 different anatomical images of interest. The results showed that the mean global efficiency of these networks was greater in healthy controls (1.25± 0.25) compared with PD patients (0.95±0.17). In both healthy controls and PD patients the top 30 nodes where observed in the precuneus, cuneus, superior occipital and middle frontal regions. These regions comprise aspects from the resting network that has been described as the “Default Mode Network”. Regions such as the left supplementary motor cortex, contiguous precentral regions, the Calcarine cortices, secondary visual regions and regions within the cerebellum appeared increased efficiency in controls than PD patients. Authors suggested that such algorithmic approaches and graph metrics are accustomed to understand better and track neurodegenerative diseases. Although a lot of research must be done so as to separate on a case by case basis the PD subjects from the controls [48].

Another significant research was that of *Baudrexel et al.* where they investigated the functional connectivity changes of the subthalamic nucleus - motor cortex (STN) using

resting-state BOLD correlations, on a voxel by voxel basis in fMRI. They choose to investigate the STN because it plays an essential role in normal motor functioning and also in pathophysiology of PD. Firstly from an anatomical and physiological perspective its position is special because it is part of two functional loops, a slow indirect (cortex-striatum- external pallidum (GPe) –STN- internal pallidum (GPi)/ substantia nigra pars reticularis (SNr)-thalamus cortex) and a fast hyperdirect pathway (cortex- STN- GPi/SNr-thalamus- cortex). Secondly for patients that are in advanced stage of the disease, the deep brain stimulation of STN along with basal ganglia nuclei constitutes the most effective target. In that study were participated thirty one early stage PD patients and forty four healthy controls. Except from the classical analysis between PD patients and healthy controls, there was another one where patients divided into subgroups according to the presence (Number of patients = 16) or absence (Number of patients = 15) of tremor. The imaging performance was carried out on a 3T MR scanner system where subjects lie still, relax and keep their eyes closed without thinking anything specific or falling asleep. Also patients scanned while they were in an off medication state. The functional scans from the whole brain were acquired with EPI sequence. As for the data preprocessing, that was performed using SPM8 with custom built programs written in MATLAB. After that, functional connectivity was analyzed with a common seed-region approach that conducted in MNI space. The last step was the conduction of a voxel based morphometry because the alterations in the structural of the brain may confound the results of functional connectivity. The analysis of the results showed increased functional connectivity between the STN and cortical motor areas in PD patients in accordance with electrophysiological studies. Comparing the results between healthy controls and tremor patients, increased STN FC was observed in the hand area of M1 and the primary sensory cortex. As for non-tremor patients increased FC was observed between the STN and midline cortical motor areas including the supplementary motor area (SMA). From the aforementioned findings the authors suggested that PD rigor and tremor symptoms may be resulted in a connection of these areas and lead to the conclusion that STN is a key node for the modulation of the motor network in PD patients [49].

Tessitore et al. were interested in investigating another motor symptom of Parkinson's disease, freezing of gait. Freezing of gait (FOG) is a common cause of disability and falls in patients, that is characterized by the feeling of "glued" to the floor that prevents locomotion generally occurring during gait initiation and/or turning. Using resting-state functional MRI they studied a group of patients with (Number of patients = 16) and without (Number of patients = 13) FOG and they compared them with fifteen age and sex matched

healthy controls. All subjects were evaluated (clinical and cognitive) 60-90minutes after their morning dose of levodopa and then were scanned in the "on medication" state. In that case the magnetic resonance images were acquired on a 3T GE scanner equipped with an 8-channel parallel head coil. The fMRI data were consisted of 240 volumes of a repeated gradient- echo planar imaging T2*-weighted sequence. Also three dimensional high resolution T1-weighted sagittal images were acquired for registration and normalization of the functional images. As for the computational techniques they used the Brain Voyager QX for data preprocessing and statistical analysis (the data were co-registered and spatially normalized to the standard Talairach space before the statistical analyses). Also ICA was used for single-subject and component analysis. So as to map the distribution of the whole brain of the components of interest, single-group one sample t-tests were used in all the participants. Then so as to define the search volume for within network group comparisons, they created an inclusive mask from the control group component. After that, a two-sample t-test was computed to produce a T map of the differences between the groups. The results showed that patients with freezing of gait exhibit reduced functional connectivity within "executive attention" network, namely in the right middle frontal gyrus and in the angular gyrus, and also visual networks, namely in the right occipito-temporal gyrus. These findings suggest that the phenomenon of FOG is generally associated with both early cognitive frontal dysfunction and mood changes, suggesting a tight relation between these symptoms [50].

Another interesting resting-state fMRI study was that by *Luo et al.*. They studied functional connectivity in a group of twenty-seven early-stage drug-naive Parkinson's disease patients compared with fifty-two age and sex-matched healthy controls. In that study they focused on the functional connectivity of the substriatum subregions. It is interesting to refer that this study was the first resting state fMRI which examined brain network integrity in a large group of patients in early-stage drug-naïve along with the relationship between the Non-motor Symptoms Scale (NMSS) and alteration of functional connectivity. The acquisition of the magnetic resonance images was performed as always with a 3T MRI scanner. The statistical analysis and preprocessing was carried out using SPM8 while for functional connectivity analysis, a seed voxel correlation approach was used. The seeds that have been selected were the left and right putamen and caudate, just like previous researches. Also they used the tool REST to investigate the functional connectivity. The last analysis that they performed was a voxel-based morphometry, so as to investigate if functional results influenced potentially by structural differences among groups. Although

the deceased functional connectivity within cortical sensorimotor areas was only evident within the foremost affected putamen subregion, a reduction of functional connectivity within mesolimbic regions was prevalent throughout the striatum. Increased functional connectivity was not obtained during this cohort. By studying a group of early-stage drug-naïve PD patients, they excluded the potential confounding effect of extended antiparkinson medication use on the functional integration of neural networks. Decreased functional integration obtained across neural networks involving striatum, mesolimbic cortex and sensorimotor regions and hypothesized that the prevalent disconnection in mesolimbic-striatal loops caused by some early clinical nonmotor features in PD. Although prolonged antiparkinson medication may result in reorganization of functional neural networks through unknown mechanisms and confound our understanding of the first pathological process, their findings of prevalent reduced functional connectivity of neural networks in early-stage drug-naïve PD patients reflect the first pathological changes within the natural disease course [51].

Baggio et al. studied about frontostriatal functional connectivity in Parkinson's disease patients that suffer from apathy, a symptom that affect 23% - 70% of the patients and is related to frontostriatal dopamine deficits. Using resting-state functional magnetic resonance imaging they investigated thirty-one healthy controls and sixty-five age, gender and education matched PD patients. From the group of PD patients, the twenty-six were classified as apathetic. Using 3T MRI scanner were acquired structural T1-weighted images, FLAIR images as well functional resting-state images. AFNI and FSL had been used for the preprocessing of the resting-state images. Also the structural data were analyzed with FSL-VBM which is a voxel-based morphometry (VBM) style analysis. As for the statistical analysis a voxelwise general linear model was applied, using a non-parametric testing for connectivity and VBM. Furthermore before the analysis, the definition of regions of interest took part. More detailed the frontal cortices were divided into limbic (anterior, posterior, medial orbital gyri, gyrus rectus, subcallosal gyrus/ventral anterior cingulate), executive (rostral superior and middle frontal gyri and dorsal prefrontal cortex), rostral motor (caudal portions of lateral and medial superior frontal gyrus, caudal middle and inferior frontal gyrus) and caudal motor (precentral gyrus and caudal premotor area). Reductions of functional connectivity showed the apathetic PD patients while comparing them with non-apathetic patients and healthy controls. These reductions were observed in left-sided circuits and predominantly involving limbic striatal and frontal territories. As for the structural analyses there was not found any significant effects. From the results, authors

suggested that the presence of apathy in PD patients is related to the reductions of functional connectivity in frontostriatal circuits, predominating within the left hemisphere and mainly involving its limbic components but also extending to premotor and primary motor regions. That is applicable even in the absence of significant structural degeneration and while controlling for associated depression and cognitive decline [52].

Another resting-state study that will be referenced is that of *Engels et al.* where they focused in dynamic functional connectivity (dFC) of both the default mode network (DMN) and the frontoparietal network (FPN) as neural correlates of cognitive functioning in patients with PD. Also they investigated symptoms such as pain and motor problems of PD in relation to dFC. The individuals that participated in that study were twenty-four PD patients and twenty-seven healthy controls. All the participants underwent resting-state functional connectivity from which dFC was defined by calculating the variability of functional connectivity over variety of sliding windows within each scan. The assessment of the pain happened with the Numeric Rating Scale (NRS) while for the motor symptom severity the Unified Parkinson's Disease Rating Scale, was used. Patients underwent MRI two times with and without Parkinson medication, but in that study only the without medication phase imaging was used so as to reduce the effect of dopaminergic medication. As always the MRI data were collected with a 3T GE Signa HDxT MRI scanner along with structural and functional images. The analysis of the data happened using FSL FMRIB software library and custom built scripts in bash and MATLAB. As for the statistical analysis were performed with IBM SPSS. The results showed that patients performed worse on tests of visuospatial memory, verbal memory and working memory compared with healthy controls. The cause of that may be the lower level of education of patients. Between groups the dFC had no differences in the DMN or the FPN with the rest of the brain regions. Although a positive correlation existed between dFC of the DMN and visuospatial memory. This association was not found when investigated motor symptoms or pain, which suggests that dFC of the DMN may be specifically linked to cognitive functioning. That study helps to understand which of the factors contribute to cognitive functioning in PD [54].

The last resting-state study that will be referenced is a latest study about the functional brain network of motor reserve that is related to patients with early PD. They proposed the notion of motion reserve in Parkinson's disease, which is similar to the notion of cognitive reserve in Alzheimer's disease, so as to explain the heterogeneity of symptom severity in Parkinson's disease regardless the analogous level of nigostriatal dopamine depletion on dopamine transporter (DAT) scans. From a total number of one hundred fifty six

participants only one hundred thirty four were included on the study because of apparent artifacts and motion artifacts. The twenty two participants were excluded at the step of preprocessing of fMRI data. All of the participants were de novo PD patients who underwent dopamine transporter (DAT) imaging and showed appropriate DAT defects in the posterior putamen. Also they underwent MRI, including high resolution of T1-weighted MRI and resting state fMRI at baseline evaluation. The preprocessing of the fMRI data was performed using SPM12 and custom codes running on MATLAB while the Toolbox of Network-Based Statistic and their custom codes running on MATLAB was applied for the network analysis. Furthermore they examined longitudinal changes in dopaminergic medication doses at a subset of participants (n= 109) according to the motor reserve network strength. That happened using a linear mixed model named LED. Last but not least they performed a voxel-based morphometry analysis to estimate if alterations in gray matter were related to the level of motor reserve. The DAT imaging was performed using a Discovery 600 device while the processing of the acquired images was performed using SPM8 implemented in MATLAB. After that the motor reserve of each patient separately was estimated, dependent on their baseline UPDRS-III score and dopamine transporter availability in the posterior putamen. The UPDRS-III score is a clinical criteria for the diagnosis of PD. They defined the motor reserve estimate as the standardized value for the residual that was calculated as (raw value - A)/B, where A and B were the mean and standard deviation of the residuals of all patients with PD. The MRI images were acquired using 3.0T scanner both for the high resolution axial T1-weighted MRI scans and T2*-weighted single-shot echo planar imaging sequences. From the network-based statistic analysis the results showed that brain regions such asbasal ganglia, inferior frontal cortex, insula and cerebellar vermis are included in the motor reserve network. Also the presence of a bigger degree of functional connectivity within the motor reserve network was found in patients with greater motor reserve. Moreover the interaction that was observed within the motor reserve network strength and time in the linear mixed model resulted in that motor reserve network strength and levodopa-equivalent dose are inversely proportional sizes. So as a more general result, functional connections within the motor reserve network are connected to the individual's capacity to cope with pathologies that concern PD [107].

3.2 An overview of the literature

In the following table (Table 3.1) is presented an overview on recent literature methods.

Table 3. 1: An overview of the literature.

Authors	*Dataset*	*Regions*	*Imaging technique*	*Computational technique*	*Results*
U. Sabatini et al 2000 [44]	6 akinetic patients 6 normal subjects All participants were right handed Motor task	Rostral part of SMA, right DPC, PSC, LPC, IPC, caudal part of SMA & ACC	fMRI	SPM96	These fMRI data confirm that the frontal hypoactivation observed in patients with PD is restricted to the rostral part of SMA and to the DPC. Also other cortical motor areas of these patients showed increase signals.
T. Wu et al 2005 [45]	15 patients (3 of them were excluded because they could not achieve automaticity) 14 age-matched normal subjects Automatic movement task Visual letter-counting tasks	BSPL, LIC, Cerebellum, premotor area, parietal cortex, precuneus, prefrontal cortex	fMRI 1.5 T MRI	SPM99	For both groups, the activation was observed in similar brain regions before and after automaticity was achieved. PD patients require more brain activity to compensate for basal ganglia dysfunction so as to perform automatic movements.
P. Péran et al 2009 [46]	14 non-demanded Italian PD patients Event-related task	Premotor and prefrontal cortices, pre and post central gyri bilaterally, left frontal operculum, left SMA, right superior temporal cortex	fMRI 3T MRI	SPM2	The direct comparison of brain activity during the production of action-words and of object names did not reveal any major differences. However there is a relationship between motor system dysfunction in PD and the extent of activation in verb generation, a task which implies processing of semantic representation of actions.
Y. Kwan et al 2010 [47]	25 mild to moderate stage PD patients 24 healthy controls Resting-state	Caudate, putamen, dorsal prefrontal cortex, DCP, ventromedial prefrontal & orbitofrontal regions for inferior ventral striatum, frontal	fMRI 3T MRI	SPM5 ANOVA	The results showed that PD and L-DOPA are variables that affect striatal RS BOLD signal oscillations and cortico-striatal network coherence.

		eye regions for superior ventral striatum & dorsal caudate, PMC, Secondary MA			
F. Skidmore et al 2011 [48]	14 idiopathic PD patients 15 healthy controls Resting- state	Cortical and subcortical regions	fMRI 3T MRI	Wavelet –based correlation analysis	PD patients showed decrease in nodal and global efficiency. For identifying and tracking neurodegenerative diseases, the use of graph metrics and algorithmic approach it might be necessary.
S. Baudrexel et al 2011 [49]	31 early stage PD patients(right handed) 44 healthy controls Presence of tremor 16 patients Absence of tremor 15 patients Resting-state	PMC, STN, cortical motor areas, basal ganglia	fMRI 3T MRI	Voxel by voxel basis SPM8	Increased FC between the STN and cortical motor areas was observed in PD patients. FC analysis of the PMC hand area revealed that the FC increase was primarily found in STN area within the basal ganglia. Tremor and non tremor patients showed increased FC in STN.
A. Tessitore et al 2012 [50]	29 PD patients(16 presented with freezing of gait) 15 healthy controls Resting-state	Right middle frontal gyrus and in angular gyrus, right occipito-temporal gyrus	fMRI 3T MRI	ICA BrainVoyager QX	Patients with freezing of gait exhibit reduced FC within both executive- attention and visual networks.
C. Luo et al 2014 [51]	52 early-stage drug naïve PD patients 52 healthy controls Resting- state study	Mesolimbic-striatal, corticostriatal loops, CSA, putamen subregion,meso limbic cortex, sensorimotor regions	fMRI 3T MRI	SPM8 REST	PD patients showed decreased functional integration across neural networks and postulate that the prevalent disconnection in mesolimbic-striatal loops is associated with some early clinical nonmotor features in PD.

H.C. Baggio et al 2015 [52]	65 PD patients 26 apathetic PD patients 31 healthy controls Resting-state	Left-hemispheric limbic ventromedial, premotor and primary motor regions	fMRI 3T MRI	Voxel based morphometry analysis	The presence of apathy in PD patients is related to the reductions of functional connectivity in frontostriatal circuits, predominating within the left hemisphere and mainly involving its limbic components.
R.G. Burciu et al 2016 [53]	112 individuals:46 PD, 13 MSA, 19 PSP, 34 healthy controls Task-based fMRI (1 year research)	Putamen, PMC(M1), SMA, superior motor regions of the cerebellum (lobules V-V1)	fMRI	ANOVA	PD patients showed a decline in functional activity compared with controls. MSA patients showed a reduction of functional activity in M1, SMA and superior cerebellum. All regions in PSP were less active after 1 year. In healthy controls there was no change in these regions.
G. Engels et al 2018 [54]	24 PD patients 27 healthy controls Resting-state	DMN, FPN, visuospatial memory	fMRI 3T MRI scanner3D	FSL FMRIB MCFLIRT SPSS	The results suggest that dynamics during the resting-state are a neural correlate of visuospatial memory in PD patients. Also brain dynamics of DMN could be a phenomenon specifically linked to cognitive functioning in PD, but not to other symptoms.
S.J. Chung et al 2020 [107]	134 de novo PD Resting state	Motor reserve network composed of basal ganglia, inferior frontal cortex, insula, cerebellar vermis.	fMRI MRI Dopamine transporter imaging (DAT)	Network based statistic analysis, SPM8, SPM12, Voxel based Morphometry analysis	Functional connections within the motor reserve network are connected to the individual's capacity to cope with pathologies that concern PD. Patients with increase of functional connectivity within the motor reserve network had greater motor reserve.

Chapter 4: Methodologies for connectivity extraction

4.1 Preprocessing of fMRI data

While fMRI identifies neuronal activity via hemodynamic response to alterations in metabolic consumption of oxygen, the acquired time-series have, most of the times, confounds of non-neurally related sources of variations. Such sources include subject's head motion, magnetic field inhomogeneity, physiological oscillations like heart beats and respiration and differences in the timing of image acquisition. These unwanted fluctuations may cover the intrinsic patterns of neural activity, alter experimental conclusions by introducing structured noise that affects the real neurally-related results and also decrease the detection of a possible following statistical analysis. In general all these lead to spatial and temporal inaccuracy of the fMRI data. For that reason several computational procedures have been developed, termed as the *preprocessing pipeline*, so as to remove unwanted variations and increase the *functional signal to noise ratio* (fSNR) before further analysis. In the most frequently steps are included, motion correction (realignment), slice timing correction, coregistration, spatial normalization and spatial smoothing [24].

4.1.1 Motion correction (realignment)

The basic aim of that preprocessing step is to correct artifacts that are related to the movement. Most of the times the movement is large and particularly subject's head

movement is a prominent concern in most fMRI studies. In cases where the duration of scan is long, subjects become increasingly drowsy and restless as time goes by. Also, when the study is task-based subject's motion synchronizes with the on-going stimulus or different types of subjects, such as elderly and diseased people affect the movement [24]. Due to the fact that head movement in the scanner cannot fully be eliminated, different mathematical transformations focus on the removal of the movement. Furthermore the statistical results are affected by movement in different ways. For example, when motion induces distance-dependent variance (more similar between voxels nearby than far apart) that causes alterations in the intrinsic correlation structure of the data. Another way is when motion interplays with field inhomogeneity and slice excitation, causing more complicated noisy fluctuations [116].

The first step in motion correction is the best possible alignment within the input image and the target image. Usually the target image is the first or the intermediate image. Due to the fact that the brain is assumed to be a rigid object that estimates at each time point its displacement from a reference position, rigid body transformation involving six variable parameters is used in realignment. So as to match the target image with the input image, the last one is translated (shifted in the x, y and z directions) and rotated (altered roll, pitch and yaw). It is necessary to use a cost function in order to determine the optimal value of parameters. Figure 4.1 demonstrates the raw and corrected images after the motion correction step.

From the mathematical perspective, a position $x = [x_1, x_2, x_3, 1]^T$ in image f is mapped to a position $y = [y_1, y_2, y_3, 1]^T$ in image g by rigid body transformation and is expressed by the following equation:

$$y = M * x \,, \tag{4.1}$$

where $M = M_{f^{-1}} M_t M_\theta M_\varphi M_\omega M_g$ is the transformation matrix.

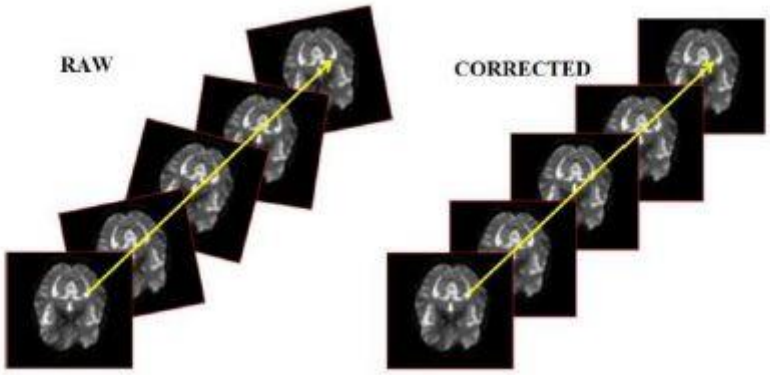

Figure 4. 1: Motion correction [117].

More specifically, M_t is the matrix that implements the translations and $M_\theta, M_\varphi, M_\omega$ are the matrices that implement the rotations about the x, y, z axes respectively. The other two matrices, M_f and M_g, are the transformation matrices into Euclidian space for images f and g that are to be registered together. The matrices are represented below [118].

$$M_t = \begin{bmatrix} 1 & 0 & 0 & x_t \\ 0 & 1 & 0 & y_t \\ 0 & 0 & 1 & z_t \\ 0 & 0 & 0 & 1 \end{bmatrix}, M_\theta = \begin{bmatrix} 1 & 0 & 0 & 0 \\ 0 & \cos\theta & \sin\theta & 0 \\ 0 & -\sin\theta & \cos\theta & 0 \\ 0 & 0 & 0 & 1 \end{bmatrix} \quad (4.2, 4.3)$$

$$M_\varphi = \begin{bmatrix} \cos\omega & 0 & \sin\omega & 0 \\ -\sin\omega & 0 & \cos\omega & 0 \\ 0 & 0 & 1 & 0 \\ 0 & 0 & 0 & 1 \end{bmatrix}, M_f = M_g = \begin{bmatrix} x_{mm} & 0 & 0 & -\frac{a}{2}x_{mm} \\ 0 & y_{mm} & 0 & -\frac{b}{2}y_{mm} \\ 0 & 0 & z_{mm} & -\frac{c}{2}z_{mm} \\ 0 & 0 & 0 & 1 \end{bmatrix} \quad (4.4, 4.5).$$

Where x_{mm}, y_{mm}, z_{mm} are the voxel's dimensions and a, b, c the dimensions of images. The best possible fit for all j voxels within the two images f and g is obtained by minimizing the following equation and solving the parameters p:

$$l(p) = \sum_j (Mx_v - sy_v)^2, \quad (4.6)$$

where $p = [x_t, y_t, z_t, \theta, \varphi, \omega]^T$ is the parameter vector, v is the voxel and s the parameter that is used to offset the differences in voxel intensity of two images [117].

4.1.2 Slice-timing correction

This preprocessing step, also, causes inaccuracies in time-series and is related to the sequential collection of slices within each volume (Figure 4.2) [118]. The major part of fMRI studies use a two-dimensional pulse sequence that illustrates one slice at a time, leading to inconsistent acquisition time among different brain slices within one TR. That kind of slice-timing errors, if uncorrected, may present inaccuracy in cases where the temporal information is critical, for example, in rapid event-related experiments or in studies with positing causal association among different cortical regions. The acquisition order defines the scan time of an individual slice. There are three options for the acquisition order, known as interleaved slice acquisition, ascending and descending sequential acquisitions. The first one is used more frequently because is collecting all of the odd slices at first and then all of the even slices, avoiding cross-slice excitation. In this acquisition order, the adjacent slices are collected a full TR/2 apart. The less common ascending and descending sequential acquisitions, are collecting the slices consecutively and particularly the last slice is collected almost one TR after the first slice. It is important to be mentioned that the data acquired via interleaved acquisition at a long TR, the step of slice-timing correction must be performed first, before the motion correction [30].

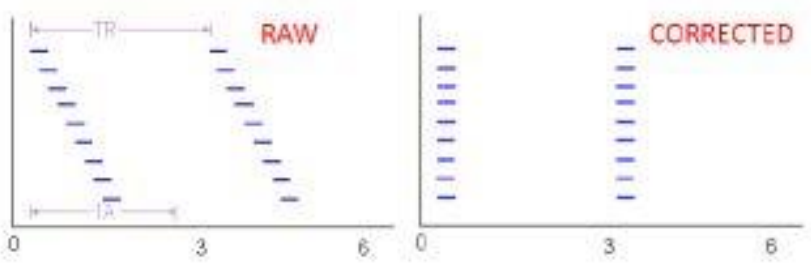

Figure 4. 2: Slice-timing correction [117].

The statistical analysis accepts that every voxel is sampled simultaneously, so the main point of slice-timing correction is to relocate each voxel's time course in order to consider them as they were measured at exactly the same time point. Due to this fact, phase shifting of the sines that comprise of the signal must be performed. Furthermore, the time-series of the voxels is transformed in the frequency domain, the data is performed to phase shifting and the inverse Fourier is used so as to execute the corrected time-series recovery [29].

From the mathematical aspect, each image volume that has q slices with $m\,x\,n$ pixels (m is the number of the rows and n is the number of columns), the matrix that is formed is the following:

$$A_{cq} = \begin{bmatrix} a_{11} & a_{12} & \dots \\ \vdots & \ddots & \vdots \\ a_{k1} & a_{k2} & \dots \end{bmatrix}, \tag{4.7}$$

where c ranges within 1 and n ($c = 1, \dots, n$) and k represents the time points. The element α_{ij} expresses the intensity value of the voxel that is localized in slice q. Consequently, the first column of the matrix illustrates the time-series of the voxel $(c, 1, q)$. The performing convolution is applied for each column of the matrix in the frequency domain with a shifting vector. The number of slices, TR, TA and the acquisition order (ascending, descending and interleaved) affect the shifting vector [117].

4.1.3 Co-registration

In general this preprocessing step maps the functional and structural images to each other applying computational procedures. The collected 3D stack of functional and structural images, usually do not match each other. That happens because of differences in MR contrasts and acquisitions, e.g. inconsistent slice orientation, voxel resolution and image distortion, leading to problems in mapping activity to the structural image. The computational procedures, basically, at first resample the structural data to the spatial resolution of the functional data and then employ a rigid body transformation where mutual information (cost function) is minimized [24].

4.1.4 Intensity normalization

With the intensity normalization step, is occurred the rescaling of all intensities in an fMRI volume by the same amount and is applied at each volume separately. That happens because, during an fMRI experiment, a supplementary scan-to-scan variance appears at very low spatial frequencies that may be caused by the scanner itself (scanner drift). In most studies, first the calculation of the mean intensity across all voxels happens, for every fMRI volume that has been at intensity above a predetermined threshold. Then follows the rescaling of all intensity values by a constant value and last the new mean intensity turns into a present value. The usage of mean intensity value of each volume as confounding variables is required so as to be applied in statistical analysis later, based on other approach. But there is a disadvantage in the case of a strong activation. Particularly, when there is a strong activation, the mean intensity increases and results in the negative correlation of the

non-activated sections of the volume with the stimulation after normalization. So, the final statistical image will include a part of deactivation [29].

4.1.5 Spatial normalization

Due to the fact, that in most fMRI studies there is comparison between brain activation across multiple individuals, this step is necessary. The shape and the size of brains are inconsistent within subjects so a comparison between different images is difficult. With spatial normalization each individual's brain is normalized to a template, which is usually based on specific populations or published ones. The most common templates are Talairach atlas, Tournoux atlas and Montreal Neurological Institute space (MNI). A large number of normal MRI scans are applied in the MNI space, so it is more representative of the population, in contrast, with the other two which are based on one subject's brain.

Spatial normalization can be based on intensity, landmark or even on surface. Typically, it is implemented by registering each individual's functional images to a functional template. This can happens directly or in two steps, where the co-registration of functional and structural images is the first step and then follows the registration of the anatomical images to a high-resolution structural template. Each of the two approaches has advantages and drawbacks. The first one prevents inconsistent geometric distortions induced by different imaging contrasts, while the second approach is more robust because of the improved resolution and quality of structural image [24].

In a more detailed description, in the first step occurs the determination of the optimum 12-parameter registration within the template and the image to be normalized. While in the second step follows the estimation of the nonlinear deformations determined by a linear combination of three-dimensional discrete cosine transform (DCT) basis functions. A maximum a posteriori (MAP) approach is applied for the determination of the optimum affine transformation. The affine transformation is represented as:

$$y = M * x, \tag{4.8}$$

where $M = M_{f^{-1}} M_t M_\theta M_\varphi M_\omega M_z M_s M_g$. Focus matrix is represented as M_z and shearing matrix as M_s, as you can see below [119].

$$M_z = \begin{bmatrix} x_z & 0 & 0 & 0 \\ 0 & y_z & 0 & 0 \\ 0 & 0 & z_z & 0 \\ 0 & 0 & 0 & 1 \end{bmatrix}, M_\theta = \begin{bmatrix} 1 & x_s & y_s & 0 \\ 0 & 1 & z_s & 0 \\ 0 & 0 & 1 & 0 \\ 0 & 0 & 0 & 1 \end{bmatrix} \quad (4.9, 4.10).$$

The estimation of the nonlinear deformations that appear throughout the normalization, it is very important. In order to achieve the distortion modeling a linear combination of basis functions are used. An example is given below:

$$y_i = x_i - \sum_j t_j b_j(x_j) \,, \quad (4.11)$$

Where t_j is the jth coefficient describing translation for each three dimensions and $b_j(x_j)$ is the jth basic function at spatial position x_i [119].

4.1.6 Spatial smoothing

The benefits of including the spatial smoothing in the preprocessing procedure are three. Firstly, with spatial smoothing the fSNR of the data can be improved. The acquired fMRI data are inherently spatially, because of the blurred signal by vascular origins and the functional similarity of adjacent brain areas. Secondly, can also be enhanced the anatomical or functional variations within different subjects. Unlikely, the optimum kernel sizes determined by different goals are not consistent. Thirdly, spatial smoothing may improve the validity of following statistical analysis by softening the difference within spatial structure of the data and the assumed model.

Meanwhile, several disadvantages of spatial smoothing in relation with the correct size of the kernel, must be considered. For conventional studies that adopt fixed kernel size among the brain, a recommended kernel size ~ 4mm is suitable for single subject analysis, while for a group level analysis a wider kernel size 6-8mm is suggested. So as to be sure, the examination of the results when a wide smoothing kernel is used, is recommended [24].

The most common approach is the convolution of each volume with Gaussian kernel. The amount of the image spatial smoothing relies on the full width half maximum (FWHM), as shown in Figure 4.3. The equation that represents the convolution is the following:

$$t_i = \sum_{u=-d}^{d} h_{i-u} \, f_u \,, \quad (4.12)$$

where d is the length of the kernel, h is the kernel and f is the image that undergoes the spatial smoothing. The kernel amplitude A, at u units away from the center is characterized as: $A_u = \frac{e^{-\frac{u}{2rl^2}^2}}{\sqrt{2\pi rl^2}}$, where $rl = \frac{FWHM}{\sqrt{8ln2}}$ and the FWHM is the full width at half maximum of the Gaussian kernel.

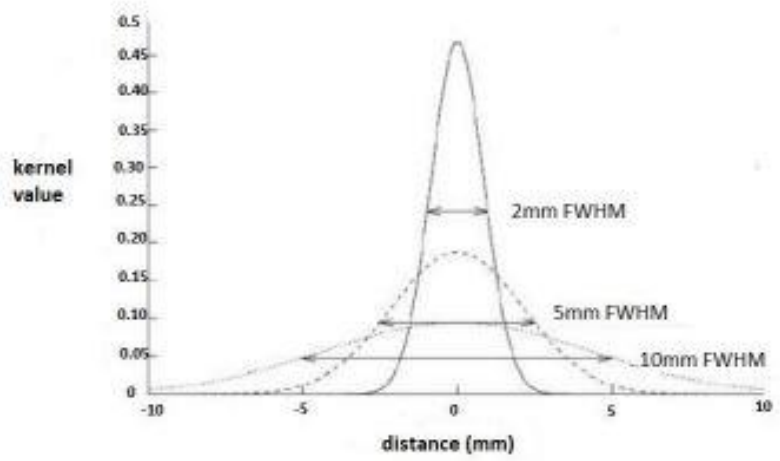

Figure 4. 3: Width of Gaussian kernel [117].

4.2 Brain connectivity

4.2.1 Functional organization and brain connectivity

In the recent past (18th century), neuroscientists believed that many brain functions were deliberated by its structure and that its structure was programmed by the genes. However, in past decades, this perspective has changed and has been believed that the neural pathways of the brain are flexible, connected, adaptable and moldable by alterations in the environment of the individuals or by injury or disease. Briefly, the brain is quintessentially plastic and can adapt and adopt new functionalities through necessity. This understanding depends on the mean of connectionism, with the hypothesis that the function of the brain can be characterized as the interaction among simple units, for example, neurons connected by synapses that cause a connected whole which changes over time. After some other ideas, the notions of functional segregation and functional integration have been introduced. Since their appearance, there has been a trend to move from functional segregation toward functional integration [55]. The notion of functional segregation implies that a certain cortical area is responsible for some aspects of perceptual or motor

processing. Although the notion of functional integration supports that many specialized areas are functionally integrated [56]. So later the integration within and between functionally specialized areas are described by functional and effective connectivity [57].

A long term goal of neuroscience is to develop models that integrate brain structure and function to predict human perception, cognition and behavior, but unfortunately they lack of characterization at the level of the individual subject. Neuroimaging research has only start to address this gap of knowledge and substantial work needs to be carried out before the study of individuality and variation of brain networks. The brain connectome is comprised of both grey matter (GM) regions representing neuronal units of information processing (the nodes of Figure 4.4) and white matter (WM) tracks, serving as structural communication pathways (the edges of Figure 4.4) [58].

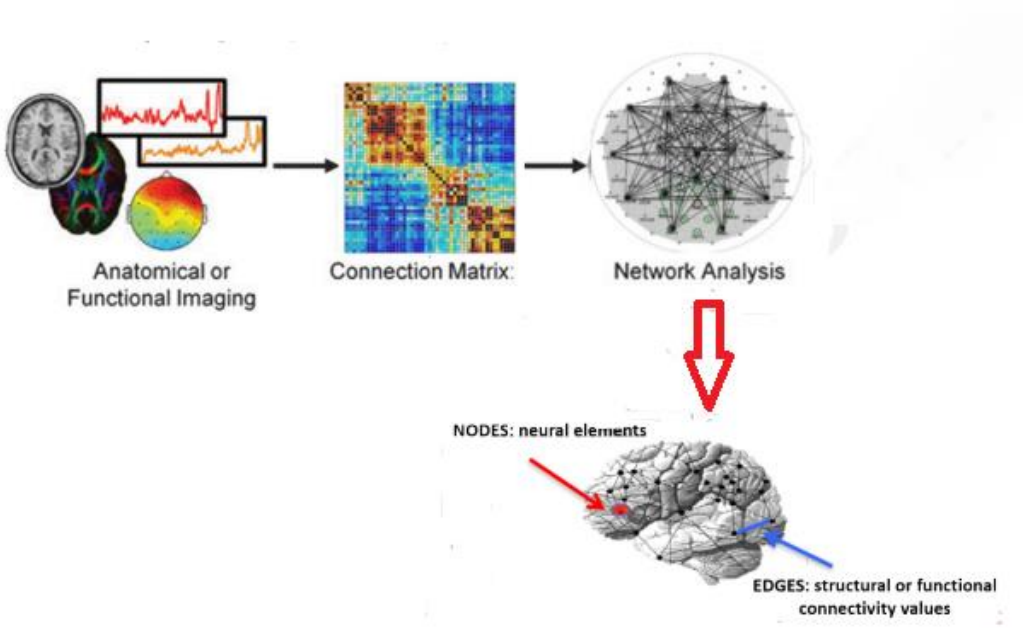

Figure 4. 4: Connectome nodes and edges. Cortical termination of the arcuate fasciculus. Yellow higher, red lower termination density. Two magor WM tracts, cortico-spinal tract (CST) & arcuate fasciculus [58].

Generally brain connectivity describes the relationship between brain regions that may be spatially close or distant, anatomically different and also are connected either functionally –spontaneous intrinsic synchronization- or structurally –neuronal axons [59]. Due to its diversity, connectivity divided into three forms. These are structural, functional and effective connectivity [60].

4.2.2 Structural connectivity

As it has already been mentioned, connectivity is the study of the interaction within two different brain regions. The structural or elsewhere the anatomical connectivity describes the physical connections or interactions through synaptic contacts within neighboring neurons or fiber tracks connecting neuron pools in spatially distant brain regions. All these fiber tracks are known as white matter of the brain. Persistence and stability on short time scales as well as substantial plasticity on longer time scales (may be observed sometimes) are characteristics of that type of connectivity [60, 61]

The anatomical connectivity can be acquired using techniques of structural imaging along with diffusion tensor tractography methods. DTI and fiber tractography allow the researchers to measure the properties of the connectome in living human brains at the meso- and macro-scale (mm to cm), providing information about brain computational machinery that changes all the time. Recent technologies identify major white matter tracts in living brains. These tracts are the most prominent edges within the connectome, information highways that implement communication about the senses, motor control, language and cognition. The variability of the connectome leads to the following limitations; firstly the dependency of connectomes on the tracking methods and secondly the insufficient reliability of connectome estimates in individual brains or even in intra-individual brain when explored at different times [58, 120].

Basically DTI measures the water diffusion tensor with the use of diffusion weighted pulse sequence as they are sensitive to the random water motion in microscopic level [59, 64]. The diffusion of the water can be characterized due to the motion (constrained or not constrained), as anisotropic and isotropic. The diffusion is anisotropic when the motion is constrained in white matter tracks or in other words when the motion prevails towards one direction than another. On the other hand, the characterization of isotropic refers to the case where diffusion occurs in all directions in equal and random rate. That happens deep in brain, in ventrices where the fluid covers large areas and the motion is not constrained [62]. However these methods suffer from low spatial resolution. In DTI literature the most mentioned frequent diffusivity indicators are the mean diffusivity (MD), franctional anisotropy (FA) and Mode. MD is based on the volume of the diffusion ellipsoid which describes the average displacement of water molecules as an outcome of diffusion in a given amount of time. Lowest number of MD is observed in tissues where diffusivity is restricted (e.g WM), while highest in tissues where there are some impediments to water diffusion (e.g CSF). As for the FA, is known as a measure of the sphericity of the diffusion ellipsoid. The

values range from zero, which indicates the spherical diffusion, to one which indicates absolutely aspherical diffusion. Also reduced FA means that there is damage to the axon membrane, reduced axonal myelination, reduced axonal packing density and/or reduced axonal coherence; on the other hand increased FA leads to supranormal levels of myelination or axonal sprouting. A relatively recently development of such indicators is the Mode. That type, provides furthermore information expressed by the 3D shape of the diffusion ellipsoid than the one that provided by FA. Basically describes whether the shape of the diffusion ellipsoid is cylinder (highly "tubular" anisotropy) or disk (highly "planar" anisotropy) for a given FA value [63].

DTI fiber tracking

The aim of DTI fiber tracking is to specify intervoxel connectivity based on the anisotropic diffusion of water. The diffusion tensor of every single voxel is used by fiber tracking so as to observe an axonal tract in three dimensions from voxel to voxel through the human brain.

DTI divided into two broad categories, the deterministic and the probabilistic that they include reconstruction methods for WM tracts. For the first category (e.g Fiber Assignment by Continuous Tracking), line propagation algorithms along with local tensor information for each step of propagation have been applied. For the second category, the global energy minimization, which detects a path within two predetermined voxels with minimum energy violation, is the main characteristic. That type also is effective for tracking fibers in areas of reduced anisotropy, not excepting gray matter [64].

4.2.3 Functional connectivity

With the term functional connectivity (FC) is meant "the temporal correlations between spatially remote "neurophysiological events". In addition with anatomical and effective connectivity, functional connectivity investigates regional interactions in the brain at a macro scale using datasets from electroencephalographic (EEG), magnetoencephalographic (MEG), positron emission tomography (PET), single-photon emission computed tomography (SPECT), local field potentials (LFP) and functional magnetic resonance imaging (fMRI) [65]. Another useful clue is that FC does not explain how these correlations are mediated, but only provides information about the correlation that is noticed [22]. As it is mentioned the use of different neuroimaging modalities is required so as to measure FC. This is because of the statistical behavior of FC, as it relies on statistical measures such as correlation, coherence, spectral coherence or phase locking [7]. From the aforementioned modalities, fMRI is the most commonly used and therefore the most important as it studies the blood

oxygen-level-dependent (BOLD) signal of the data. As it is commonly accepted, the methods that are used for FC analysis via fMRI are generally grouped into two types: model-based methods and data-driven methods (Figure 4.5). The first type is based on prior knowledge, methods with many variables are included and its use is widely. The second type does not need any prior knowledge, methods with one variable are included and it is useful for resting-state fMRI studies, where spatial and temporal pattern are unknown [11, 124].

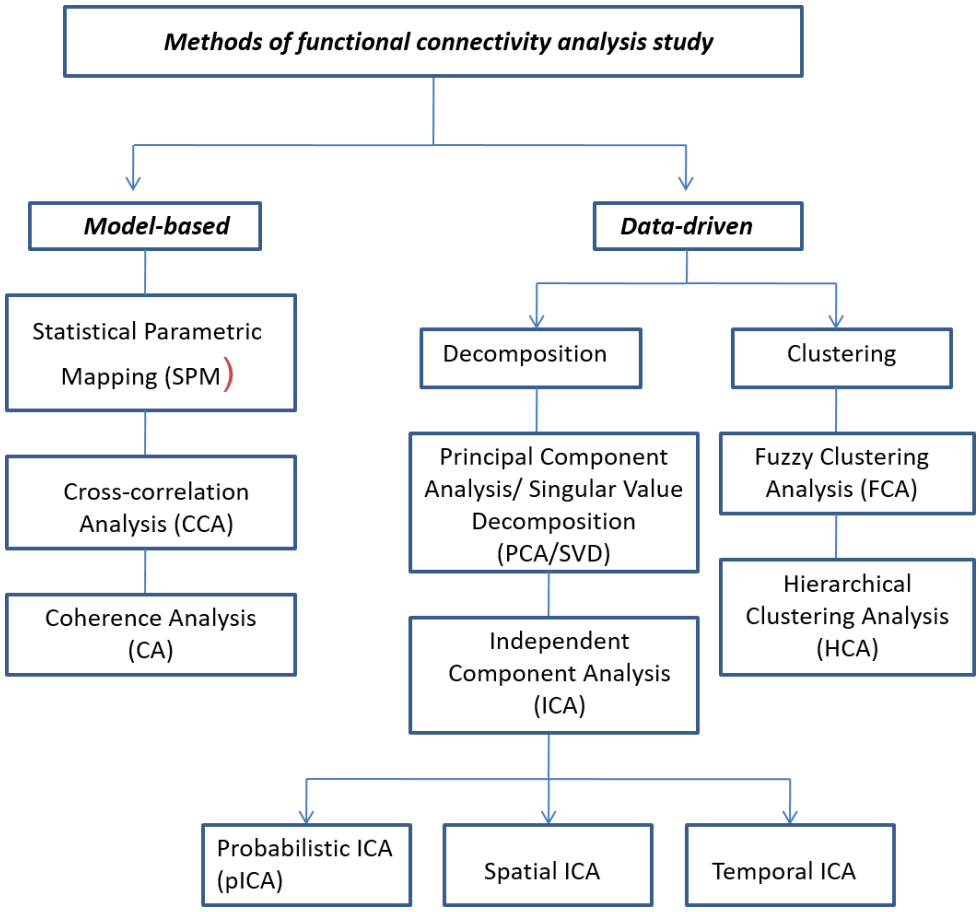

Figure 4. 5: Current Methods for FC fMRI study [65].

The correlations in activity that are mentioned all the time, which describe the FC, can result from a number of reasons. As it is shown in Figure 4.6, there are in general three ways to describe the correlations. At first, the direct influence from one region to another region which is known as effective connectivity. More specifically the signal along connection between two regions one of which sends the efferent connections to the other can be interpreted as a correlated activity. Secondly, the indirect influence where a third region operates as a mediator between the two regions. At last, the shared influence where a third region works as a common input for both of the regions. This is named as the

problem of stimulus-driven transients. The critical point is that only in the first case does functional connectivity reveal a direct causal influence between regions. For that reason, results from functional connectivity analysis must be interpreted with great caution [66].

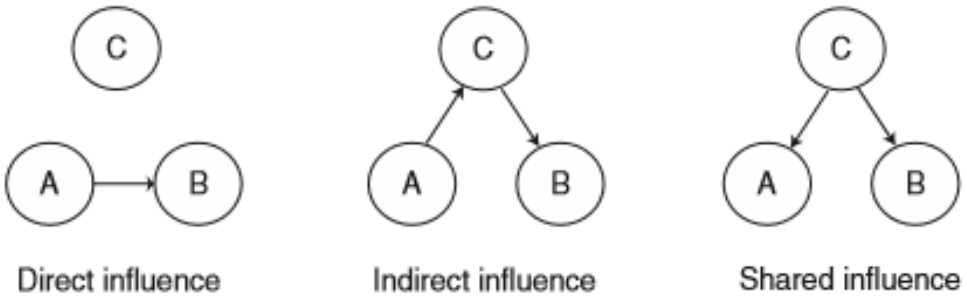

Figure 4. 6: Direct influence (left panel), indirect influence through a third region (centre panel) and shared influence of a common input region (right panel) [66].

Model-based functional connectivity analysis

Essentially in a model-based analysis it is important to select a seed or region of interest (ROI) and find the linear correlation of this seed region with all the other voxels in the entire brain, thereby yielding a seed-based FC map. For that reason this method is also referenced as seed-based analysis. Because of the fact that this analysis is dependent on the definition of the ROIs, it is difficult to test the FC of the whole brain using this technique [60]. As it is known this method is based on prior knowledge or experience as it is required a priori selection of a voxel, cluster or atlas region from which the extraction of time-series can be accomplished [65]. Also seed-based analysis was the first method that has been used by *Biswal et al.* to identify the resting-state networks [67]. In accordance to the metrics that have been used for the measurement of connectivity, the model-based methods could be classified in cross-correlation analysis, coherence analysis, and statistical parametric mapping (SPM) [65].

Cross-correlation analysis (CCA)

That type of analysis is a technique that has been widely used in many fields. Basically this analysis suggests that if one region of the brain is functionally connected to a certain seed, there should be correlation in terms of their BOLD time courses. Mathematically for fMRI

BOLD time course $F_x(k)$ and $F_y(k)$ is a seed (which is also a time course), then the CCA estimates the correlation at lag μ as:

$$Corr_{x,y}(\mu) = \frac{Cov_{x,y}(\mu)}{\sqrt{Var(x) \times Var(y)}}, \quad (4.13)$$

where $Var(x)$ and $Var(y)$ are the variances of $F_x(k)$ and $F_y(k)$, respectively; $Cov_{x,y}(u)$ is the cross variance of $F_x(k)$ and $F_y(k)$ at lag μ:

$$Cov_{x,y}(\mu) = E\{((F_x(k) - E(F_x)) \times ((F_y(k) - E(F_y))\}, \quad (4.14)$$

E is the expected value, $E(F_x)$ and $E(F_y)$ are the expectation or the mean of $F_x(k)$ and $F_y(k)$, respectively. If $Cov_{x,y}(\mu)$ is above a certain threshold, the two BOLD time courses $F_x(k)$ and $F_y(k)$ are considered as functionally connected.

An advantage of that analysis is that it is not needed the full-lag-space calculation of cross-correlation of the hemodynamic response of blood, where its computational cost is high in order to calculate the cross-correlation of all lags. Although the hemodynamic response function (HRF) varies, its duration is restricted. That happens because it will return to baseline after some time (few dozen seconds). Therefore the correlation must be computed with a time window of a dozen time points or so. In fact many cross-correlation researches compute the correlation with zero lag [65].

Although CCA has been used for fMRI data analysis on both task-based and resting-state dataset, the use of correlation at zero lag has been controversial. From the one perspective, correlation is sensitive to the shape of HRF while from the other high correlation can be detected within regions that have no blood flow fluctuations. The presence of noises such as blood vessel activity and cardiac activity in the brain would also conclude to delusion of high correlation. All these problems overcame by the appearance of a new analysis, called coherence analysis [65].

Coherence analysis

While correlation is defined in the time domain, coherence is defined in the frequency domain. The first is responsible for time delays comprising the effects of one region on another and it has great usage as statistic for the functional connectivity studies. In the case that the ordinary zero-order correlation within two different regions is moderate or low,

means that the time-series in one region is broadly similar to that in another, but with a time delay. In contrast, the coherence is high between the bandwidth of the curve [68].

For the same time courses $F_x(k)$ and $F_y(k)$, the coherence is expressed as:

$$Coh_{x,y}(\lambda) = \frac{|F_{x,y}(\lambda)|^2}{F_{x,x}(\lambda)F_{y,y}(\lambda)}, \quad (4.15)$$

where $F_{x,y}(\lambda)$ is the cross spectrum, defined by the Fourier transform of the cross covariance as follows:

$$F_{x,y}(\lambda) = \sum_u Cov_{x,y}(u) \times e^{-j\lambda u}, \quad (4.16)$$

where $F_{x,x}(\lambda)$ is the power spectrum, such as the $F_{y,y}(\lambda)$. They are defined as following:

$$F_{x,x}(\lambda) = \sum_u Cov_{x,x}(u) \times e^{-j\lambda u}, \quad (4.17)$$

$$F_{y,y}(\lambda) = \sum_u Cov_{y,y}(u) \times e^{-j\lambda u}. \quad (4.18)$$

The study of time course relationships can be achieved via the expression of correlation in frequency domain. For example, at high frequency around 1.25 Hz the coherence may be caused by the cardiac activity instead of the functional connectivity. While at low frequency values below 0.1 Hz the coherence can be related to functional connectivity [65].

Statistical parametric mapping (SPM)

The last model-based method that will be referenced is statistical parametric mapping (SPM). Its use is based on finding the patterns of activity that are induced by cognitive tasks in a fMRI experinment. Although is considering from scientists as a method for task studies, recently, SPM methodology has been applied for the detection of functional connectivity under resting-state [70]. The point of this method is to copy a stimulus based on the selected seed, then to use it in the same way as the real stimulus did in cognitive tasks. This happens because in resting-state studies there are no designed cognitive activities. As for the modeling and statistical inference, these are following the basic steps of the classical SPM [65].

In general this analysis averages the voxels in certain seed, after the steps of scaling and filtering across all brain voxels, and is considering it as a covariate of interest in the first level of the analysis. Then the second-level random effect of analysis took place where contrast images were determined individually for each subject, that are corresponding to that regressor. The aim of this step is the definition of the brain areas that exhibit significant functional connectivity across subjects [65].

SPM is, basically, a voxel-based approach that adapts the classical inference, in order to gain the remark of particular regional responses related to experinmental factors. Nowadays statistical parametric maps are considered as a way to make classical inferences about spatially extended data with the joining of general linear model (GLM) and gaussian random field (GRF). That joint of the two models is not random. GLM estimates the parameters that could explain the data, while GRF solves the multiple comparison problems so as to make statistically powerful inferences [65,69].

Although the use of model-based methods, especially CCA, is remarkable there are some disadvantages that have to be mentioned. It is common that different seeds would lead to detection of different connectivity, so seed-based methodology renders the detected functional connectivity sensitive to seed selection [71]. Also the need of prior knowledge constrains the exploration of possible functional connectivity. This lead to the conclusion that only brain regions related to the prior knowledge will be investigated, neglecting other parts or functions of brain. So this method is not capable to explore the whole brain and might need other type of methods to achieve that. Data-driven methods assume to solve this problem [65].

Data-driven functional connectivity analysis

The development of data-driven methods lead to overcome the limitations that where observed on the model-based methods and also make possible to investigate the functional connectivity of the whole human brain. This new type for detection of the functional connectivity has two main categories. The first category is known as decomposition and is composed of principal component analysis (PCA), singular value decomposition (SVD) and independent component analysis (ICA). The goal of this category is to represent the original fMRI data as linear combination of basis vectors (PCA/SVD) or as statistically independent components (ICA). Clustering analysis is the second category and is composed of fuzzy clustering analysis (FCA) or hierarchical clustering analysis (HCA). The aim of this category is to apply traditional clustering techniques to fMRI data [65].

Decomposition-based methods

Principal Component Analysis and Singular Value Decomposition

Principal component analysis and singular value decomposition are two techniques that have been used in a lot of researches and because of their similarity in their theoretical background, they are considered as one type. To begin with PCA/SVD is a method that reexpresing a dataset in terms of a set of components that are uncorrelated, or orthogonal to one another. The first principal component is equivalent to the direction through the data that has the biggest amount of variance, while the second component is the direction with the next biggest amount of variance and also is uncorrelated with the first principal component and so on. The numbers of components is the minimum against the number of observations or dimensions. Another important information about PCA is that it can analyzes only the data from the first few principals components, which accounts from the majority of the variance in the data. Thats why it can be applied as a data reduction technique [66].

From the mathematically perspective, the aim of PCA/SVD is to represent the observed fMRI time courses X with a combination of orthogonal contributors. Each from the contributors is made of a temporal pattern (principal component) multiplied with a spacial pattern (an eigen map). The SVD of X (T time points $\times$ N voxels) is:

$$X = USV^T = \sum_{i=1}^{p} S_i U_i V_i^T, \tag{4.19}$$

where S_i is the singular value of X, U_i is the ith principal component, V_i is the corresponding eigen map and p is the number of the collected components. The generated eigen maps reveal the connectivity of different regions of brain, regions with high absolute values (positive or negative) are considered as correlated [65].

To perform PCA on fMRI data, a two dimensional matrix is applied that has been created by the reformation of the data, with voxels as columns and time-points/subjects as rows. Then a set of components will be provided from PCA that have a value for each time-point, which reveals the combinations of voxels that account for the most variance. Also every component has a loading for each voxel, denoted the contribution of the voxel to each component [66].

In general this technique is simple and easily implemented. However it has the disadvantage of being sensitive only to signals that follow a Gaussian distribution. Although some signals in fMRI data follow such distribution, there also many signals of interest that do not follow such distribution [66]. Another issue is that its use is constrained in functional connectivity detection. That happened because it fails to identify activations at lower

contrast to noise ratios (CNR) when there are other sources present. Last but not least PCA/SVD is used some times as a preprocessing step for reduction of the dimensions for further analysis, just like ICA [65].

Independent Component Analysis

Independent component analysis was developed to give a solution to the problem called the blind source separation, which means to detect the unknown signals in a given dataset [66]. Blind signal separation is an explorative technique which is used in the field of image and sound analysis. Because of the fact that signals are from various types of fMRI recordings, blind separation techniques are suitable to isolate and distinguish the source of these signals separation [72].

ICA is a popular method for functional connectivity detection with no need of prior knowledge about the spatial or temporal patterns of source signals; so it has been applied for both task-based and resting-state studies. Particularly for an rs-fMRI signal, ICA facilitates the effective extraction of distinct rs-fMRI networks by using mathematical algorithms to decompose the signal from the whole brain voxels to temporally and spatially independent components. ICA investigates multiple simultaneous voxel to voxel interactions of distinct networks in the brain. It is assumed as a powerful technique which utilizes for both group level analysis and same group analysis, having different conditions such as psychological, physiological and pharmachological [60, 124].

From the mathematically perspective, ICA searches for linear combination of components in the dataset. In contrast with PCA/SVD, ICA finds components that are as statistically independent as possible. For fMRI data X (T time points $\times$ N voxels), the ICA model can be written as:

$$X = AC = \sum_{i=1}^{N} A_i C_i, \tag{4.20}$$

where C_i is the ith underlying signal source, A is the mixing matrix with dimension equivalent with $T \times N$. Every different source is independent from one another:

$$P(C_1, C_2, \dots, C_N) = \prod_{i=1}^{N} P(C_i), \tag{4.21}$$

where $P(C_i)$ presents the probability of the ith underlying signal source. Assuming as the pseudo reverse of A the W, the independent components can simply obtain by the following equation [14]:

$$C = WX. \tag{4.22}$$

In the initial stage, ICA decomposes the concatenated multiple fMRI data, so as to identify distinct patterns of functional connectivity in every subject. In the next stage identifies for all the subjects, the spatial maps and the associated time courses. In the third stage a generation of different component maps, is happening, for different subjects and are complied into a single four-dimensional file to perform the non-parametric analysis. That kind of analysis is a methodology of statistical test which aims to extract statistical significance across groups or across subjects in a group [60].

During the performance of ICA, two different assumptions can be made that are leading to different results. Firstly for both of the assumptions, the reconstruction of the original 4D matrix into a 2D matrix is needed. Afterward, the first assumption claims that the data composes of T random variables (time-points) where all of them are measured in N voxels. So T three-dimensional maps of activity are generated while there is possibility to analyze the 3D map into an original $N \times T$ matrix. The result from this is that the mixing matrix A has $T \times T$ dimensions. According to the second assumption, the expression of data is described as N random variables where all of them are measured in T time-points. Consequently, the output is N independent time-series with T as the length. This leads to an original $T \times N$ matrix with X dimensions and a mixing matrix A with $N \times N$ dimensions. For the solution of ICA there have been used two common algorithms, Infomax and Fixed-Point. Both of them are attempt to minimize the mutual information of components C_i. Infomax manages to accomplish this aim, using adaptively minimization of the output entropy of neural network with as many outputs as the number of ICs to be estimated. As for Fixed-Point, this is based on the notion of negentropy. Several studies reveal the conjoint efficiency and accuracy of the findings after the use of both algorithms. Obviously they have their own separate advantages. Fixed-Point algorithm prevails over Infomax in the level of spatial and temporal accuracy, while Infomax shows competitive superiority in global model estimation and the decrease of noise [65, 72].

The ICA can be divided into spatial ICA and temporal ICA which depends on the way the data are decomposed. Spatial ICA is based on the analysis of spatially independent components and spatially independent time-course. In contrast, temporal ICA is denoted to the data decomposition into temporarily independent components and temporarily independent time-course. The nature of the task determines which of the two methods is the most suitable, because these methods lead to different results in relation to the characteristics of the underlying signals that are to be assessed. For example, when the

underlying signals are spatially but not temporarily correlated, temporal ICA is the proposed method. When, in contrast, signals are temporarily but not spatially correlated, spatial ICA must be applied [65].

Although the widely use of ICA algorithm to fcMRI studies and especially on resting-state fMRI dataset, there are some "traps" that have to be on concern. As it has already been mentioned, this decomposition-based method relies on the independence of the components (signal sources) even it is spatially or temporally. If something like that hindered, the conclusion will be the decrease of effectiveness of ICA. Another issue is the selection of the number of independent components and how to threshold the IC maps. These questions have been studied by Ma et al. and the conclusions that were referenced were the following; when the number of ICs is smaller than that of the source signals then ICA results are highly dependent on the number [71]. Because of the difficulty of the direct thresholding of IC maps, it is widely accepted the conversion of an independent map with a non-Gaussian distribution into a z-map with a Gaussian distribution [65]. Ma et al.'s results showed that the conversion of z-map is inclined to overestimate the false positive rate (FPR) [71]. However this overestimation is in many cases acceptable. The last issue that has to be mentioned is about the consideration of ICA as a non-free generative model, which expresses in detail the fMRI data through source signals and the mixing matrix A. Because of this fact, the evaluation of the statistical significance of the source within the framework of null-hypothesis is not allowed. The solution of this ''trap'' comes from a newly development of a model called probabilistic ICA. As stated in pICA, a set of q $(q < p)$ statistically independent non-Gaussian sources (spatial maps) produce the observed p dimensional time-series through a linear and instantaneous 'mixing' procedure violated by additive Gaussian noise $\eta(t)$:

$$X_i = AS_i + \mu + \eta_i, \tag{4.23}$$

where X_i is the p-dimensional column vector of individual measurements at voxel location I, A is mixing matrix, S_i refers to the q-dimensional column vector of non-Gaussian source signals contained in the data, μ is the constant part and $\eta_i$is the Gaussian noise $\eta_i \sim N\,(0, \sigma^2 \Sigma_i)$ [14, 21].

ICA is not able to naturally generalize to a method suitable to make significant results about a group of subjects, in comparison with univariate methods. In contrast using for example GLM approach on a dataset, the regressors of interest will be specified by the scientist. This is the reason that inferences about group data arise naturally as all subjects in

the group use common regressors. From the other perspective with the implementation of ICA there is not the capability to clarify directly the way of making inferences about group data, because different subjects in the group have different time-courses and so the classification follows different way. For that reason, several ICA multi subject approaches have been recommended. There are five categories of these approaches, including single subject ICA, group ICA with temporal concatenation or spatial concatenation, pre-averaging and tensor ICA. Their distinction relies on the way the data has been grouped before the analysis, what kinds of output are available and the way of the processing of the statistical inference [74].

In the first category a large amount of approaches are included. The first step is the performance of a single-subject ICA and then follows the application of other approaches like self-organized clustering or spatial correlation of the components in order to combine the output into a group post hoc. Typically this category identifies unique spatial and temporal features, in contrast with the fact that the components are not certainly mixture similarly for each subject, because of the noise of the data. As for the other four approaches, those include the computation of ICA on the whole group dataset. After the examination of the temporal and spatial concatenation, the single performance of ICA is an advantage that has been referenced. Subsequently, it is able to be separated into subject-specific parts and because of that is quite simple to make a comparison between subject differences within a component. While temporal concatenation approach gives unique time courses for individual subjects and supposes same aggregate spatial maps; spatial concatenation approach provides unique spatial maps with common time-series. Even though there are differences between them in the organization of the data, there are proofs that temporal concatenation suits better on fMRI data. This conclusion arise from the fact that ICA time courses are greater concerning temporal variations in contrast with the variation in the spatial maps at conventional field strengths of 3T and below.

As a less computationally demanding approach is averaging the data before ICA. Of course allows the possession of a common time course and a common spatial map. Last but not least, recently great interest arises from the multidimensional or multi-way or N-way decompositions which represent the tensor decomposition approaches. However their effectiveness on group and multi-group fMRI data, have not been proven. According to a typical approach, a three-dimensional tensor used so as to assess a single spatial, temporal and subject-specific process for every component to reorganize the multidimensional structure of the data in the level of estimation. Definitely a preprocessing procedure is

necessary as a precaution of existence of different time courses within subjects. It is comprehensible that this works in resting-state MRI studies, where there is no synchronization of time courses within subjects; while in task-based experiments similar timing between subjects are existed [75].

Clustering Analysis

The second category of the data-driven analysis of functional connectivity is known as clustering analysis. The variety of the methods of this analysis has been applied in many functional MRI studies so as to investigate the activity patterns. Fuzzy clustering analysis, vector quantification, self-organizing maps and neural gas network are the methods that are included in the notion of clustering. The aim of these methods, and in general in clustering analysis, is to division the data into different clusters that rely on the intensity proximity of the time course. When time courses are close enough, they are considered as one cluster [65]. In the case of an fcMRI study the use of clustering analysis based on the intensity proximity is not able to give the desired detection of functional connectivity. For that reason instead of characterizing the distance by intensity proximity, they use the similarity within time courses as measurement of distance [76].

Fuzzy Clustering Analysis (FCA)

The term fuzzy clustering analysis means an allowing fuzzy partition of the dataset. The main concept of this method is the minimization of an objective function, which is defined, most of the times, as the total distance within all patterns and their cluster centers [65]:

$$J(M,C) = \sum_{i=1}^{i=N} \sum_{j=1}^{j=K} M_{ij}^{\varphi} D_{ij}^{2}, \tag{4.24}$$

where M_{ij} is a metric that measures the probability of a voxel i relates to j, D_{ij} is the distance within voxel i and the centroid C_j of a cluster j, N is the amount of voxels in brain, K is the number of the primary clusters and φ is a weighting component. The objective function is subject to [65]:

$$\sum_{j=1}^{j=K} M_{ij} = 1,\ i = 1,2,\dots,N \quad , \tag{4.25}$$

$$\sum_{i=1}^{i=N} M_{ij} = 1,\ j = 1,2,\dots,K; M_{ij} \in [0,1], \tag{4.26}$$

A solution that provided by Bezdec for the membership matrix M and clustering centroids C, is presenting below [79]:

$$M_{ij} = \frac{D_i^{\frac{2}{\varphi-1}}}{\sum_l^{l=K} D_{il}^{\frac{2}{\varphi-1}}}, \begin{cases} i = 1,2,\dots,N; \\ j = 1,2,\dots,K; \end{cases}, \tag{4.27}$$

$$C_j = \frac{\sum_{i=1}^{i=N} M_{ij}^{\varphi} X_i}{\sum_{i=1}^{i-N} M_{ij}^{\varphi}}, j = 1,2,\dots,K;, \tag{4.28}$$

where X_i is a vector which includes the coordinates of a cluster centroid i. After a repetitive process the membership matrix M and centroids can be acquired.

For fcMRI study has been proposed two distance metrics D_{cc}^1 and D_{cc}^2 that was based on Pearson's correlation coefficient $CC_{x,y}$ within two time courses $F_x(k)$ and $F_y(k)$. The two distance metrics are shown below:

$$D_{cc}^1 = \left(\frac{1-CC_{x,y}}{1+CC_{x,y}}\right)^{\beta}, \tag{4.29}$$

$$D_{cc}^2 = 2(1 - CC_{x,y}), \tag{4.30}$$

where $CC_{x,y}$ is the cross-correlation of $F_x(k)$ and $F_y(k)$ at lag zero. The two proposed distances describe the degree of correlation within two fMRI time courses. It is known that as functionally connected brain areas are those where their distance is under a certain threshold.

However a significant question concerns about the number of clusters that should be selected and generally which would be the typical number so as to investigate the connectivity. Different reports had been shown that a variety of numbers lead to a significant affection of the connectivity. This observation happens especially when the initially chosen clusters are less than the number of underlying function networks [77]. Several studies have been done so as to give an appropriate answer, just like *Golay et al.*[65] which suggested the use of a large number of clusters initially. This suggestion will lead to obtain a complete description of the clusters without acquisition of insignificant cluster centers. Despite these recommendations this issue is an intrinsic problem for FCA and might not be completely solved within the framework of FCA. Another issue concerns the distance metrics. *Golay et al.*[65] proposed that might be mixed with noises, such as human heart beat and respiration. These noises contribute to the distance metrics at a relatively high frequency domain (around 1 Hz), while the distance contributors that are of interest, are low

frequency oscillations (<0.1 Hz). At this frequency domain observed synchrony in cerebral blood flow and oxygenation between different brain regions [65].

Hierarchical Clustering Analysis

This analysis have been introduced by *Cordes et al.*[65] in order to give a solution to the aforementioned problems of the FCA, applying a new distance measurement based on frequency analysis. Hierarchical clustering analysis, in contrast with FCA, considers each voxel as one cluster at the initial stage and combines the close clusters according to a certain distance measurement. Applying different ways lead to measure the closeness of the clusters, which distinguishes single-linkage from complete-linkage and average-linkage clustering. Is characterized as an expensive computational technique and is thought to be more effective when applied to 3D human brain data.

The recently developed single-linkage HCA algorithm measures the distance combining correlation analysis along with frequency decomposition. The decomposition of Pearson's correlation coefficient within two time courses $F_x(k)$ and $F_y(k)$ can be expressed as below:

$$CC(x,y) = \frac{N\sum_f Re(\omega_f)Re(\varphi_f) + Im(\omega_f)Im(\varphi_f)}{S}$$

$$= \Sigma_f \frac{N(Re(\omega_f)Re(\varphi_f) + Im(\omega_f)Im(\varphi_f))}{S} = \Sigma_f CC_f(x,y), \quad (4.31)$$

where ω_f and φ_f are complex frequency components of $F_x(k)$ and $F_y(k)$ respectively, $Re(*)$ and $Im(*)$ describe the real and imaginary component of signal * and S is expressed as below:

$$S = \sqrt{\sum_{k=0}^{N-1} F_x^2(k) \sum_{k=0}^{N-1} F_y^2(k)}, \quad (4.32)$$

The distance $D(x,y)$ within the two time courses has been defined as below:

$$D(x,y) = 1 - \sum_{f=0}^{0.1\,Hz} CC_f(x,y), \quad (4.33)$$

In conclusion, a low-pass filter to Pearson's correlation coefficient applies this distance and then creates a reverse increase function to map the output into distance. From

the above filtering process, the extraction of the information from correlation coefficient happens. That information is the one that reflects synchrony in cerebral blood flow and oxygenation between different brain areas. Results from experiments, that have investigated both simulated data and human brain data, have proven the successful remove of the structured contaminations (respiratory or cardiac noises) [65].

Because of some disadvantages, such as the high complexity, sensitivity to outliers and the poor scaling, HCA has not been used in resting-state fMRI analysis just like other methods that have been used fluently. Something that should not been forgotten is the fully deterministic character of this approach and also the ability to express data as stratum through a hierarchical structure [78].

Model-based methods against Data-driven methods

A number of researches have investigated the issue about when the use of model-based or data-driven methods is most appropriate or elsewhere which of the two methods is more capable and with the best results. However, no one outperformed the other in an all around way. The choice or the preference of a model-based or data-driven method depends on the concept of the experiment. In general there is no reason to forget the knowledge and the experience from the one type of method and only use it in every situation. From the other hand is not reasonable to use CCA instead of ICA in order to detect extensive regions of correlated voxels [65].

4.2.4 Effective Connectivity

As it has been mentioned, the aim of functional connectivity methods is to find temporal correlations between spatially remote neurophysiological events. However a very important issue is whether the activity, from the neurophysiological events, has a causal influence in the activity of another brain region. Effective connectivity methods were created and applied for that reason, specifically to test causal models that concern the interactions within regions either at a synaptic or population level. Such models of causal processes are described in terms of directed graphs, just like in Figure 4.7. There is also another definition of them, named as path diagrams in parts of path analysis and SEM. More specifically the nodes (circles) in Figure 4.7 illustrate the brain areas while the edges (lines with arrows) illustrate the causal relations [66].

Aertsen and *Preibl* [80] proposed that “the term of effective connectivity should be understood as the experiment and time dependent, simplest possible circuit diagram that would replicate the observed timing relationships between the recorded neurons”. This

proposal leads to the conclusion that effective connectivity is dynamic, namely activity dependent, and also that it relies on a model of coupling or interactions [80].

While FC is an observable phenomenon that uses measures of statistical dependencies, such as correlations, coherence or transfer entropy so as to be quantified; effective connectivity wants to explain observed dependencies (functional connectivity) that corresponds to the parameter of a model. This is very important because in this way the analysis of effective connectivity can be reduced to model comparison, i.e. compare a model with and without a specific connection to infer its presence. In this sense, in the analysis of effective connectivity, every model corresponds to an alternative hypothesis about the cause of the observed data. In general the key aspect of effective connectivity is that it relies on the comparison or the optimization of the given models. In contrary, the functional connectivity is essentially descriptive [80].

It is obvious that effective and functional connectivity have differences in practice, even though their common use in the areas of neuroimaging and electrophysiology. For example, it could be an attractive approach of using temporal dynamics (dynamic FC) on the development of FC but it is restricted because of the lack of the causal explanation. This happens because of the fact that FC focuses on the definition of second-order data characteristics, preventing the interpretation of neurophysiological time-series under a mechanistic point. Thus is it important to divide the notions of functional and effective connectivity as it forms the character of the inferences coming from functional integration and solves different problems that result from intricate interrelationship within effective and functional connectivity [81].

Despite the fact that effective connectivity analysis is implemented to fMRI data, it is important to know that the underlying neuronal signals concern the causal interactions, which are the main focus of the study. Thus, the evaluation of the causal relations from variables, that derived from observed signals and also contain noise and systematic distortion of the signal, is required. But during the estimation, the recorded noise heads to identify causal relations that are not actually existent. Also another problem relies on the use of temporal information for the extraction of the causal relations. In that case the alterations of the hemodynamic response across brain areas are an additional purpose for fake causal association.

Except for the aforementioned information about the relations within the observed activity through brain areas, an interesting perspective is to study about the connectivity in inferences that showed up in a bigger amount of individuals rather than in a set of subjects.

Parameters such as age, genetics and experience e.g. maybe affect the connectivity pattern, even in the case of same causal structure. This leads scientists to the conclusion that the development of methods, at a population level, for effective connectivity evaluation is required. The combinational approach that consisted of data across individuals and also the model's estimation in the complex dataset is not recommended. That happened because the conclusion would be an observed pattern of independence and conditional independence interactions that did not correspond to any individual of the group. Thus a random effect analysis for the accurate and effective evaluation of connectivity across individuals is needed [66].

The diverse nature of the observed causal inferences of the effective connectivity and its various interpretations lead to the development and application of different methods of effective connectivity [82]. Two models are used to describe the effective connectivity, the linear and the non linear. Those models give details of the mathematical perspective about the way of connection of brain regions, and also of the neuroanatomy perspective about which regions are connected. Due to some previous knowledge, while the linear model provides sufficient results, the non linear model is that of more interest. Specifically, it is known that the brain responds at simple and well-organized experiments in a directed process, in contrast with the non linear neurophysiological interactions that make the linear model's efficiency controversial [22].

The most commonly used approaches for the study of effective connectivity with fMRI, are the structural equation modeling (SEM), Granger causality analysis, dynamic causal modelling (DCM), graphical causal modeling, dynamic Bayesian networks, switching linear dynamic systems (sLDSf) and psychophysiological interactions (PPI). Those have been applied in a variety of clinical studies and will be analyzed below [24].

Structural Equation Modeling (SEM)

The first method that will be described, for the analysis of effective connectivity is the structural equation modeling. SEM is a method in which hypotheses about causal inferences within variables can be examined. Elsewhere defines a set of equations with supporting assumptions of the system being analyzed, and the parameters are adapted from statistical observations [66, 83].

SEM belongs to the category of linear statistical technique which illustrates steady-state connection within brain areas using the covariance structure of the data, while the temporal dynamics of the fMRI time-series are not of concern. It is worth noting that is an

ideal method for the estimation of effective connectivity on fMRI data [84]. The path coefficients for every link are estimated by the changes in activity of an area that has been affected by a given unit change. Also they indicate the average influence throughout the measure of the time interval.

From the mathematical perspective, a SEM model can be expressed as:

$$Y = MY + \varepsilon, \tag{4.34}$$

where Y is the data matrix, M is a path coefficients matrix and ε is independent and identically distributed Gaussian noise.

The previous equation can be expressed and in another form as below:

$$Y = (I - M)^{-1}\varepsilon, \tag{4.35}$$

where I is the identify matrix. So as to acquire the result for the unknown coefficients that are included in M, the empirical covariance matrix Y is used [85].

As well as the modeling connectivity within regions, SEM can also have extraneous variables along with error terms for the observed variables. Therefore can include *latent* variables which are hypothesized but unobserved variables, that are associated (in some way) with the observed variables.

SEM, instead of comparing the actual and predicted data, achieves the estimation of the parameters by minimizing the difference within the actual and predicted covariance between the variables. The estimated parameters are called as path coefficients and illustrate how a change of a variable can lead to a change in another variable, while all other variables are staying constant. After the estimation level, the use of statistical test is required so as to see the fitting of the observed data [66]. This technique is advantageous besides others because of the fast and robust computations and also due to the implementation on large scale simulations applying neuroimaging data. Also because of the early development, there is access in many software packages and algorithmic variations. Notably this technique can be used on PET, fMRI and also EEG data and because of that it suits in cognitive networks including those arbitrating motor control, visual perception, language function, associative learning and pain processing [86].

Even though the important use of it, SEM has some complications when it is applying on fMRI data. Firstly SEM provides a reduction of temporal information when there is the assumption of normally distributed and independent from sample to sample data. That fact leads to the creation of the same path coefficient as the original data on the permuted one, since the assumed independence is interfered with the analysis of a single subject [85]. Disadvantages such as the primary estimation of the connection directions, the incapability of utilizing fully reciprocal models and the high dependency of the sample size on the absolute evaluation of the model, are also involved [87].

Granger Causality Mapping (GCM)

In general Granger causality is a method that has been advanced in order to model causality by testing the time relation within variables, for the analysis of economic data. Its base is on the notion that causes always antedate effects in time [66]. Also its use in a whole-brain manner is named as *Granger causality mapping (GCM),* through which the comparison between the time course in a seed voxel and all other voxels in the brain is tested, and the Granger causality for every voxel is computed. GCM depends on the idea of Granger causality in order to define the existence and direction of influence from information in the data [88].

The multivariate autoregressive (MAR) model can describe how Granger causality functions, so as to observe interactions among brain areas. This happens by reporting a causal and dynamic system of linear interaction driven by stochastic innovations [87, 89]. Therefore because of the use of past values of one brain area so as to predict the current values of another area, a priori specification of a structural model is not needed [85].

The theory behind this analysis is based on the use of a vector autoregressive (VAR) modeling of fMRI time series in the concept of Granger causality. With the hypothesis that $x[n]$ and $y[n]$ are the measured time courses of two brain areas (voxels), Granger causality specifies the quantity of the usefulness of unique information in one of the time series in predicting values of the other. In the case that incorporating past values of *x* improves the prediction of the current value of y then x "Granger causes" y. In this way, temporal precedence is applied for the identification of the direction of causality from the information in the data. So as to achieve the computation of Granger causality maps (GCMs), the temporal precedence is used, that identifies voxels that are sources or targets of directed influence for any region of interest. Therefore the analysis does not need the specification of a directed graph model and is investigative in nature.

From the mathematical perspective, the VAR process of order p can be applied so as to model the discrete zero-mean vector time series $x[n] = (x_1[n], \dots, x_M[n])^T$ can be described as below:

$$x[n] = -\sum_{i=1}^{p} A[i]x[n-i] + u[n], \tag{4.36}$$

where $u[n]$ is (multivariate) white noise. As autoregression (AR) coefficients are named the matrices $A[i]$ because they regress $x[n]$ onto its own past. As it has already been mentioned, the VAR model can be characterised as a linear prediction model. Thus the current value of a component $x_i[n]$ is predicted by a linear combination of its own past values and the past values of the other components. With this it is understandable the matter of importance of the use of VAR model in the quantification of Granger causality within components.

It is also important to describe the use of temporal precedence in Granger causality approach. More specifically, if $x[n]$ and $y[n]$ are given time courses, it is easy to identify independently influence from the two directions with suitable models. The proposal measure of linear dependence $F_{x,y}$ within $x[n]$ and $y[n]$ which applies Granger causality in terms of vector autoregressive models, is shown below:

$$F_{x,y} = F_{x\to y} + F_{y\to x} + F_{x.y}, \tag{4.37}$$

where $F_{x,y}$ will evaluate to zero if there is no value at a given instant that can be described by a linear model that contains all the values of the other. Therefore the two directed components $(F_{x\to y}, F_{y\to x})$ take advantage of the time so as to decide on the direction of influence. However, the total linear dependence does not depend on only these two components, but also at the undirected instantaneous influence $F_{x\cdot y}$. Basically the last component quantifies the improvement in the prediction of the current value x by including the current value of y, and inversely, in a linear model that already includes the past values of x and y. It is understandable that $F_{x\cdot y}$ does not contain information about the direction but illustrates residual correlations in the data. Basically, the directed influence within x and y can demonstrate from the nonzero values of $F_{x\cdot y}$ [88].

While Granger causality and especially GCM is an attractive approach for the model of effective connectivity without the requirement of the specification of an anatomical network, in contrast with SEM and DCM, when applying in fMRI data become problematic

due to the temporal features of them. The first disadvantage that will be mentioned concerns the slice timing, since Granger causality depends on the relative activity of regions in time. Potentially, the alterations in relative timing of acquisition through slices are probably much larger than the relative timing effects caused by neural processing. Secondly, the assumption of Granger causality about the similar timing features of the hemodynamic response across brain is false. Actually, there are many researches that show that generation of accurate causal influence by Granger causality on fMRI time series does not exist, against the use of electrophysiological and fMRI recordings. Only in the case that time series are deconvolved, accurate outcomes can be acquired. The third disadvantage concerns the problem about sampling the data at a rate slower than the causal process. A possible solution might be the acquirement of residuals from a time series analysis and after that the use of graphical causal model. At last, the multivariate extension (when required) must be done carefully because the results might be unstable due to the involvement of a large amount of regions [66, 87].

Dynamic Causal Modeling (DCM)

Dynamic causal modeling is a powerful tool that has been applied in a lot of studies. It can be both used in fMRI and EEG/MEG studies with the generation of mutually confirmative outcomes that might be more robust and show deeper insights into cortical physiology than separately [90]. In general DCM addresses causal interactions within distinct predefined brain areas with the construction and the test of realistic models of the interacting neuronal areas. DCM estimates the coupling within brain areas and tests how the changes of the experimental context affect the coupling. Basically, in a neuronal model of interacting cortical regions DCM adds a forward model, which explains the transformation of the neuronal or synaptic activity into a signal that can be measured by fMRI (BOLD) or EEG/MEG. Particularly, a hemodynamic response model is contained in the case of fMRI so as to explain the transformation [58]. For an fMRI experiment DCM is composed of two sections. The first concerns about a model of the neurodynamics (i.e. the underlying neuroactivity) and the second section concerns about a model of the hemodynamics (i.e. the blood flow response induced by the neurodynamics).

The neurodynamic model in DCM is described by the following equation:

$$\frac{dz}{dt} = \dot{z}_t = \left(A + \sum_{J=1}^{\cdot J} u_t(J) B^{(J)}\right) z_t + C u_t, \qquad (4.38)$$

where t is the time, $\dot{z}_t$ is the derivative of neuronal activity in time, $u_t(j)$ is the jth of J extrinsic inputs at time t and A, $B^{(j)}$and C are connectivity matrices. More specifically, the matrix A describes the intrinsic connections, which specifies which regions are connected to one another and also the type of the connections (unidirectional or bidirectional). The input connections are described by the matrix C, which specifies which regions are influenced by which extrinsic inputs $u_t(j)$. The $B^{(j)}$ matrix describes the modulatory connections, which specify the alterations in intrinsic connections in A by each of the $u_t(j)$ inputs.

From the other hand, the hemodynamic model in DCM is alike to the balloon-windkessel model which aims to model the relation within neuronal activity and alteration in blood volume, blood flow and blood oxygenation that result in the measured fMRI signal [66]. The Balloon model is composed by equations that define the association within four hemodynamic state variables using five parameters.

Due to the involvement of the interaction of two linear effects, DCM is usually mentioned as a bilinear model. However the use of DCM has been extended to nonlinear cases in which connections are modulated by a third region [91].

As it is already mentioned, the combination of hemodynamic and neurodynamic models leads to the full forward model that describes the DCM. The following equation presents the full model where θ is a joint parameter vector:

$$\dot{x} = F(x, u, \theta), \tag{4.39}$$

$$y = \lambda(x). \tag{4.40}$$

Supposing a set of given parameters θ and inputs u, the predicted BOLD response $h\,(u, \theta)$ outcomes from the integration of the joint state equation and its pass across the output nonlinearity λ. The observation model that contains observation error e and confounding effects X can be expressed as [99]:

$$y = h(u, \theta) + X\beta + e. \tag{4.41}$$

Just like the previous methods that have been referenced, DCM has some important limitations. Firstly, it is known that the validity of the outcomes relies on the anatomical models that are specified and the regions that are used for data extraction. A possible solution might be the use of graphical search techniques so as to construct a set of plausible candidate models and then applying DCM to examine particular assumptions about those models. Secondly, the current implementation of DCM is restricted because of the models

that have relatively few regions; MATLAB memory limitations are responsible for this disadvantage. This might be relieved by the use of 64-bit systems. Furthermore it is a high computational cost technique with the weakness to estimate effective connectivity in more than six areas. Finally, in cases where there are correlations within different parameter values, the estimation of the parameter can be relatively unreliable, while DCM is highly reliable in model selection [66].

Spectral Dynamic Causal Modelling (spDCM)

The extension of DCM named as spectral DCM aims to model intrinsic dynamics on resting-state fMRI data, in order to define effective connectivity among populations of coupling neurons which contains the observed functional connectivity in the frequency domain [99]. Spectral DCM, typically, provides a constrained inversion of the stochastic model with the parameterization of the spectral density neuronal fluctuations. Through this process it is possible to compare parameters that encode neuronal fluctuations among groups.

The main notion of spectral DCM is to add a stochastic parameter to model endogenous neuronal fluctuations in the ordinary differential equations that were used in the standard DCM. In this way, the equations of motion become stochastic and the stochastic model for the resting-state fMRI time-series includes the Langevin form of evolution equation *(ż)* and the observation equation *(y)*. It is worth to be mentioned that the observation equation illustrates a static non-linear mapping from the hidden physiological states to the observed BOLD activity. The two types of equation that are mentioned are expressed below:

$$\dot{z} = f(z, u, \theta) + v\,, \tag{4.42}$$

$$y = h(z, u, \varphi) + e\,, \tag{4.43}$$

where $\dot{z}$ is the rate in change of the neural states z , θ and φ are unknown parameters of the evolution and observation equation respectively, v *i*s the stochastic process (state noise) which models the random neuronal fluctuations concerning the resting-state activity and u is the exogenous inputs (that are not presence in resting-state condition). In a resting-state experiment, the Langevin equation will be expressed as below:

$$\dot{z} = Az + Cu + u\,, \tag{4.44}$$

where A is the Jacobian, that describes the effective connectivity close to its stationary point when fluctuations v are not presented [99].

Spectral DCM estimates the time-invariant parameters of their cross spectra. Efficiently this is performed with the replacement of the original time series with their second-order statistics (cross spectra), which means that instead of estimating time-varying hidden states, covariance has been estimated. Consequently, the definition of covariance of the random fluctuations is required. Thus the observation noise can be expressed as:

$$g_v(\omega, \theta) = \alpha_v \ \omega^{-\beta v}, \tag{4.45}$$

$$g_e(\omega, \theta) = \alpha_e \ \omega^{-\beta e}, \tag{4.46}$$

where $\{\alpha, \beta\} \subset \theta$ are the parameters that controls the amplitudes and exponents of the spectral density of the neural fluctuations [55].

While the three aforementioned methods, SEM, DCM, Granger Causality, are the most used and most qualified in the study of effective connectivity in fMRI data; there are some other approaches that they are not that common. Those are described below briefly.

Graphical Causal Models

For the characterization of the causal structure of a given dataset, Graphical causal models have been introduced. The general concept of that approach is that the causal relations in a graph have consequences concerning the conditional independence relations within different sets of variables in the graph. With the term conditional independence is meant that two variables are independent only when they conditioned on some other variables. Therefore this idea could be described from the point of regression. According to that, when two variables are correlated via a third variable, means that is equivalent to include it as a covariate in the statistical model. Thus the third variable functions as regressor that will remove the correlation and still let the other variables independent.

Over the past twenty years, a set of methods that have been developed in the field of machine learning has made available to investigate efficiently such graphical structures. There are a lot of search algorithms for graph investigation, where the most of them are implemented in TETRAD software. After the identification of the optimal graphs applying these graph search approaches, then they can be used as basis on experiments with other effective connectivity approaches (SEM, DCM) [66].

The combination of the data across multiple subjects is a very challenging stage in a method like this. Although there are obvious solutions, these have the ability to obtain false results. As it is mentioned, the independence relations within variables in a given dataset may not reveal the relations that present for any of the individuals. Ramsey et al. introduced a method named IMaGES in order to solve this problem. This method searches across multiple subjects for the best fitting graph structure, focusing at each subject in each step of the search and then combining the fit across subjects, so as to find the model that suits beat across the entire group [92].

Dynamic Bayesian Models

In order to address dynamic systems modeling, another approach was introduced named as Dynamic Bayesian Models. This approach is a temporal extension of Bayesian networks and is included in the group of graphical models [93, 94]. Dynamic Bayesian networks are based on a multi-dimensional expression of a random process, in contrast with Bayesian networks which is characterized by a cumulative probability distribution in a set of random variables that are independent of time [93]. Due to its dynamic features, it has been used in studies so as to illustrates the alterations within healthy and control individuals. Also the application of static Bayesian networks could lead to examine problems such as in genetics, speech recognition, identification and target tracking, probabilistic expert systems and medical diagnostic systems. Recently dynamic Bayesian models have been applied to investigate the genomic regulation [94, 95].

Switching Linear Dynamic System (sLDSf)

In fMRI, Switching Linear Dynamic system provides infinite variability over time in the parameter values of connectivity and also instantaneous connectivity by probabilistically combining a small amount of static models regimes [96]. The observation equations that are used in sLDSf and are based on the linear convolution model are presented below:

$$y_t = \beta \Phi z_t + D v_t + \zeta_t, \zeta \sim N(0, R), \tag{4.47}$$

$$z_t = \left[x_t, x_{t-\tau}, x_{t-2\tau}, x_{t-3\tau}, \dots, x_{t-(h-1)\tau}\right], \tag{4.48}$$

where the variable z_t includes h errorless lagged copies of the signals x from $x_t - (h-1)\tau$ to x_t .

While the observation equation y_t describes the instantaneous linear function of z_t any additional observation level input v_t and noise ζ_t with a diagonal covariance matrix $R^{ij} = 0 \, for \, i \neq j$. The priori known set of basic vectors is the matrix Φ, which connect the possible variability in the hemodynamic impulse response function (hIRF), similar to a canonical hemodynamic response and its derivatives with respect to time and dispersion. Regionally specific weights for these bases are included in matrix β so as to generate a unique hIRF $\beta^i \Phi$. In this way the linear output $\beta^i \Phi \, Z_t^i$ is able to convolve every signal with a regionally specific hemodynamic response. In order to achieve the estimation, the sLDSf output equations with three basic vectors need three additional parameters per region [97].

Psychophysiological Interactions (PPI)

The last approach of this category that will be discussed is the Psychophysiological interactions and the related technique of psychophysiologocal interactions (ΦPI). That approach is based on extensions to statistical models of factorial designs. Both of them can be considered as models of "contribution". Another important issue is that PPIs are on the border within functional (FC) and effective (EC) connectivity. It is already mentioned that FC is defined as the temporal correlation within spatially remote neurophysiological events, are typically model-free and do not specify a direction of influence [98]. On the other hand, PPIs are relied on regression models and also the direction of influence is based on the model selection. As for EC, is defined as the affect that has one neural system to another. Thus, even if PPIs are more related to EC models, because of their simplicity they are very restricted models of EC [99]. As observed in every other approach, PPI presents some potential problems due to its simplicity. For example PPI hypothesizes that the fit of hemodynamic model is precise. Thus in the case of misspecification of the model, this could result to correlation that reflect activation-induced effects instead of reflecting functional connectivity [66].

4.2.5 Network Analysis and Graph Theory

In neuroscience, the aim of graph theory is to establish mathematical models of complex network functions within the human brain. The main characteristics of these networks are the connections and associations within different regions and subregions of the brain, where the combination of their dynamics form a larger single network [60]. The explanation of the brain networks can be achieved in micro-scale, meso-scale and last in macro-scale or large-scale. But most of the studies use large-scale networks because of some technical restrictions and computational requirements [100].

In general the approach of graph theory is based on the study of nodes and edges. Their relation can be described as $G = (V, E)$, where V characterizes the nodes that are connected with edges E, which describes the interaction within nodes [101]. Due to the term of directionality, the graphs usually divided into categories. The main categories are the directed or undirected graphs, while another classification is the weighted or unweighted graphs, as shown in Figure 4.7. As unweighted graph is characterized, when an equal weight of 1 in every edge of the graph, while as weighted when there are different strengths at every edge. In the cases of undirected and unweighted graphs $G = (V, E)$, the connectivity patterns could be represented by a $V \times V$ symmetric square matrix, the adjacency matrix A. When there is an edge within node i and j, the entry of α_{ij}, that ranges between $1 - V$, is 1 and it takes the value of 0 in the reverse situation [100].

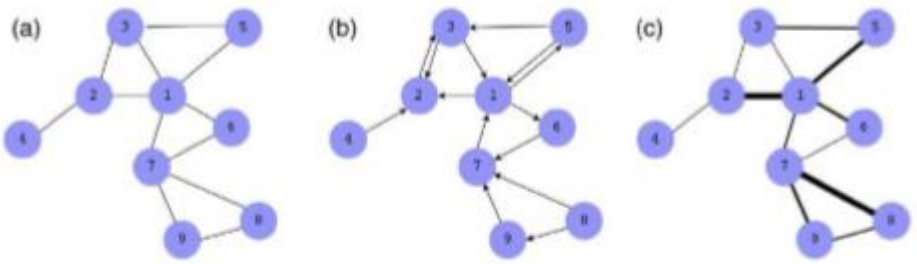

Figure 4. 7: Different types of graphs: (a) undirected, (b) directed, (c) weighted networks [106].

In brain functional connectivity analysis, the application of graph theory has lead to answer a variety of issues that are of interest using information from different graph parameters. Such parameters are the average path length, degree of node, clustering coefficient, level of modularity and measures of centrality. More specifically the path length is graph theoretical metrics that represents the level of global communication efficiency of the given network. The shortest path length indicates the smallest number of edges that are needed to attach all the nodes together. Therefore, the characteristic path length of node i demonstrates the proximity of node i to all the other nodes in the network. The simplest measurement of all these is the degree of node. Typically this measurement achieves the quantification of the total number of connections of the node. An unavoidable role in the flow of information plays the node with the higher degree, for a particular network. The clustering coefficient parameter represents the local connectedness of the

graph. Also is the ratio within the number of connections between direct neighbors of node i and the maximum number of possible connections between the neighbors of node i [100].

The notion of modularity is based on the ability of the networks to create couples on modular or community structure. As modules, are described a set of nodes with thick connections among them in contrast with the connections along the whole brain network which are weak. The performance of the modularity can be achieved through different algorithms, which give the opportunity to comprehend the anatomical or functional components [100].

Graph metrics such as global efficiency and average path length point out the integration of the brain networks. As it is already mentioned, global efficiency tests the ability of a brain network to spread information on a global level, while the average path length represents the shortest number of edges that are able to connect two nodes in a network. Consequently the segregation of the networks can be described through the terms of local efficiency, clustering coefficient and centrality. Thus local efficiency signifies the information flow in a local network (subpart of a whole brain network), while clustering coefficient indicates which nodes tend to create clusters. At last the parameter of centrality points out the importance of a node and tests whether the particular node operates as a central or leading role in the spread of the information to other nodes in the network [60].

Another notion that is of interest is the hierarchical networks. This network is composed of hubs that are connected to nodes, which from a different sight are not connected to each other. Basically this means that the value of the parameter clustering coefficient is lower in the case where the degree is larger. The benefits that are observed are the better top-down relations within the nodes and minimize of the wiring cost. The weak part concerns of the hubs attacking [102].

It has to be mentioned that as small world network is characterized the one with high value of local and global efficiency and a small characteristic path length [103, 104]. On the other hand a large scale network, according to *Supekar et al.*[60], is characterized the one that has short range of connectivity and more supremacy from the part of long range functional connectivity [60].

While the main focus of the seed-based analysis is the strength of correlation within the regions of interest, graph theory examines and measures the topological properties of the regions of interest within the whole brain or that network that is related to a particular function. The keys for the representation of brain networks are the integration and segregation due to the brain regions that works in such a manner. So anyone can

understand the significance of graph theory but there are some limitations that have to be mentioned. Primarily the human brain consists of neurons and physical elements that have differences and so the estimation of the functional networks is very complicated. Applying the graph theory, which is depends on voxels or anatomically –or functionally-defined ROIs, it is understandable that it is not quite easy to acquire results. At last even if the selected nodes are the appropriate (no many differences), the complication of the brain networks and the unknown pathways make this impossible [105].

Taking advantage of the classical steps of the preprocessing, that were described in this chapter, with a combination of statistical methods we tried to extract brain connectivity (functional and effective) from our data. We demonstrate three different studies, where the two of them focus on extracting functional connectivity and the other one focus on extracting effective connectivity. More details about the exact steps that we follow and the results that we take are shown in Chapter 5.

Chapter 5: Results

5.1 Imaging protocol

The fMRI data that was used in this thesis was acquired from the OpenNeuro database[1] [108]. MRI was performed on a 1.5 T MR scanner system (Magnetom Avanto, software version Syngo MR B17, Siemens, Erlangen-Germany) equipped with a 12-element matrix radiofrequency head coil and SQ-engine gradients. All subjects underwent high resolution 3D T1-weighted imaging and resting-state fMRI (rsfMRI), the latter with simultaneously cardiorespiratory monitoring. T1-weighted MR images were acquired with an axial high resolution 3D sequence (Magnetization Prepared Rapid Gradient Echo, MPRAGE) with repetition time (TR) = 1900ms, echo time (TE) = 3.44ms, inversion time (TI) = 1100ms, flip angle = 15˚, slice thickness = 0.86mm, field of view (FOV) = 220mm x 220mm, matrix size = 256 x 256, number of excitations (NEX) = 2. A fluid attenuated inversion recovery (FLAIR) sequence (TR = 9000ms, TE = 88ms, TI = 2500ms, slice thickness = 3mm, FOV = 172.5mm x 230mm, matrix size = 154 x 256, turbo factor = 16, NEX = 1) was also obtained in the axial plane. For the rsfMRI experiments, they used a T2*- weighted echo-planar imaging (EPI)

[1] https://openneuro.org/datasets/ds001354/versions/1.0.0

sequence (TR = 2130ms, TE = 40ms, flip angle = 90˚, slice thickness = 5mm, FOV = 256mm x 256mm, matrix size 64 x 64; number of slices = 32; interleaved slice acquisition) exploiting the blood-oxygen-level-dependent (BOLD) effect. Three hundred volumes were acquired for a total acquisition time of about 8 minutes and 10 seconds. The slices were oriented along and parallel to the bi-commissural plane and covered the entire brain. During rsfMRI acquisition the subjects were instructed to lie still with their eyes closed and not to think of anything particular. Cushions were used to minimize head motion during the scan.

5.2 Subjects

In this thesis fourteen (3 women and 11 men, age 63.7±11.1 years, mean ± standard deviation) patients with de-novo PD and fourteen age and gender-matched healthy subjects (controls) (3 women and 11 men, age 64.7±9.6 years, mean ± SD), with no history of neurological disease and normal neurological examination, take part. The functional images received from MRI are transformed into image *.img and image *.hdr files with the use of MATLAB code, while the structural images are transformed into image *.img and image *.hdr with the MRIcro application. After the transformation every subject has 600 functional images (300 images in *.img format and the corresponding 300 images in *.hdr format) and 2 structural images (1 image in *.img and 1 image in *.hdr).

The following studies have been performed.

5.3 Study 1: Functional connectivity using seed-based analysis

The main aim of the first study of this thesis is to extract functional connectivity measures using a seed-to-voxel analysis. This analysis calculates the temporal correlation between brain activity of a selected region and all other regions applying a General Linear Model approach. For that reason, CONN functional connectivity toolbox v17[2]is utilized.

The preprocessing is the first step that has to be done in order to start the analysis. The preprocessing pipeline for volume-based analysis, that is used, includes the following stages: (1) functional realignment and unwarping (subject motion estimation and correction), (2) functional center to (0, 0, 0) coordinates (translation), (3) functional slice timing correction, (4) functional outlier detection (ART- based identification of outlier scans for scrubbing), (5) functional direct segmentation and normalization (simultaneous GM/WM/CSF segmentation and MNI normalization), (6) structural center to (0, 0, 0) coordinates (translation), (7) structural segmentation and normalization (simultaneous GM/WM/CSF segmentation and MNI normalization), (8) functional smoothing (spatial

[2] https://www.nitrc.org/projects/conn

convolution with Gaussian kernel). After the preprocessing step, a denoising clean up step is followed so as to remove physiological subject motion and other confounding effects from BOLD signal.

The seeds that are selected in seed-to-voxel analysis and ROI-to-ROI analysis are different brain networks such as Sensorimotor, Salience and Default Mode Network (DMN). Although all these networks are affected by Parkinson's disease, the DMN is chosen for functional connectivity analysis since it is used more often in studies. DMN includes Medial Prefrontal Cortex (MPFC), right and left Lateral Parietal Cortex (LPC) and Posterior Cingulate Cortex (PCC).

Results

The following tables (Table 5.1 and Table 5.2) present the results of the coordinates of the maximum voxel, the size of the cluster, the associated brain areas and their figures from the seed-to-voxel analysis. These tables concern the results from the analysis using the medial prefrontal cortex as seed for both of groups (PD and controls). The tables for the other three regions of DMN are stored in Appendix (Table 7.1-Table 7.6).

Table 5. 1: Brain areas that are functionally connected with the medial prefrontal cortex (MPFC) concerning PD group.

MNI coordinates of maximum voxel	*Cluster Size (voxels)*	*Brain areas*	*Size p-FWE*	*Size p-FDR*	*Size p-unc*	*Peak p-FWE*	*Peak p-unc*
[06, 50, -04]	14435	Orbital Medial Frontal Gyrus Right	0.000000	0.000000	0.000000	0.000000	0.000000
[-08, -50, 30]	5344	Posterior Cingulum Left	0.000000	0.000000	0.000000	0.000032	0.000000
[-42, -64, 32]	1533	Angular Gyrus Left	0.000000	0.000000	0.000000	0.000318	0.000000
[64, -18, -16]	1424	Middle Temporal Gyrus Right	0.000000	0.000000	0.000000	0.021562	0.000000
[48 -58, 26]	1144	Angular Gyrus Right	0.000000	0.000000	0.000000	0.006738	0.000000
[-62, -20, -12]	770	Middle Temporal Gyrus Left	0.000000	0.000000	0.000000	0.263724	0.000002
[48, -34, 62]	748	Postcentral Gyrus Right	0.000000	0.000000	0.000000	0.832015	0.000019
[-44, -40, 58]	684	Postcentral Gyrus Left	0.000000	0.000000	0.000000	0.767841	0.000015
[-26, 16, -18]	269	Insula Left	0.000573	0.000162	0.000022	0.078735	0.000000
[10, -50, -40]	244	Cerebellum 9 Right	0.001125	0.000286	0.000043	0.757389	0.000014
[-02, -16, 06]	213	Thalamus Left	0.002683	0.000620	0.000103	0.420169	0.000004
[02, 06, 72]	202	Supplementary Motor Area Right	0.003689	0.000782	0.000142	0.858180	0.000022
[-34, -74, -40]	156	Cerebellum Crus2 Left	0.014904	0.002932	0.000578	0.394032	0.000003
[20, -74, -50]	149	Cerebellum 8 Right	0.018625	0.003409	0.000723	0.698248	0.000011
[20, -80, -36]	107	Cerebellum Crus2 Right	0.075735	0.013328	0.003029	0.905015	0.000029
[-04, 10, 52]	91	Supplementary	0.132889	0.022623	0.005484	0.505882	0.000005

		Motor Area Left					
[28, -26, -12]	87	ParaHippocampal Gyrus Right	0.153188	0.024829	0.006395	0.900756	0.000028

Table 5. 2: Brain areas that are functionally connected with the Medial Prefrontal Cortex (MPFC) concerning controls group.

MNI coordinates of maximum voxel	***Cluster Size (voxels)***	***Brain areas***	***Size p-FWE***	***Size p-FDR***	***Size p-unc***	***Peak p-FWE***	***Peak p-unc***
[08, 50, -08]	13555	Orbital Medial Frontal Gyrus Right	0.000000	0.000000	0.000000	0.000000	0.000000
[-10, -54, 24]	5195	Precuneus Left	0.000000	0.000000	0.000000	0.000303	0.000000
[22,-38, 72]	2442	Postcentral Gyrus Right	0.000000	0.000000	0.000000	0.000335	0.000000
[50, -66, 32]	1902	Angular Gyrus Right	0.000000	0.000000	0.000000	0.002801	0.000000
[-52, -66, 26]	1501	Angular Gyrus Left	0.000000	0.000000	0.000000	0.001790	0.000000
[-62, -34, 40]	1406	Supramarginal Gyrus Left	0.000000	0.000000	0.000000	0.010132	0.000000
[60, -02, -24]	1119	Middle Temporal Gyrus Right	0.000000	0.000000	0.000000	0.039505	0.000000
[-54, -10, -16]	748	Middle Temporal Gyrus Left	0.000000	0.000000	0.000000	0.150799	0.000001
[-04, -58, -40]	725	Vermis 9	0.000000	0.000000	0.000000	0.001772	0.000000
[08 ,-86, -40]	599	Cerebellum Crus2 Right	0.000000	0.000000	0.000000	0.215302	0.000001
[-18, -02, -12]	380	Amygdala Left	0.000033	0.000007	0.000001	0.751830	0.000014
[-50, -50, -18]	272	Inferior Temporal Gyrus Left	0.000502	0.000096	0.000019	0.524980	0.000006
[-46, 14, -44]	153	Inferior Temporal Gyrus Left	0.015861	0.002816	0.000610	0.330386	0.000002
[00, 14, 46]	118	Supplementary Motor Area Left	0.050551	0.008484	0.001979	0.603778	0.000008
[-42, 38, 20]	116	Middle Frontal Gyrus Left	0.054143	0.008497	0.002124	0.901128	0.000028
[24, -64, 50]	90	Superior Parietal Lobule Right	0.135044	0.020761	0.005536	0.997806	0.000112
[-16, -86, -40]	79	Cerebellum Crus2 Left	0.200356	0.030114	0.008532	0.987653	0.000069
[34, 30, -18]	77	Orbital Inferior Frontal Gyrus Right	0.215251	0.030832	0.009250	0.752090	0.000014

In order to have a visual aspect of the results that will be helpful to understand them, ROI-to-ROI results carried out. The specific type of results display functional connectivity results but at a different resolution. Instead of demonstrating a whole brain

connectivity map, as it is common, ROI-to-ROI results present only ROIs that are significantly correlated with other ROIs. As shown in Figure 5.1 and Figure 5.2 the red lines indicate which ROIs are significantly correlated with a selected seed, while the blue lines indicate significantly negative correlations.

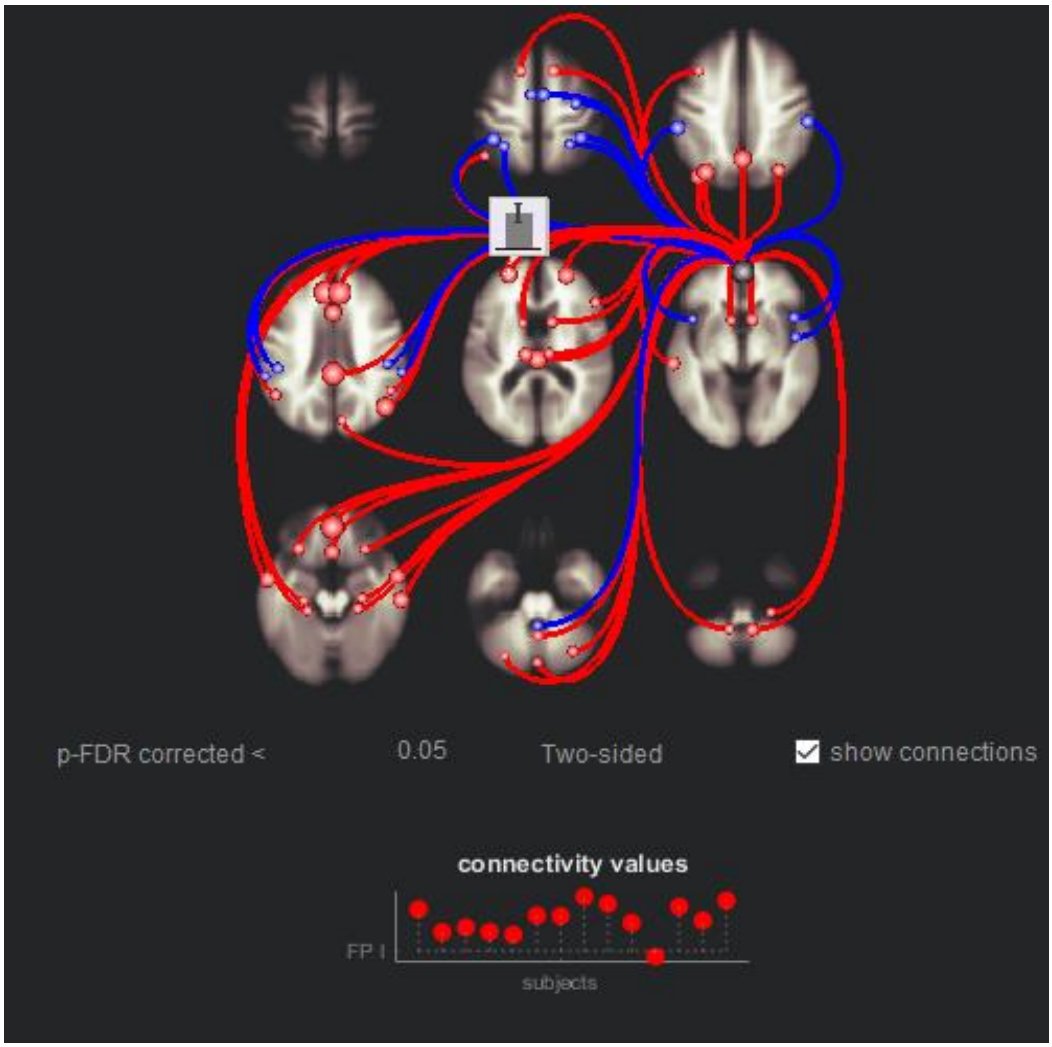

Figure 5. 1: Functional connectivity results between ROIs of the MPFC for PD group.

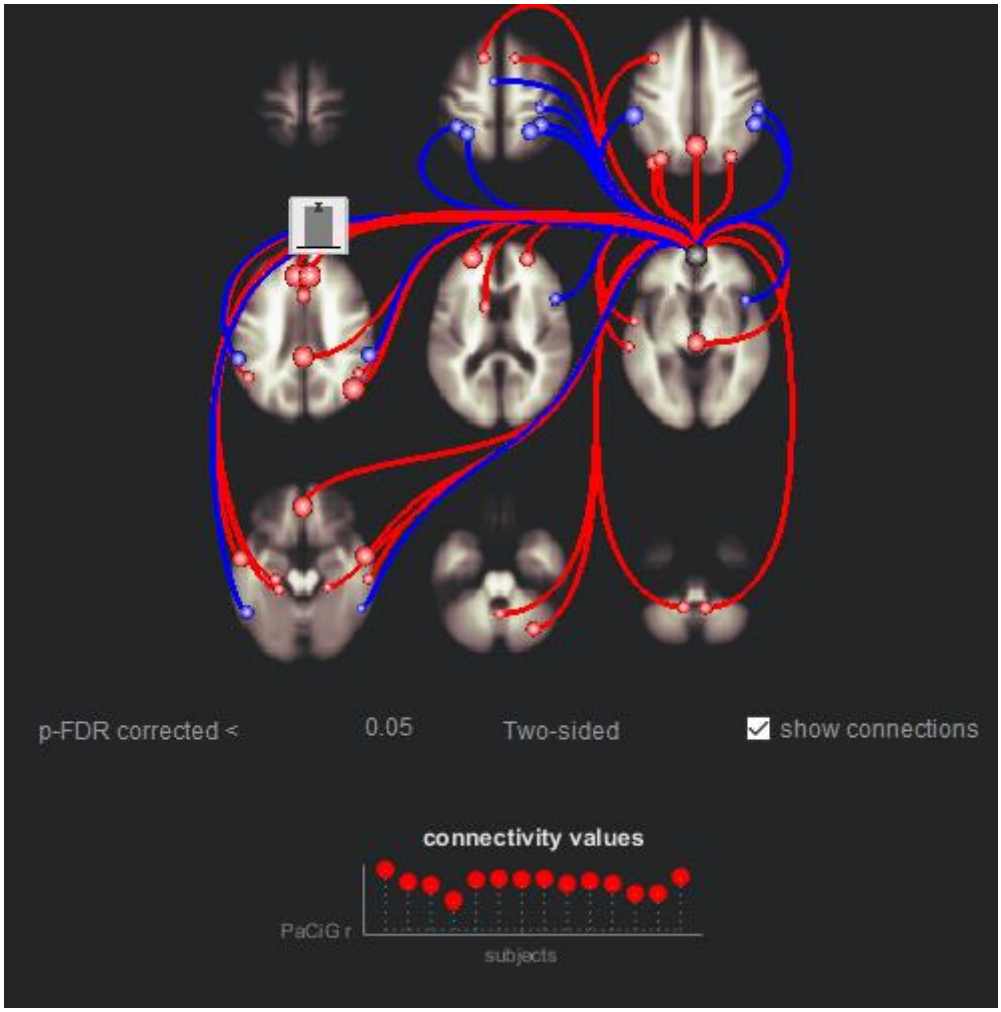

Figure 5. 2: Functional connectivity results between ROIs of the MPFC for the controls group.

Also, ROI-to-ROI results allow anyone to see in more detail how nodes of certain networks are correlated with other nodes in the brain. The following figures (Figure 5.3, Figure 5.4) demonstrate the more detailed images which are known as connectograms. Again the red lines show significant positive correlation between the nodes whereas the blue lines show significant negative correlation between them.

More specifically, the PD group shows greater positive correlation between MPFC and PCC and LPC regions, due to the fact that these areas belong to the same network, while the negative correlation is observed within MPFC and Dorsolateral Attention Network. It is important to be mentioned that significant correlation is observed within MPFC and Salience Network. As for controls group greater positive correlation is observed within MPFC and LP while negative correlation is noticed between MPFC and Dorsolateral Attention and Salience Networks.

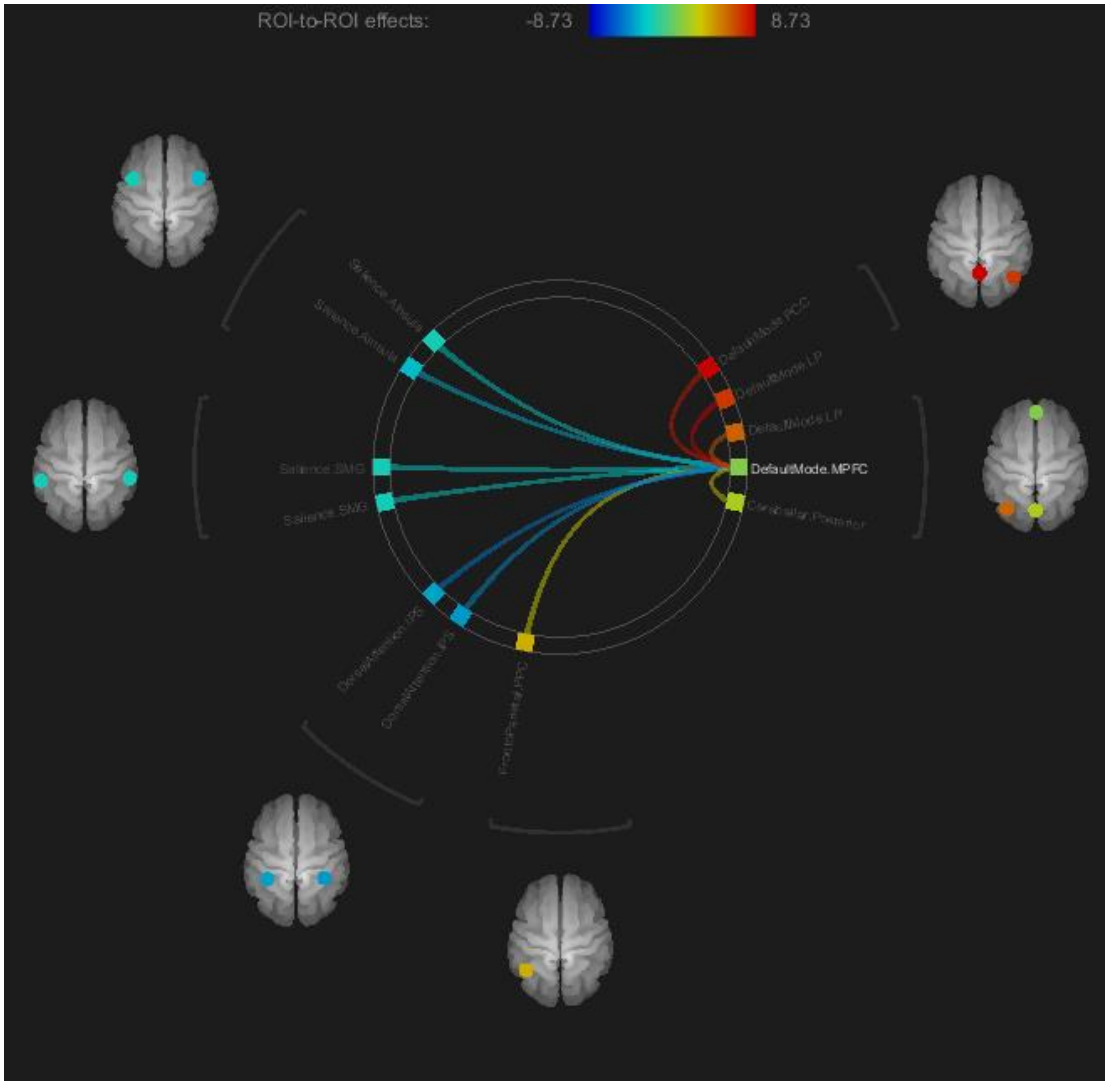

Figure 5. 3: Connectogram using as seed MPFC for PD group.

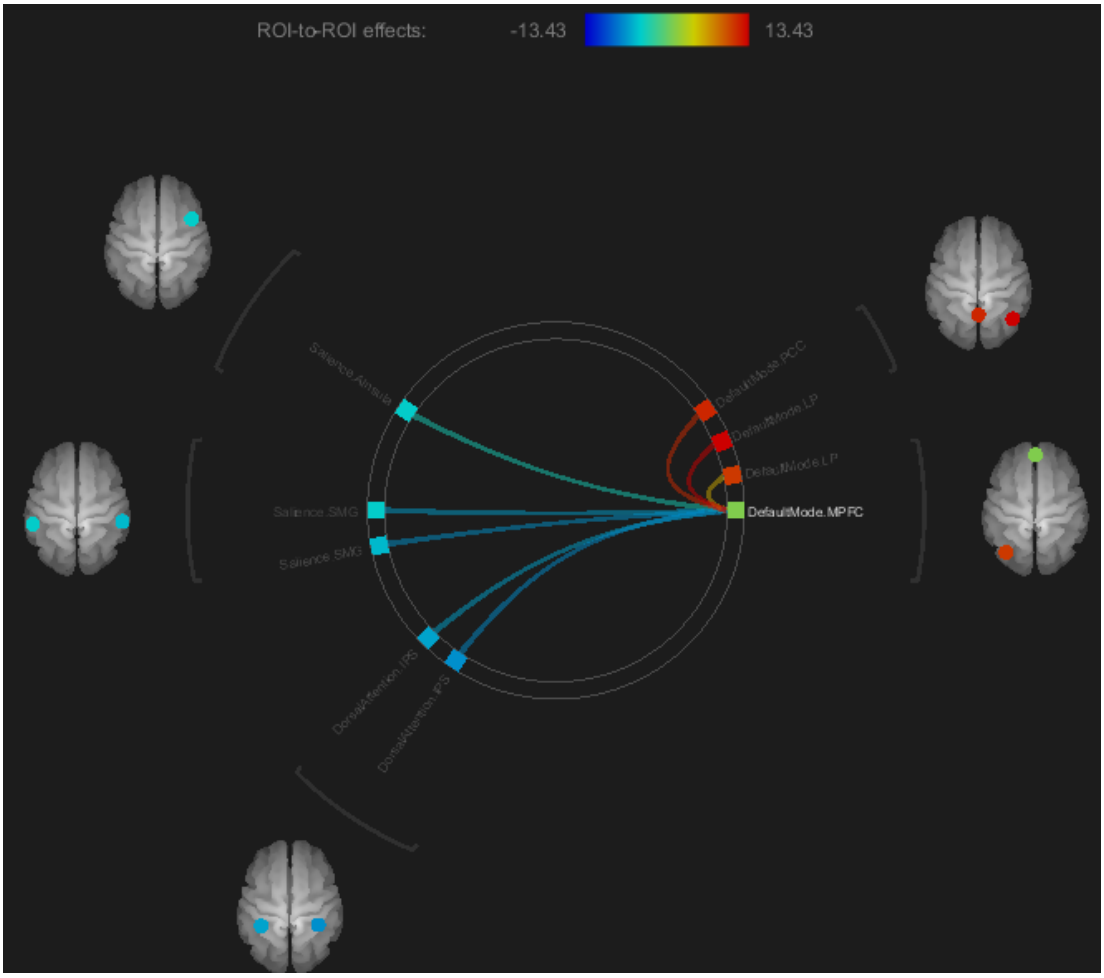

Figure 5. 4: Connectogram using as seed MPFC for controls group.

Discussion

Comparing the results that are acquired from CONN for the two groups, one can conclude the following. At first the brain regions that are functionally connected with the MPFC are pretty similar between PD and controls group, with the size of clusters to be different. For example, grouping in lobes the regions that are functionally connected with MPFC (Table 5.1, Table 5.2), it is obvious that the same lobes concern all the subjects except from some differences. Specifically, the frontal lobe, parietal lobe, temporal lobe and cerebellum are shown in both groups, while insula and diencephalon are shown only in PD. The brain regions that are connected are similar because patients of PD group are in the early stages of the disease, so there is not a lot of alteration in brain connections.

At first, the activation in dienchephalon and precisely in left thalamus in PD patients is an important issue that has to be discussed. The role of the thalamus is to receive and process information from the basal ganglia, limbic system and cerebellum and then to transfer the information to the cerebral cortex. It also plays a noticeable role in complex

somatosensory and motor, just like in controlling cognition and emotion. Although changes in thalamus are shown to be related with the symptom of dyskinesia in PD patients, according to previous studies, nonmotor symptoms are also related with thalamus [109]. In our case, due to the fact that PD patients are in the early stages of the disease, the activation in thalamus is related with nonmotor symptoms. Additionally, insula is a highly interconnected region with the basal ganglia and it is related to the sensorimotor integration.

As it is previously noticed, significant correlation observed within MPFC and Salience Network. This finding along with the activation of parahippocampal gyrus, observed only in PD group, corresponds to PD and the memory impairment caused by the disease [110]. Another finding is the activation in amygdala, only in controls group, which means that the same brain region in PD group has been affected by the disease even in the early stages. The primary role of amygdala is the processing of memory, emotional responses and decision-making.

It is important to be mentioned that the connections in controls group are stronger than in PD group. Definitely that is caused by the disease. All the brain regions that are referenced on the tables are in accordance with the bibliography findings. Also all the symptoms that are related with the brain activations are definitely nonmotor symptoms, since the UPDRS score of our patients is very low.

5.4 Study 2: Functional connectivity using data-driven method

The second study of this thesis investigates the functional connectivity by applying a different type of method, compared to the previous study, known as data-driven method. The Independent Component Analysis (ICA) is used for this study, which is a widely used method especially for studies that include resting-state fMRI data. The GroupICAT of fMRI toolbox (GIFT) version 4.0b[3] is utilized. It is important to be mentioned that the ICA study of a specific group requires the simultaneous analysis of all data, no matter how many subjects are included in that group.

Before the set up of the ICA analysis, preprocessing of the resting-state fMRI data must be done. For that reason SPM12[4]is used and the steps that are followed are described below:

1. Slice-timing correction

[3] https://trendscenter.org/software/gift/
[4] https://www.fil.ion.ucl.ac.uk/spm/software/spm12/

All the raw images are selected and the time that the image was acquired is corrected within the slices. The corrected images have an 'a' as prefix.

2. Realignment (Motion correction)

   All the slice-timing corrected images are selected and realigned according to the mean image of 300 functional images. The name of realigned images has an extra 'r' as prefix.

3. Co-registration

   In this step all the functional images are co-registered with the structural image in order to maximize the mutual information. When the co-registration step is done, are displayed the voxel-to-voxel affine transformation matrix, the histograms of the images with the original orientations and the final orientation as well as the registered images (Figure 5.5).

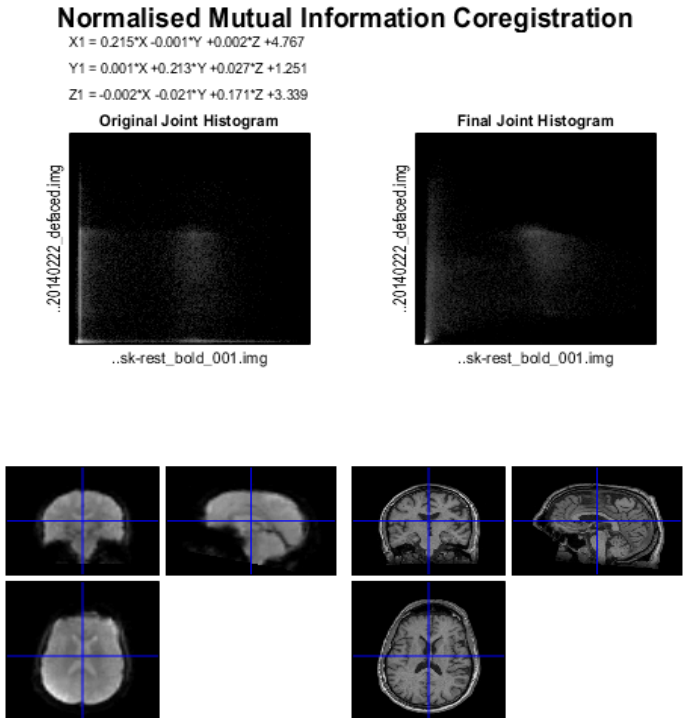

Figure 5. 5: The co-registration step of a subject.

4. Segmentation

   In this step gray and white matter images are produced along with a bias field corrected structural image that will be used in the next step.

5. Normalization

All the realigned and re-sliced functional images and the preprocessed structural image are normalized to the MNI (Montreal Neurological Institute) space. The images have the 'w' as prefix.

6. Smoothing

   In this step all the normalized images are smoothed with Gaussian kernel of a specified width (10mm). In the last step all the preprocessed images have the prefix 's'.

The analysis of data via ICA happens simultaneous for all the subjects of a group. For that reason, all the 28 subjects must be classified into two groups depending on their condition (control or PD patient). Afterwards the set up of the analysis is followed with the selection of the data and the estimation of Independent Components (ICs). In order to eliminate complicated computations, GIFT adopts the use of Principal Component Analysis in which the data was reduced into 12 Independent Components for every group separately. The algorithm that is used in the dataset is Infomax since it maximizes the transferring information from the input to the output of a network, using a non linear function. Spatial maps are reconstructed from the final mixing matrix data, depending on the courses of each participant and component. Due to the fact that number of subjects and the number of Independent Components are the same for both of the groups, the number of spatial maps is also equal. More specifically, 168 spatial maps are produced for every group (14 participants x 12 Independent Components x 1 session = 168 spatial maps). For every subject are recorded the coordinates of maximum voxel according to the z-scores. Also, the components are spatially sorted, that is a way to classify components spatially, using maximum voxel criteria. All these are carried out in group context for both the PD and control subjects but also for every subject separately.

Results

First, the findings of IC analysis are studied in a group level and then separately for every subject. In group level and specifically in PD group, the maximum z-score is located in voxels in pons, supplementary motor area right and in cerebellum crus 1 right. Similarly, controls group showed maximum z-score in voxels in paracentral lobule left, pons and cerebellum crus 1 right. The brain areas that are found to be active on both of the groups are pons, cerebellum crus 1 right and left, fusiform gyrus left and precuneus right. The tables with detailed information about the coordinates of maximum voxel and the associated brain areas of every group are presented in Appendix (Table 7.7 and Table 7.22).

Concerning the findings of each PD subject, the brain areas with the maximum voxel values are pons, paracentral lobule left, precuneus left, lingual gyrus right and supplementary motor area right. Also different locations of cerebellum such as cerebellum crus 1 right and left and cerebellum 9 left, are included. The results from every control subject present activation in brain areas such as pons, lingual gyrus left and right, paracentral lobule left and occipital inferior right. Areas such as cerebellum crus 1 right and left and cerebellum 9 left are also included. The Tables 7.8 - 7.21 concerns each subject from controls group, while Tables 7.23 – 7.36 concerns each subject from PD group in the Appendix.

Observing the functional connectivity matrix (Figure 5.6) of the PD group, the maximum positive correlation that is demonstrated in dark red colour, is between the components 7 [38,-80,-25] and 3 [-26,-84,-30], 10 [-42,-52,55] and 9 [2,-4,75] that correspond to the areas of cerebellum crus 1 right, cerebellum crus 1 left, inferior parietal lobule left and supplementary motor area right respectively. Furthermore, between the components 11 [2,-76,55] and 2 [34,56,5], 12 [-62,-20,15] and 10 [-42,-52,55] which correspond to the areas of precuneus right, middle frontal gyrus right, rolandic operculum left and inferior parietal lobule left. On the contrary, high negative correlations (dark blue colour) are observed within the components 7 [38,-80,-25] and 5 [-6,-28,-50], 9 [2,-4,75] and 6 [34,16,-25] which correspond to the cerebellum crus 1 right, pons, supplementary motor area right and superior temporal pole right, respectively. There is also observed positive correlations in some other components with light red colour, such as between the components 4 [-50,-60,30] and 1 [2,-72,40], 8 [-38,-80,-15] and 1 [2,-72,40], 11 [2,-76,55] and 6 [34,16,-25], 12 [-62,-20,15] and 8 [-38,-80,-15], 12[-62,-20,15] and 9 [2,-4,75]. All the previously mentioned components correspond to angular gyrus left, precuneus right, fusiform gyrus left, superior temporal pole right, rolandic operculum left, supplementary motor area right. Except from the light red colour, it can be observed the light blue colour which concerns negative correlations. More specifically, negative correlations are observed between the components 8 [-38,-80,-15] and 2 [34,56,5], 8[-38,-80,-15] and 3 [-26,-84,-30]. The associated areas are fusiform gyrus left, middle frontal gyrus right and cerebellum crus 1 left.

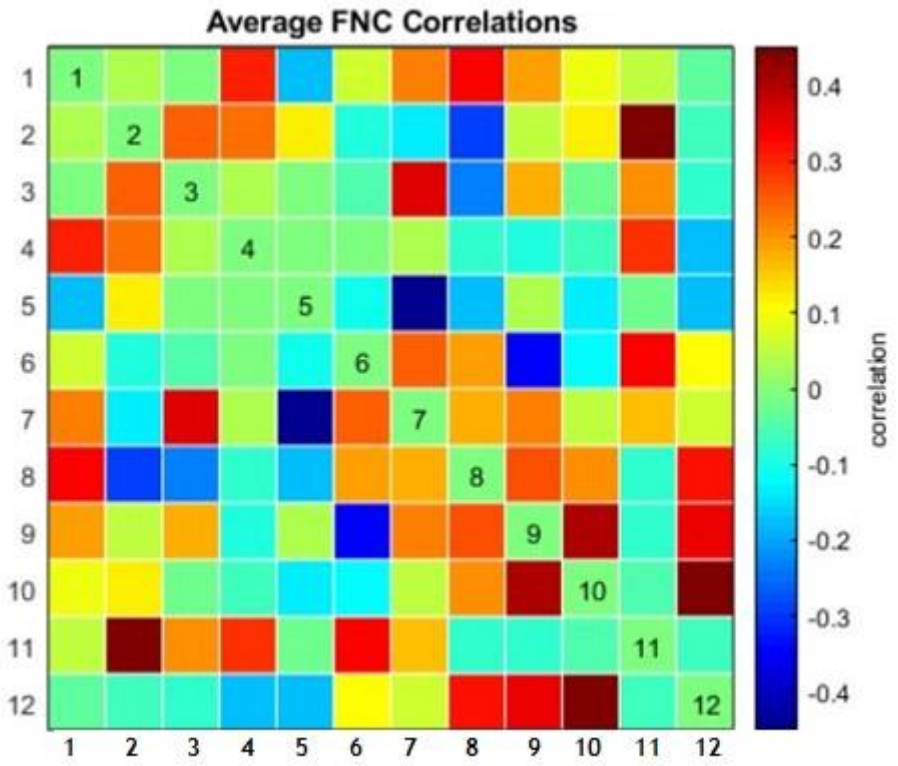

Figure 5. 6: Functional connectivity correlation matrix of PD group.

Furthermore, functional connectivity correlation matrix is acquired for the controls group, demonstrating the correlations with positive and negative values within the components. Figure 5.7 shows the matrix for controls group.

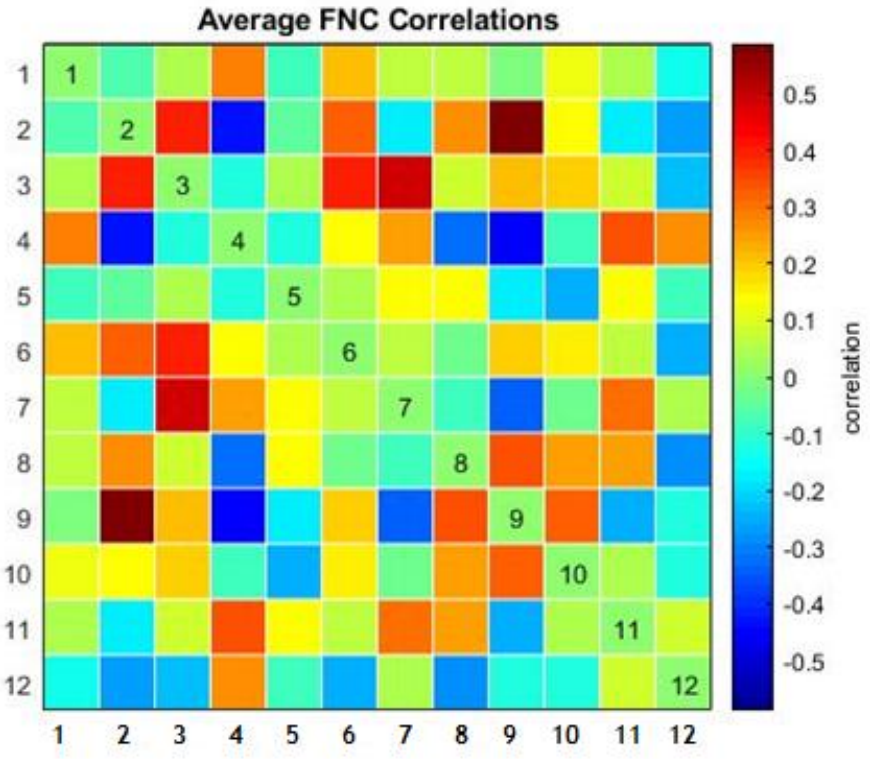

Figure 5. 7: Functional connectivity correlation matrix of controls group.

In order to have a different aspect of the results, the Network Summary tool is used from GroupICAT. That tool organizes all the independent components by network names. In this case, the components and precisely the associated brain regions are divided into groups depending on which lobes are being involved. For the PD subjects, the twelve components are grouped into seven lobes of the brain as shown below:

1. Parietal Lobe contains the precuneus right (1, 11), angylar gyrus left (4), inferior parietal lobule left (10).
2. Frontal Lobe contains the middle frontal gyrus right (2) and supplementary motor area right (9).
3. Cerebellum contains the cerebellum crus 1 left and right (3, 7).
4. Brainstem contains the pons (5).
5. Temporal Lobe contains the superior temporal pole right (6).
6. Occipital Lobe contains the fusiform gyrus left (8).
7. Insula contains the rolandic operculum left (12).

For the controls subjects, the twelve components are grouped into six lobes of the brain as shows below:

1. Parietal Lobe contains the precuneus right (6) and superior parietal lobule right (10).
2. Frontal Lobe contains the orbital inferior frontal gyrus left and right (1, 5), paracentral lobule left (9) and olfactory sulcus left (11).
3. Cerebellum contains the cerebellum crus 1 right and left (3, 4) and cerebellum 6 left (7).
4. Brainstem contains the pons (12).
5. Occipital Lobe contains fusiform gyrus left (2).
6. Insula contains the insula right (8).

From the Network Summary is acquired the functional connectivity correlations matrix, as well as a connectogram that shows the correlations within components and regions in another way. Figure 5.8 and Figure 5.9 demonstrate the connectograms for both of groups.

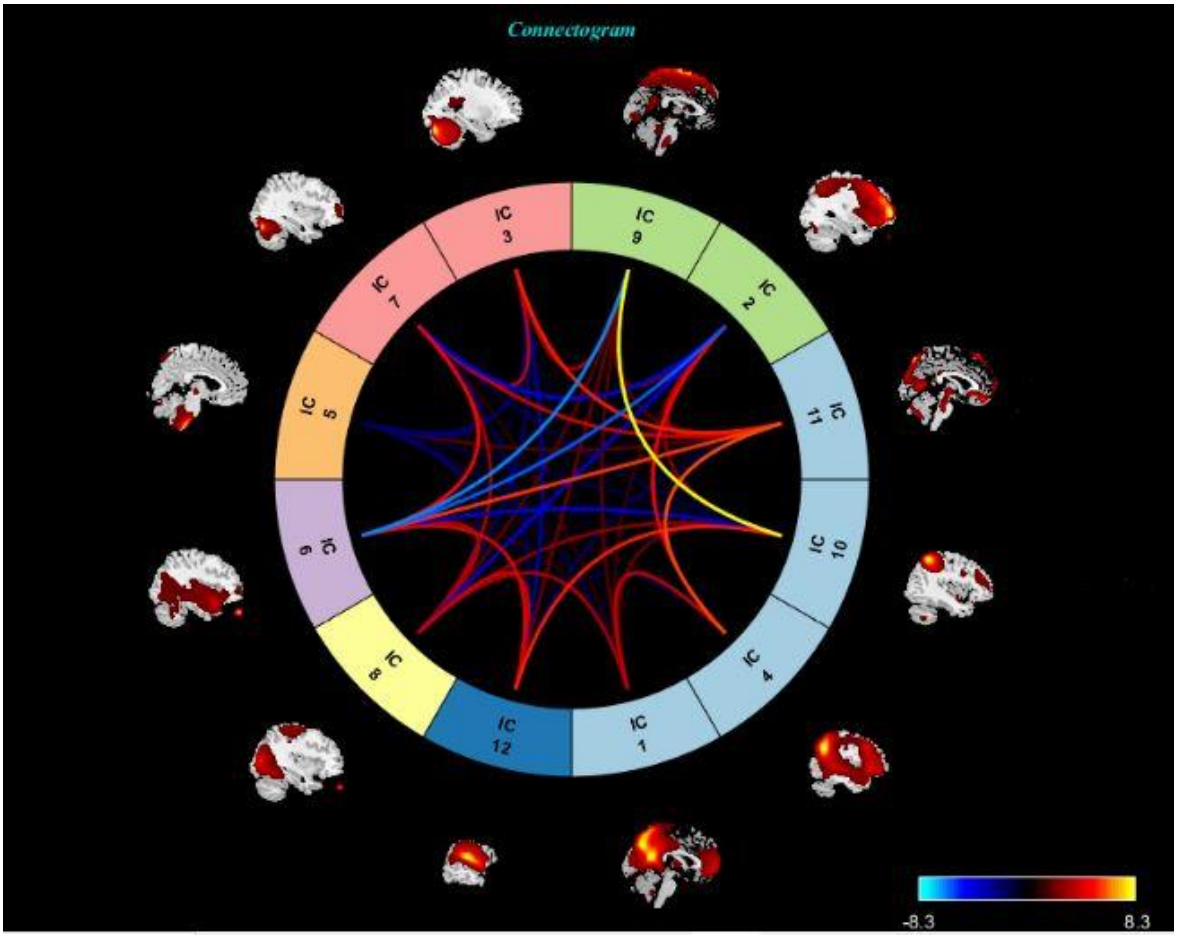

Figure 5. 8: Connectogram of the 12 components of PD group.

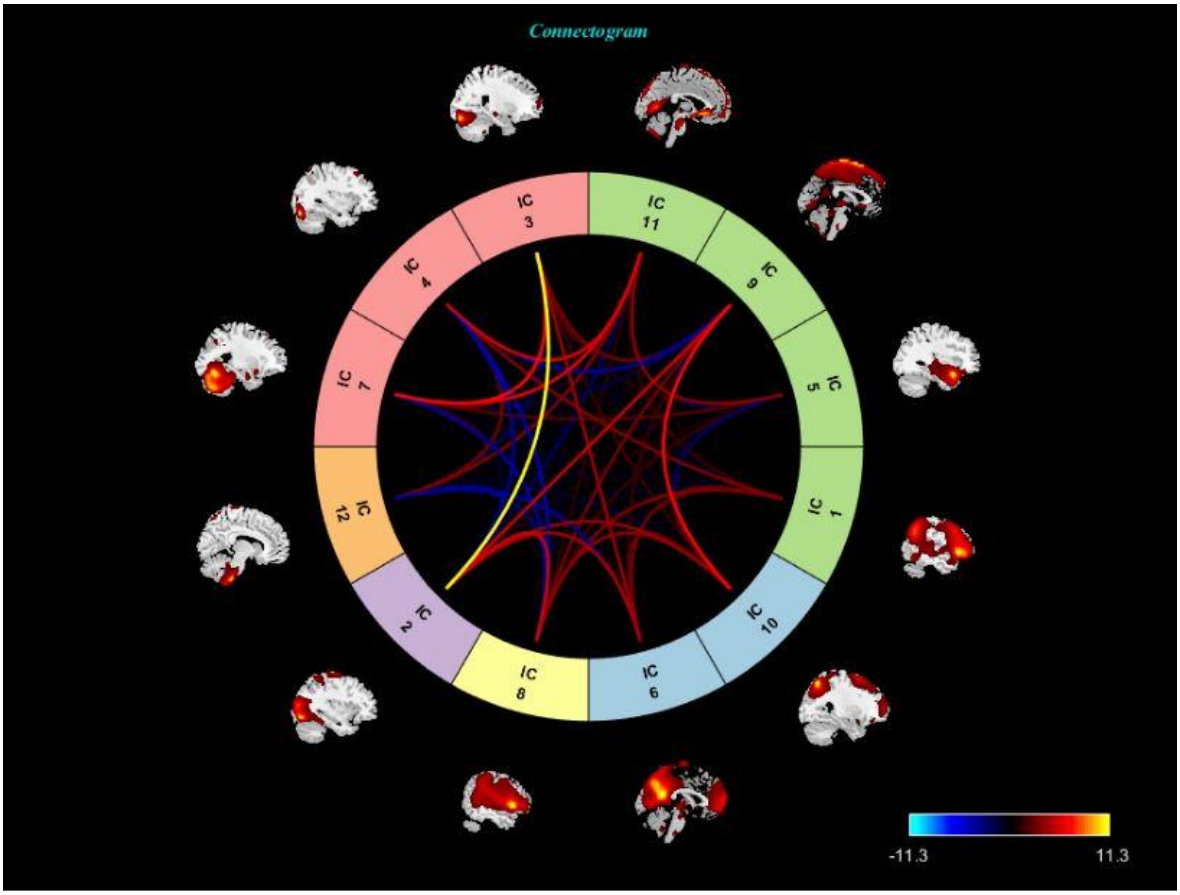

Figure 5. 9: Connectogram of the 12 components of controls group.

In the connectograms there is a coloured circle with the names of independent components where components within the same network are shown in the same color. Particularly, blue color corresponds to parietal lobe, green color to frontal lobe, pink color to cerebellum, orange color to brainstem, purple color to temporal lobe, yellow color to occipital lobe and dark blue corresponds to insula (there is only in Figure 5.8). Also, around the circle are thumbnails of spatial maps for every component. The curves inside the circles are known as Bezier curves. Those curves show the functional connectivity correlations within components and have different colors according to their negative or positive correlation. Negative correlation is demonstrated with the blue color while positive correlation is demonstrated with red and yellow color.

In Figure 5.8, the connectogram for PD group, the highest positive correlation is observed within parietal and frontal lobe and more specifically within inferior parietal lobule left and supplementary motor area right. While in Figure 5.9 the highest positive correlation is observed within occipital lobe and cerebellum and specifically within fusiform gyrus left and cerebellum crus 1 right. Also comparing the two connectograms in controls group there

are more positive correlations within components, while in PD group there are positive and negative correlations in similar proportion. It is worth to be mentioned that within the components of the same network there are only positive correlations with the negative correlations of the connectogram to be within the different networks. Comparing the connectograms with the functional connectivity correlation matrices (Figures 5.6, 5.7) that are acquired from ICA analysis the correlations within regions are identified.

Discussion

Setting side by side the findings from the analysis, one can understand that most of the activated brain regions are regions of the cortex. From the other side there are areas such as middle frontal gyrus and supplementary motor area of the right hemisphere in frontal lobe, angular gyrus and inferior parietal of the left hemisphere in parietal lobe, superior temporal pole of the right hemisphere in temporal lobe, fusiform gyrus of the left hemisphere in occipital lobe and rolandic operculum of the left hemisphere in insula that appear only in PD subjects. This finding leads to the conclusion that these areas are related to the disease. While, a significant activation is observed only in controls group and is the activation in olfactory sulcus. It is important to be referenced that the region of insula is activated in both of the groups. But in controls group the activation is restricted only in the region of insula of the right hemisphere while in PD group affects a wider area, the rolandic operculum. Also observing the lobes that are affected in both groups, temporal lobe is the one that concerns only PD group.

Particularly, the existence of activation in insula which is highly interconnected with the basal ganglia and other cortical regions including supplementary motor area indicates its possible role in sensorimotor integration [107]. Observing the connectogram between insula and supplementary motor area there is strong positive correlation, a fact that confirms the presence of Parkinson's disease. As for angular gyrus has been found to acts as a hub region wherein multisensory information is converged and integrated together. Specifically, the left angular gyrus that is found in this thesis, has been implicated in speech processing with the most common feature of hypophonia in PD [111]. Our PD patients may not have experienced the symptom of hypophonia but they will for sure. Furthermore, the activation of temporal lobe leads to the conclusion that there is temporal pole atrophy in patients which is an early sign in PD according to previous description of Braak *et al.* [112]. As for activation in fusiform gyrus that leads also in brain atrophy. Fusiform gyrus is an area that is involved in the visual network that's why a lot of PD patients appear visual common symptoms such as blurred vision, visuoperceptual impairments and visual hallucinations.

Also fysiform gyrus has constantly been found to be involved in the perception of faces and body regions since is part of the visuoperceptive ventral stream [113]. That symptom is occurred even in the early stages of the disease, just like in our PD group. The last thing that has to be discussed is about the activation in olfactory sulcus, only in controls group. That finding means that olfactory sulcus is affected by the disease in PD group that's why there is no activation in that group. There is evidence that the disease begin in the peripheral autonomic nervous system and/or the olfactory bulb and then spreading through central nervous system affecting the lower brainstem structures before involving the substantia nigra [17]. Also patients maybe experienced that symptom, the loss of olfaction, even years before the diagnosis of the disease.

All the aforementioned findings agree with the bibliography. Differences that may be occurred between the Study 1 and Study 2 are related with the fact that the Study 1 is more focused on one area of the Default Mode Network while the Study 2 is a more general approach concerning of Default Mode Network as a whole.

5.5 Study 3: Effective connectivity using spectral Dynamic Causal Modelling

The third study of this thesis is about the investigation of effective connectivity using a model-based approach, known as Dynamic Causal Modelling (DCM). More specifically the extension of DCM named as spectral DCM is used, in order to model intrinsic dynamics on resting-state fMRI data and define effective connectivity [99]. This method is suitable for implementation in resting-state fMRI data because models BOLD signal when exogenous inputs do not exist.

The spectral DCM analysis is implemented in both control and Parkinson's disease (PD) groups. This analysis is performed using DCM12.5 routine implemented in SPM12. The images of all the subjects are preprocessed before this analysis, following the same preprocessing procedure that was described previously. After the preprocessing, four regions of interest (ROIs) are selected and the time-series from the selected ROIs are created as the residuals of a general linear model (GLM). The regressors that are part of this model are the six rigid body realignment parameters to model the movement correlated effects and the signal that is extracted from white matter (WM) and cerebrospinal fluid (CSF) so as to be used as confound [99].

The ROIs of spectral DCM analysis are the key regions of the Default Mode Network (DMN), a brain network that has increased level of involvement in PD. In general DMN is a brain system which mediates internal modes of cognitive activity, showing higher neural

activation when someone is at rest [121]. ROIs are defined as spheres with a radius of 8mm produced by the previous CONN study. The selected ROIs are shown in Table 5.3.

Table 5. 3: Selected ROIs for the spectral DCM analysis.

	ROIs	***Center of ROI***
1	Medial Prefrontal Cortex (MPFC)	[1, 55, -3]
2	Left Lateral Parietal Cortex (lLPC)	[-39, -77, 33]
3	Right Lateral Parietal Cortex (rLPC)	[47, -67, 29]
4	Posterior Cingulate Cortex (PCC)	[1, -61, 38]

After the extraction of the resting-state fMRI time-series from all four ROIs, the specification of a fully-connected model which has bi-directional connections between any pair of ROIs is performed (Figure 5.10). In Table 5.4 the effective connectivity parameters of the first PD subject are presented, where the matrix elements represent the effective influence between regions. The tables of effective connectivity parameters for the rest of the subjects are presented in the Appendix (Table 7.37- Table 7.62).

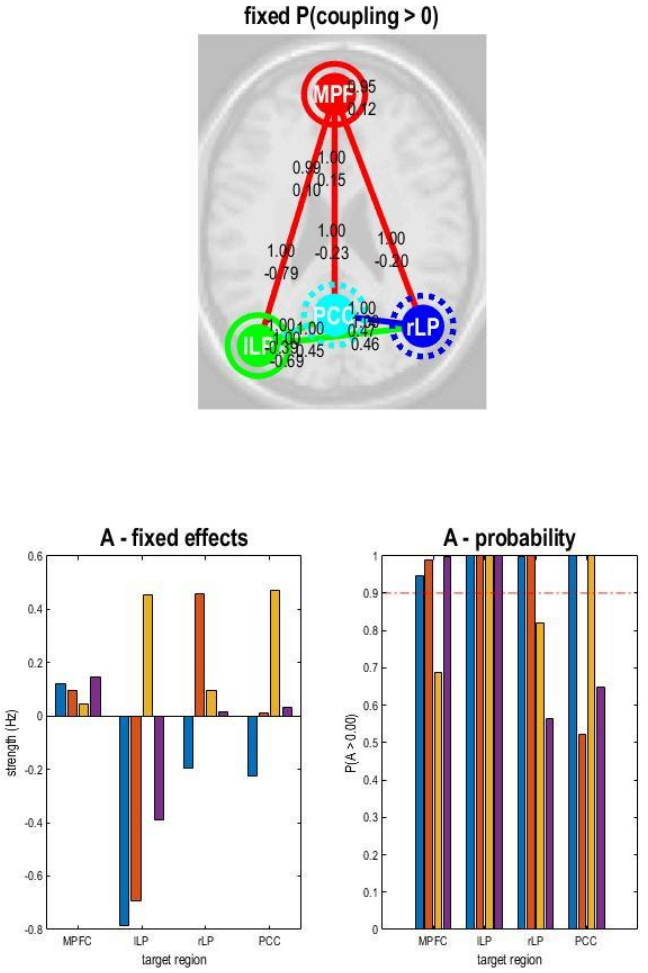

Figure 5. 10: The fully connected model with bi-directional connections between any pair of ROIs and effective connectivity parameters for the first PD subject.

Table 5. 4: Effective connectivity parameters of the first PD subject.

	MPFC	***lLPC***	***rLPC***	***PCC***
MPFC	0.1219	0.0972	0.0431	0.1466
lLPC	-0.7871	-0.6943	0.4536	-0.3913
rLPC	-01972	0.4580	0.0966	0.0159
PCC	-0.2266	0.0102	0.4708	0.0300

The next step of this analysis is the selection of a Bayesian Model and the use of Fixed Effects Inference Method (FFX) in order to compare the winning model that effectively describes and fits to the data. For that reason, eight different connectivity models are specified for both PD and control groups. More specifically, a fully connected model, three

models where different regions primarily affected the other ones (MPFC, PCC, bilateral modulation) and the same models without direct connections between rLPC and lLPC, as shown in Figure 5.11 and Figure 5.12 are specified.

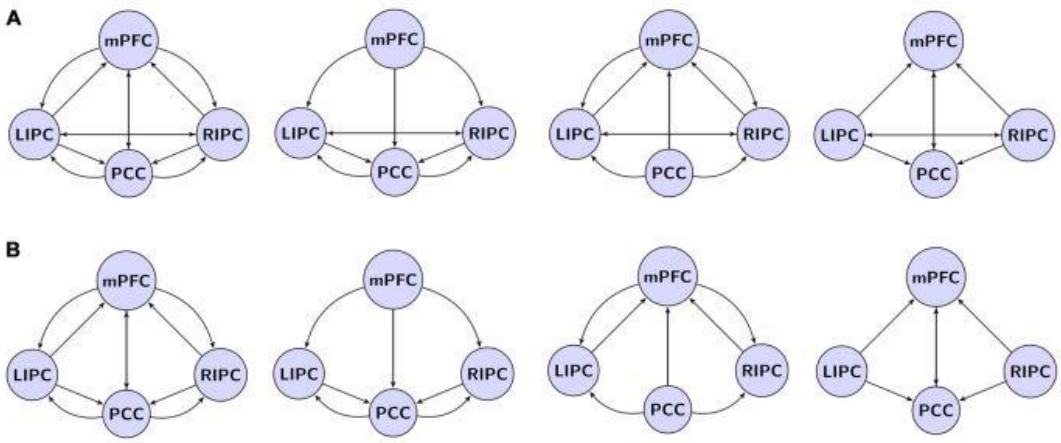

Figure 5. 11: The investigated models. (A) Models with direct connections between bilateral RLP and LLP, left to right: fully connected model (DMN), MPFC, PCC, bilateral modulation. (B)Models with no direct connections between RLP and LLP. Double arrows correspond to mutual connections [114].

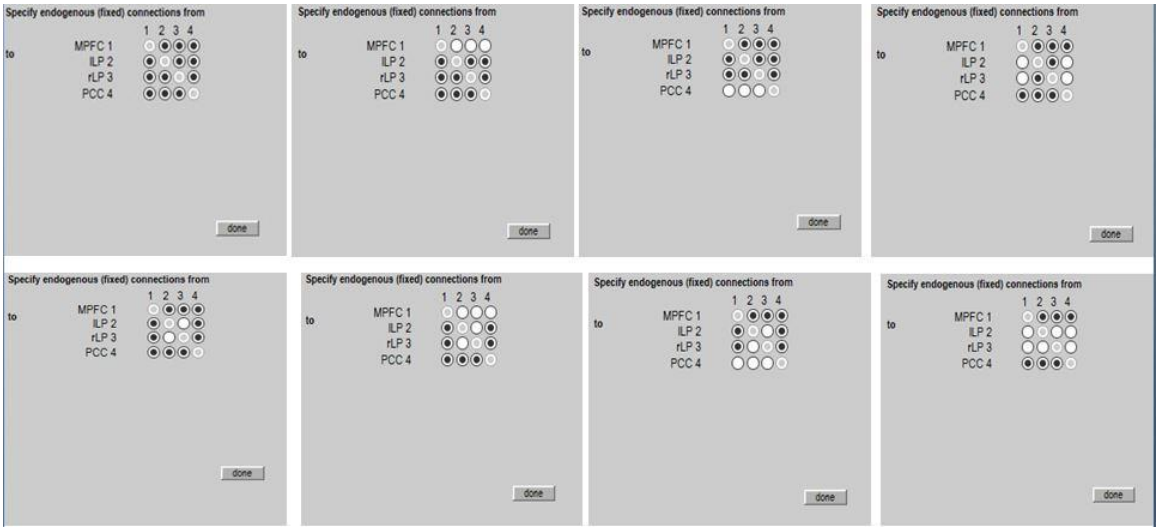

Figure 5. 12: The desirable specification of endogenous (fixed) connections for the model comparison.

Bayesian Model Selection finds that the fully connected model is the best at the group level. Moreover, this model is the best one for eight out of thirteen PD subjects and ten out of thirteen control subjects. The winning model of the first PD subject is shown in Figure 5.13.

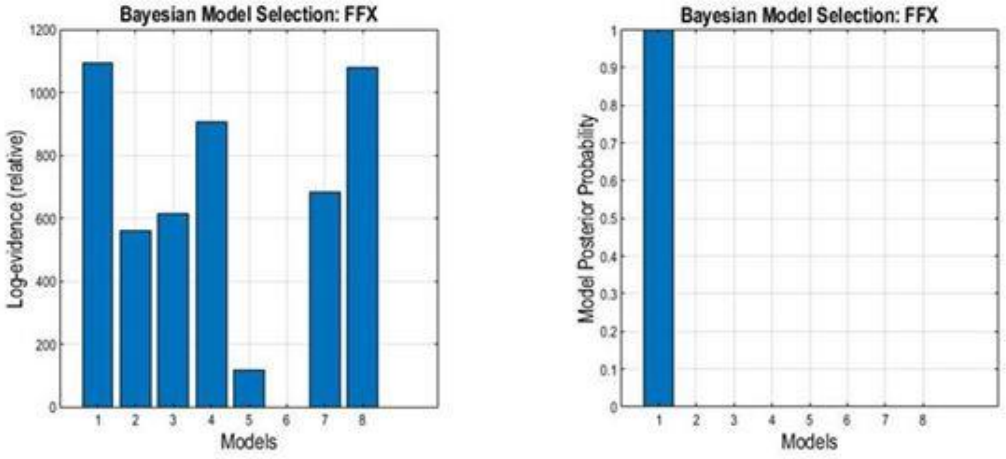

Figure 5. 13: The winning model is the first one using Fixed Effects Inference Method (FFX).

Chapter 6: Conclusions

6.1 Discussion

Parkinson's disease (PD) is the second most common age related neurodegenerative disorder after Alzheimer's disease. It is a progressive disorder that is characterized by motor symptoms, rigidity, tremor and bradykinesia. Nowadays it is well known that except from the common motor symptoms of the disease there are non-motor symptoms that occur in the early stages or even years before the diagnosis of the disease. Although the significant progress that has been made with the clarification of its pathophysiology, the variability of symptoms along with the still unknown etiology facilitates the disease an important issue for more investigation (Chapter 1).

MRI-based studies have been frequently occurred so as to better understand the disease and its alterations within the different stages and within different group of subjects. A modern application known as fMRI has been used in order to find the location of activated brain regions when subjects are at resting-state or in task condition, depending on the field of investigation (Chapter 2). There are a lot of studies for both conditions, task-based and resting-state concerning the analysis of brain imaging in Parkinson's disease (Chapter 3). After this process, the acquisition of fMRI images, patterns of connected and disconnected brain regions can be acquired applying appropriate statistical analyses (preprocessing and

brain connectivity methods) that will be empathized with the differences within healthy and patient subjects or within subjects of the same group (Chapter 4).

In this thesis resting-state functional MRI (rs-fMRI) data from drug naïve PD patients is used in order to measure functional connectivity in spatially distinctive brain regions and compared them with the patterns of healthy subjects respectively. The number of participants is 28, 14 PD subjects and 14 healthy subjects and the investigation focuses on the Default Mode Network. So as to measure functional connectivity two different approaches are applied. The first is a seed-based approach utilized via CONN toolbox where the results that provide are more specific due to the selection of only one seed (region) for investigation. While the second is a data-driven method, using ICA, which is a more general approach and gives better visualization of the brain. Differences observed within the two approaches are occurred due to the more general aspect and more pointed aspect of them. In general regions such as temporal pole, angular gyrus, insula, supplementary motor area and fusiform gyrus occurred in PD patients and consequently are related with the disease. Except from the aforementioned studies a third study carried out in order to investigate the effective connectivity in the same data. In this study the extension of DCM, named as spectral DCM, is used where compares 8 different models between healthy and PD subjects so as to find the most appropriate to describe the data. It is found that the Default Mode Network is the one (Chapter 5).

As it is already mentioned, in this work, the description of PD from the perspective of brain connectivity using fMRI data and applying appropriate analysis methods is presented. Although the use of classical methods such as ICA and spectral DCM, as a lot of researchers, the way that the results (connectograms) are presented and the significant conclusions in such early stages of PD subjects, maybe can help the investigation in this field. The analysis of brain connectivity in patients with PD and the comparison with the brain connectivity of controls subjects reveal that, even at the onset of the disease, the alteration of brain connectivity can provide significant information to the experts for the disease effects to the patient and its efficient management. The observations become even more important since do not concern a specific brain region but a network of regions, which is the innovation of this work. A lot of previous studies focus on a particular symptom such as freezing of gait (*Tessitore et al.*[50]) or apathy (*Baggio et al.*[52]) something that helps to understand that symptom but the investigation is restricted.

6.2 Limitations

The methods that are applied in the current thesis give, all of them, reliable results considering functional and effective connectivity patterns. Because of the fact that the number of the participants is restricted further studies must be done so as to make more robust results about the early stages of the disease. Also PD patients were at very early stages of the disease so we could not make a comparison between them, but only with healthy subjects, because of the similar experience of the disease. Another limitation is the fact that the results are related only with one network that has been in our interest. Furthermore, the complexity of the effective connectivity models and the large number of areas and their combinations that are necessary in order to construct each model, render the determination of the best model a not simple matter.

6.3 Future work

The target of this thesis was not to prove that there is only one method to describe the PD data, as there is no such thing, but to present both advantages and disadvantages of each method. The selection of the most appropriate method depends on the researcher's motivation and the aim of each study. Although PD's pathophysiology has been clarified, the variability of symptoms and the still unknown etiology facilitates the disease an important issue for more investigation, especially in the early stages where the symptoms can be controlled.

References

1. L.V. Kalia, A.E. Lang, Parkinson's disease, Lancet, 386, 9996, 896-912, 2015.
2. J. Campdelacreu, Parkinson's disease and Alzheimer disease: environmental risk factors, Review, Neurologia, 29, 9, 541-549, 2014.
3. S. Factor, W. Weiner, Parkinson's disease: diagnosis and clinical management, Chapter 22, 2nd Edition, Demos Medical Publishing, 2008.
4. S. Divya, S. Shrimali, R. KS, A Review on Parkinson's Disease: Its Pathophysiology, Treatment and Surgery, Pharmatutor, 3, 2, 25-32, 2015.
5. I. Litvan, K.P. Bhatia, D.J. Burn, C.G. Goetz, A.E. Lang, I. McKeith, N. Quinn, K.D. Sethi, C. Shults, G.K. Wenning, Movement Disorders Society Scientific Issues Committee report: SIC Task Force appraisal of clinical diagnostic criteria for Parkinsonian disorders, Movement Disorder Society, 18, 5, 467-486, 2003.
6. D.J. Gelb, E. Oliver, S. Gilman, Diagnostic criteria for Parkinson disease, Archives of Neurology, 56, 1, 33-39, 1999.
7. J. Massano, K.P. Bhatia, Clinical approach to Parkinson's disease: features, diagnosis, and principles of management, Cold Spring Harbor perspectives in medicine, 2, 6, 008870, 2012.
8. A.J. Hughes, S.E. Daniel, L. Kilford, A.J. Lees, Accuracy of clinical diagnosis of idiopathic Parkinson's disease: a clinic-pathological study of 100 cases, Journal of Neurology, Neurosurgery and Psychiatry, 55, 3, 181-184, 1992.
9. W. Koller, S. Kase, Muscle strength testing in Parkinson's disease, European Neurology, 25, 2, 130-133, 1986.
10. R. Cano-de-la-Cuerda, M. Pérez-de-Heredia, J.C. Miangolarra-Page, E. Muñoz-Hellín, C. Fernández-de-Las-Peñas, Is There Muscular Weakness in Parkinson's Disease?, American Journal of Physical Medicine & Rehabilitation, 89, 1, 70-76, 2010.
11. J.H. Friedman, A.M. Abrantes, Self perceived weakness in Parkinson's disease, Parkinsonism & Related Disorders, 18, 7, 887-889, 2012.
12. C.G. Goetz, W. Poewe, O. Rascol, C. Sampaio, G.T. Stebbins, C. Counsell, N. Giladi, R.G. Holloway, C.G. Moore, G.K. Wenning, M.D. Yahr, L. Seidl, Movement Disorder Society Task Force report on the Hoehn and Yahr staging scale: status and recommendations, Movement disorders: official journal of the Movement Disorder Society, 19, 9, 1020-1028, 2004.
13. M.M. Hoehn, M.D. Yahr, Parkinsonism: onset, progression and mortality, Neurology, 17, 5, 427-442, 1967.

14. C.G. Goetz, B.C. Tilley, S.R. Shaftman, G.T. Stebbins, S. Fahn, P. Martinez- Martin, W. Poewe, C. Sampaio, M.B. Stern, R. Dodel, B. Dubois, R. Holloway, J. Jankovic, J. Kulisevsky, A.E. Lang, A. Lees, S. Leurgans, P.A. LeWitt, D. Nyenhuis, C.W. Olanow, O. Rascol, A. Schrag, J.A. Teresi, J.J. van Hilten, N. LaPelle, Movement disorder Society-sponsored revision of the Unified Parkinson's Disease Rating Scale (MDS-UPDRS): Scale presentation and clinimetric testing results, Movement Disorder Society, 23, 15, 2179-2170, 2008.
15. C.A. Antoniades, R. Barker, The search for biomarkers in Parkinson's disease: a critical review, Expert Review of Neurotherapeutics, 8, 12, 1841-1852, 2009.
16. E.R. Dorsey, R. Constantinescu, J.P. Thompson, K.M. Biglan, R.G. Holloway, K. Kieburtz, F.J. Marshall, B.M. Ravina, G. Schifitto, A. Siderowf, C.M. Tanner, Projected number of people with Parkinson disease in the most populous nations, 2005 through 2030, Neurology, 68, 5, 384-386, 2007.
17. A. Kouli, K.M. Torsney, W.L. Kuan, Parkinson's Disease: Etiology, Neuropathology, and Pathogenesis, ResearchGate, 3-26, 2018.
18. R. Gray, N. Ives, C. Rick, S. Patel, A. Gray, C. Jenkinson, E. Mclntosh, K. Wheatley, A. Williams, C.E. Clarke, Long-term effectiveness of dopamine agonists and monoamine oxidase B inhibitors compared with levodopa as initial treatment for Parkinson's disease (PD MED): a large, open-label, pragmatic randomized trial, Lancet, 384, 9949, 1196-1205, 2014.
19. R.C. Helmich, D.E. Vaillancourt, D.J. Brooks, The Future of Brain Imaging in Parkinson's Disease, Review, Journal of Parkinson's Disease, 8, 47-51, 2018.
20. R.C. Helmich, L.C. Derikx, M. Bakker, R. Scheeringa, B.R. Bloem, I. Toni, Spatial remapping of cortico-striatal connectivity in Parkinson's disease, Cerecral Cortex, 20, 5, 1175-1186, 2010.
21. P.J.P. Matthews, Functional magnetic resonance imaging, Neurology, Neurosurgery & Psychiatry, 75, 6-12, 2004.
22. P.M.M.P. Jezzard, S.M. Smith, Functional MRI: An Introduction to Methods, 2001.
23. M.E. Raichle, A brief history of human brain mapping, Trends in Neurosciences, 32, 2, 2008.
24. J.E. Chen, G.H. Glover, Functional magnetic resonance imaging methods, Neuropsychology Review, 25, 289-313, 2015.
25. G.H. Glover, Overview of functional magnetic resonance imaging, Neurosurgery Clinics, 22, 133-139, 2011.

26. R.A. Poldrack, J.A. Mumford, T.E. Nichols, Handbook of functional MRI data analysis: Cambridge University Press, 1, 3, 2011.
27. C. Mulert, L. Lemieux, EEG-fMRI: physiological basis, technique and application, Springer Science &Business Media, 2009.
28. M.D. Fox, M.E. Raichle, Spontaneous fluctuations in brain activity observed with functional magnetic resonance imaging, Nature Reviews Neuroscience, 8, 700, 2007.
29. E.E. Tripoliti, D.I. Fotiadis, Recent developments in computer methods for fMRI data processing, in Biomedical Engineering, InTech, 2009.
30. S.A. Huettel, A.W. Song, G.McCarthy, Functional magnetic resonance imaging, Sinauer Associates Sunderland, MA, 1, 2004.
31. D.C.V. Essen, K. Ugurbil, E. Auerbach, D. Barch, T.E.J. Behrens, R. Bucholz, A. Chang, L. Chen, M. Corbetta, S.W. Curtiss, S.D. Penna, D. Feinberg, M.F. Glasser, N. Harel, A.C. Health, L. Larson-Prior, D. Marcus, G. Michalareas, S. Moeller, R. Oostenveld, S.E. Petersen, F. Prior, B.L. Schlaggar, S.M. Smith, A.Z. Snyder, J. Xu, E. Yacoub, WU-Minn HCP Consortium, The Human Connectome Project: A data acquisition perspective, National Institute of Health Neuroimage, 62(4), 2222-2231, 2012.
32. O. Josephs, R.N. Henson, Event-related functional magnetic resonance imaging: modeling, inference and optimization, Philosophical Transactions of the Royal Society of London B: Biological Sciences, 354, 1215-1228, 1999.
33. M. Daliri, M. Behroozi, Advantages and disadvantages of resting-state functional connectivity magnetic resonance imaging for clinical applications, OMICS J Radiology, 3, 123, 2013.
34. M.H. Lee, C.D. Smyser, J.S. Shimony, Resting-state fMRI: a review of methods and clinical applications, American Journal of Neuroradiology, 2012.
35. T. Takamura, T. Hanakawa, Clinical utility of resting-state functional connectivity magnetic resonance imaging for mood and cognitive disorders, Journal of Neural Transmission, 124, 821-839, 2017.
36. N.K. Logothetis, B.A. Wandell, Interpreting the BOLD signal, Annual Reviews Physiology, 66, 735-769, 2004.
37. J.A. Detre, T.F. Floyd, Functional MRI and its applications to the clinical neurosciences, The neuroscientist, 7, 64-79, 2001.
38. R. Henson, Analysis of fMRI Timeseries: Linear Time-Invariant Models, Event-related fMRI and Optimal Experimental Design, The Wellcome Department Of Imaging Neuroscience & Institute of Cognitive Neuroscience Chapter 10.

39. B.C. Dickerson, Advances in functional magnetic resonance imaging: technology and clinical applications, Neurotherapeutics, 4, 360-370, 2007.
40. D. Orringer, D.R. Vago, A.J. Golby, Clinical Applications and Future Directions of Functional MRI, National Institute of Health Seminars in Neurology, 32, 466-475, 2012.
41. https://www.researchgate.net/figure/Principles-of-EEG-fMRI-Indirect_functional neuroimaging-modalities-such-as-fMRI-are_fig2_283753260
42. N.H. Nasaruddin, A.N. Yusoff, S. Kaur, Functional MRI Characteristics in Visual Cortex (BA 17, 18 and 19) Corresponding to the Visual Field of Normal, Glaucoma Suspect (GS) and Primary Open Angle Glaucoma (POAG) Patients, Jurnal Sains Kesihatan Malaysia, 15, 1, 27-32, 2017.
43. J.L. McCelland, M.A.L. Ralph, Cognitive Neuroscience, International Encyclopedia of the Social &Behavioral Sciences (Second Edition), 95-102, 2015.
44. U. Sabatini, K. Boulanouar, N. Fabre, F. Martin, C. Carel, C. Calonnese, L. Bozzao, I. Berry, J.L. Montastrue, F. Chollet, O. Rascol, Cortical motor reorganization in akinetic patients with Parkinson's disease : A functional MRI study, Brain, 123, 394-403, 2000.
45. T. Wu, M. Hallett, A functional MRI study of automatic movements in patients with Parkinson's disease, Brain, 128, 2250-2259, 2005.
46. P. Péran, D. Cardebat, A. Cherubini, F. Piras, G. Luccichenti, A. Peppe, C. Caltagirone, O. Rascol, J.F. Démonet, U. Sabatini, Object naming and action-verb generation in Parkonson's disease: A fMRI study, Science Direct, 45, 960-971, 2009.
47. Y.Kwak, S.Peltier, N.I.Bohnen, M.L.T.M.Müller, P.Dayalu, R.D. Seidler, Altered resting state cortico-striatal connectivity in mild to moderate stage Parkinson's disease, Frontiers in Systems Neuroscience, 4, 143, 1-25, 2010.
48. F. Skidmore, D. Korenkevych, Y. Liy=u, G. He, E. Bullmore, P.M. Pardalos, Connectivity brain networks based on wavelet correlation analysis in Parkinson fMRI data, Neuroscience Letters, 499, 47-51, 2011.
49. S. Baudrexel, T. Witte, C. Seifried, F. Wegner, F. Beissner, J.C. Klein, H. Steinmetz, R. Deichmann, J. Roeper, R. Hilker, Resting state fMRI reveals increased subthalamic nucleus-motor cortex connectivity in Parkinson's disease, Neuroimage, 55, 1728-1738, 2011.
50. A. Tessitore, M. Amboni, F. Esposito, A. Russo, M. Picillo, L. Marcuccio, M.T. Pellecchia, C. Vitale, M. Cirillo, G. Tedeschi, P. Barone, Resting-state brain connectivity in patients with Parkinson's disease and freezing of gait, Parkinsonism and Related Disorders, 18, 781-787, 2012.

51. C. Luo, W. Song, Q. Chen, Z. Zheng, K. Chen, B. Cao, J. Yang, J. Li, X. Huang, Q. Gong, H. Shang, Reduced functional connectivity in early-stage drug-naïve Parkinson's disease: a resting-state fMRI study, Neurobiology of Aging, 35, 431-441, 2014.
52. H.C.Baggio, B.Segura, J.L.Garrido-Milan, M.J.Marti, Y.Compta, F.Valldeorida, E.Tolosa, C.Junque, Resting-State Frontostriatal Functional Connectivity in Parkinson's Disease-Related Apathy, Movement Disorders, 30, 5, 671-679, 2015.
53. R.G. Burciu, J.W. Chung, P. Shukla, E. Ofori, H. Li, N.R. McFarland, M.S. Okum, D.E. Vaillancourt, Functional MRI of disease progression in Parkinson disease and atypical parkinsonian syndromes, Neurology, 87, 709-717, 2016.
54. G. Engels, A. Vlaar, B. McCoy, E. Scherder, L. Douw, Dynamic Functional Connectivity and Symptoms of Parkinson's Disease: A Resting- State fMRI Study, Neuroscience, 10, 388, 2018.
55. A. Razi, K.J. Friston, The Connected Brain (Causality, models and intrinsic dynamics), IEEE SIGNAL PROCESSING MAGAZINE, 1053-5888, 2016.
56. K.J. Friston, Functional and effective connectivity: a review, Brain connectivity, 1, 13-36, 2011.
57. K.J. Friston, Functional and effective connectivity in neuroimaging: a synthesis, Human brain mapping, 2, 56-78, 1994.
58. P.M. Rossini, R. Di Iorio, M. Bentivoglio, G. Bertini, F. Ferreri, C. Gerloff, R.J. Miraglia, M.A. Nitsche, F. Rosanova, Y. Shirota, c. Tesoriero, Y. Ugawa, U. Vecchio, Ziemann, M. Hallett, Methods for analysis of brain connectivity: An IFCN-sponsored review, Clinical Neurophysiology, 1-51, 2019.
59. A.A. Elseoud, Exploring functional brain networks using independent component analysis, Academic Dissertation –Faculty of Medicine, 2013.
60. K.A. Smitha, K.A. Raja, K.M. Arun, P.G. Rajesh, B. Thomas, T.R. Kapilamoorthy , C. Kesavadas, Resting state fMRI: A review on methods in resting state connectivity analysis and resting state networks, The Neuroradiology Journal, 30,4, 305-317, 2017.
61. E.W. Lang, A.M. Tomé, I.R. Keck, J. Górriz-Sáez, C.G. Puntonet, Brain connectivity analysis: a short survey, Computational intelligence and neuroscience, 2012, 1-21, 2012.
62. M. Rosenbloom, E.V. Sullivan, A. Pfefferbaum, Using magnetic resonance imaging and diffusion tensor imaging to assess brain damage in alcoholics, Alcohol Research and Health, 27, 146-152, 2003.
63. T.J. Whitfford, M. Kubicki, M.E. Shenton, Diffusion tensor imaging, structural connectivity and schizophrenia, Schizophrenia research and treatment, 2011,2011.

64. C. Bougias, E.E. Tripoliti, Theory of diffusion tensor imaging and fiber tractography analysis, European Journal of Radiography, 1, 37-41, 2009.
65. K. Li, L. Guo, G. Li, T. Liu, Review of methods for functional brain connectivity detection using fMRI, Computerized Medical Imaging and Graphics, 33, 131-139, 2009.
66. R.A. Poldrack, J.A. Mumford, T.E. Nichols, Handbook of functional MRI data analysis: Cambridge University Press, 130-155, 2011.
67. C.J. Earley, G.R. Uhl, S. Clemens, S. Ferré, Connectome and molecular pharmacological differences in the dopaminergic system in restless legs syndrome (RLS): plastic changes and neuroadaptations that may contribute to augmentation, Sleep medicine, 31, 71-77, 2017.
68. D. Zhou, Functional Connectivity Analysis of fMRI Time-Series Data, University of Pittsburgh, 2011.
69. K.J. Friston, Introduction: experimental design and statistical parametric mapping, Human brain function, 2004.
70. M.D. Greicius, B. Krasnow, A.L. Reiss, V. Menon, Functional connectivity in the resting brain: a network analysis of the default mode hypothesis, PNAS, 100, 1, 253-258, 2003.
71. L. Ma, B. Wang, X. Chen, J. Xiong, Detecting functional connectivity in the resting brain: a comparison between ICA and CCA, Magnetic Resonance Imaging, 25, 1, 47-56, 2007.
72. M.J. McKeown, L.K. Hansen, T.J. Sejnowsk, Independent component analysis of functional MRI: what is signal and what is noise?, Current opinion in neurobiology, 13, 620-629, 2003.
73. V.D. Calhoun, T. Adali, G.D. Pearlson, J. Pekar, A method for making group inferences from functional MRI data using independent component analysis, Human brain mapping, 14, 140-151, 2001.
74. V.D. Calhoun, J. Liu, T. Adali, A review of group ICA for fMRI data and ICA for joint inference of imaging, genetic and ERP data, Neuroimage, 45, S163-S172, 2009.
75. E.B. Erhardt, S. Rachakonda, E.J. Bedrick, E.A. Allen, T. Adali, V.D. Calhoun, Comparison of multi-subject ICA methods for analysis of fMRI data, Human brain mapping, 32, 2075-2095, 2011.
76. X. Golay, S. Kollias, G. Stoll, D. Meier, A. Valavanis, P. Boesiger, A new correlation-based fuzzy logic clustering algorithm for fMRI, Magnetic Resonance in Medicine, 40, 249-260, 1998.

77. C. Windischberger, M. Barth, C. Lamm, L. Schroeder, H. Bauer, R.C. Gur, E. Moser, Fuzzy cluster analysis of high-field functional MRI data, Artificial Intelligence in Medicine, 29, 3, 203-223, 2003.
78. Y. Wang, T.Q. Li, Analysis of whole-brain resting-state fMRI data using hierarchical clustering approach, PLoSOne, 8, e76315, 2013.
79. J.C. Bezdek, Pattern recogniztion with fuzzy objective function algorithms, New York: Plenum press, 1981.
80. K.J. Friston, Functional and effective connectivity in neuroimaging: a synthesis, Human Brain Mapping, 2, 56-78, 1995.
81. A. Razi, K.J. Friston, The connected brain: causality, models and intrinsic dynamics, IEEE Signal Processing Magazine, 33, 14-35, 2016.
82. K.R. Sreenivasan, Connectivity analysis of functional MRI data in the latent neuronal space: Applications in science and medicine, 2014.
83. P. Tarka, An overview of structural equation modeling: its beginnings, historical development, usefulness and controversies in the social sciences, Quality & Quantity, 52, 313-354,2018.
84. X. Di, B.B. Biswal, Identifying the default mode network structure using dynamic causal modeling on resting-state functional magnetic resonance imaging, Neuroimage, 86, 53-59, 2014.
85. M.A. Lindquist, The statistical analysis of fMRI data, Statistical science, 23, 439-464, 2008.
86. G.A. James, M.E. Kelley, R.C. Craddock, P.E. Holtzheimer, B. Dunlop, C. Nemeroff, H.S. Mayberg, X.P. Hu, Exploratory Structural Equation Modeling of Resting-state fMRI: applicability of group models to individual subjects, Neuroimage, 45, 778-787, 2009.
87. A. Mclntosh, Moving between functional and effective connectivity, Analysis and function of large-scale brain networks, 15, 2010.
88. A. Roebroeck, E. Formisano, R. Goebel, Mapping directed influence over the brain using Granger causality and fMRI, Neuroimage, 25, 1, 230-242, 2005.
89. J.C. Rajapakse, J. Zhou, Learning effective brain connectivity with dynamic Bayesian networks, Neuroimage, 37, 749-760, 2007.
90. M. Bönstrup, R. Schulz, J. Feldheim, F.C. Hummel, C. Gerloff, Dynamic causal modeling of EEG and fMRI to characterize network architectures in a simple motor task, Neuroimage, 124, 498-508, 2016.

91. K.E. Stephan, L. Kasper, L.M. Harrison, J. Daunizeau, H.E.M. den Ouden, M. Breakspear, K.J. Friston, Nonlinear dynamic causal models for fMRI, Neuroimage, 42, 2, 649-662, 2008.
92. J.D. Ramsey, S.J. Hanson, C. Hanson, Y.O. Halchenko, R.A. Poldrack, C. Glymour, Six problems for causal inference from fMRI, Neuroimage, 49, 2, 1545-1558, 2010.
93. A. Łupińska-Dubicka, Modeling dynamic systems by means of dynamic Bayesian networks, Zeszyty Naukowe Politechniki Białostockiej. Informatyka, 9, 77-92, 2012.
94. H. Lähdesmäki, I. Shmulevich, Learning the structure of dynamic Bayesian networks from time-series and steady state measurements, Machine Learning, 71, 185-217, 2008.
95. L. Zhang, M. Guindani, M. Vannucci, Bayesian models for functional magnetic resonance imaging data analysis, Wiley Interdisciplinary Reviews: Computational Statistics, 7, 21-41, 2015.
96. J.F. Smith, A.S. Pillai, K. Chen, B. Horwitz, Effective connectivity modeling for fMRI: six issues and possible solutions using linear dynamic systems, Frontiers in systems neuroscience, 5, 104, 1-17, 2012.
97. J.F. Smith, K. Chen, A.S. Pillai, B. Horwitz, Identifying effective connectivity parameters in simulated fMRI: a direct comparison o switching linear dynamic system, stochastic dynamic causal and multivariate autoregressive models, Frontiers in Neuroscience, 7, 70, 1-17, 2013.
98. K.J. Friston, C. Buchel, G.R. Fink, J. Morris, E. Rolls, R. Dolan, Psychophysiological and modulatory interactions in neuroimaging, Neuroimage, 6, 218-229, 1997.
99. J. Ashburner, G. Barnes, C.C. Chen, J. Daunizeau, G. Flandin, K. Friston, A. Jafarian, S. Kiebel, J. Kilner, V. Litvak, R. Moran, W. Penny, A. Razi, K. Stephan, S. Tak, P. Zeidman, D. Gitelman, R. Henson, C. Hutton, V. Glauche, J. Mattout, C. Philips, SPM12 Manual (The FIL Methods Group), 328, 2020.
100. J. Wang, X. Zuo, Y. He, Graph-based network analysis of resting-state functional MRI, Frontiers in systems neuroscience, 4, 16, 1-14, 2010.
101. C.T. Butts, Social network analysis: a methodological introduction, Asian Journal of Social Psychology, 11, 13-41, 2008.
102. F. Ferreira-Santos, Complex network analysis of brain connectivity: An introduction, University of Porto, 2012.
103. B. Goparaju, K.D. Rana, F.J. Calabro, L.M. Vaina, A computational study of whole-brain connectivity in resting-state and task fMRI, Medical Science Monitor, 20, 1024-1042, 2014.

104. Q.K. Telesford, K.E. Joyce, S. Hayasaka, J.H. Burdette, P.J. Laurienti, The Ubiquity of Small-World Networks, Brain Connectivity, 1, 367-375, 2011.
105. D. Goldenberg, A. Galvan, The use of functional and effective connectivity techniques to understand the developing brain, Developmental Cognitive Neuroscience, 12, 155-164, 2015.
106. H. Onias, A. Viol, F. Palhano-Fontes, K.C. Andrade, M. Sturzbecher, G. Viswanathan, D.B. de Araujo, Brain complex network analysis by means of resting state fMRI and graph analysis: Will it be helpful in clinical epilepsy?, Epilepsy & Behavior, 38, 71-80, 2014.
107. S.J. Chung, H.R. Kim, J.H. Jung, P.H. Lee, Y. Jeong, Y.H. Sohn, Identifying the Functional Brain Network of Motor Reserve in Early Parkinson's Disease, Movement Disorders, 35, 4, 577-586, 2020.
108. C.Tessa, N.Toschi, S.Orsolini, G.Valenza, C.Lucetti, R.Barbieri, S.Diciotti, Central modulation of parasympathetic outflow is impaired in de novo Parkinson's disease patients, PLOS, , 14, 1, 1-17, 2019.
109. M. Li, J. He, X. Liu, Z. Wang, X. Lou, L. Ma, Structural and Functional Thalamic Changes in Parkinson's Disease With Mild Cognitive Impairment, International Society for Magnetic Resonance in Medicine, 52, 1207-1215, 2020.
110. L. Christopher, S.Duff-Canning, Y. Koshimori, B. Segura, I.Boileau, R. Chen, A.E. Lang, S. Houle, P. Rusjan, A.P. Strafella, Salience Network and Parahippocampal Dopamine Dysfunction in Memory-Impaired Parkinson Disease, Annals of Neurology, 77, 2, 269-280, 2016.
111. A.S. Mihaescu, M. Masellis, A. Gruff-Guerrero, J. Kim, M. Criaud, S.S. Cho, C. Ghadery, M. Valli, A.P. Strafella, Brain degeneration in Parkinson's disease with cognitive decline: a coordinate-based meta-analysis, Brain Imaging and Behavior, 13, 1021-1034, 2019.
112. A.R.E. Potgieser, A. Hoorn, A.M. Meppelink, L.K. Teune, J. Koerts, B.M. Jong, Anterior Temporal Atrophy and Posterior Progression in Patients with Parkinson's Disease, Neurodegenerative Diseases, 14, 125-132, 2014.
113. X. Xu, Q. Han, J. Iin, L. Wang, F. Wu, H. Shang, Grey matter abnormalities in Parkinson's disease: a voxel-wise meta-analysis, European Journal of Neurology, 27, 653-659, 2020.
114. M.G. Sharaev, V.V. Zavyalova, V.L. Ushakov, S.I. Kartashov, B.M. Velichkovsky, Effective Connectivity within the Default Mode Network: Dynamic Causal Modeling of Resting-State fMRI Data, frontiers in Human Neuroscience, 10, 14, 1-9, 2016.

115. R. Kim, D. Yoo, Y.J. Jung, K. Han, J-Y. Lee, Sex differences in smoking, alcohol consumption, and risk of Parkinson's disease: A nationwide cohort study, Parkinsonism and Related Disorders, 71, 60-65, 2020.
116. J.D. Power, B.L. Schlaggar, S.E. Petersen, Recent progress and outstanding issues in motion correction in resting state fMRI, Neuroimage, 0, 536-551, 2015.
117. E.E. Tripoliti, Automated analysis of brain function in patients with Alzheimer disease bases on random forests algorithm, Doctoral Thesis, Department of Computer Science & Engineering, University of Ioannina, 2012.
118. W. Liao, D. Mantini, Z. Zhang, Z. Pan, J. Ding, Q. Gong, Y. Yang, H.Chen, Evaluating the effective connectivity of resting state networks using conditional Granger causality, Biological Cybernetics, 1, 102, 57-69, 2010.
119. M. Kononen, The mathematical background of SPM99, Academic Dissertation, Department of Applied Physics, University of Kuopio, 2004.
120. J.K. Wong, E.H. Middlebrooks, S.S. Grewal, L. Almeida, C.W. Hess, M.S. Okun, A Comprehensive Review of Brain Connectomics and Imaging to Improve Deep Brain Stimulation Outcomes, Movement Disorders, 35, 5, 741-751, 2020.
121. T.D. van Balkom, O.A. van den Heuvel, H.W. Berendse, Y.D. van der Werf, C. Vriend, The effects of Cognitive Training on Brain Network Activity and Connectivity in Aging and Neurodegenerative Diseases: a Systematic Review, Neuropsychology Review, 30, 267-286, 2020.
122. A.C. Nobre, F.van Ede, Under the Mind's Hood: What We Have Learned by Watching the Brain at Work, Journal Neuroscience, 40, 1, 89-100, 2020.
123. K. Specht, Current Challenges in Translational and Clinical fMRI and Future Directions, Frontiers in Psychiatry Neuroimaging and Stimulation, 10, 924, 1-9, 2020.
124. B. Hart, I. Cribben, M. Fiecas, A longitudinal model for functional connectivity networks using resting-state fMRI, NeuroImage, 178, 687-701, 2018.

Appendix: Tables with results from the three studies

Table 7. 1: Brain areas that are functionally connected with the left lateral parietal cortex (lLPC) concerning PD group.

MNI coordinates of maximum voxel	*Cluster Size (voxels)*	*Brain areas*	*Size p-FWE*	*Size p-FDR*	*Size p-unc*	*Peak p-FWE*	*Peak p-unc*
[-06, -54, 46]	5435	Precuneus Left	0.000000	0.000000	0.000000	0.010201	0.000000
[24, 36, 44]	3518	Superior Frontal Gyrus Right	0.000000	0.000000	0.000000	0.391603	0.000003
[-40, -70, 28]	3356	Occipital Middle Left	0.000000	0.000000	0.000000	0.000008	0.000000
[40, -58, 26]	2556	Angular Gyrus Right	0.000000	0.000000	0.000000	0.005809	0.000000
[54, -08, -16]	248	Middle Temporal Gyrus Right	0.000721	0.000294	0.000026	0.989613	0.000068
[00, -80, -24]	235	Cerebellum Crus2 Left	0.001046	0.000356	0.000038	0.553290	0.000006
[30, -38, -14]	227	Fusiform Gyrus Right	0.001319	0.000385	0.000048	0.320430	0.000002
[-22, -12, -22]	142	Hippocampus Left	0.018878	0.004863	0.000695	0.518074	0.000005
[-58, -56, 00]	121	Middle Temporal Gyrus Left	0.039000	0.009023	0.001450	0.991725	0.000073
[-60, -06, -22]	93	Middle Temporal Gyrus Left	0.107645	0.023250	0.004152	0.983103	0.000058

Table 7. 2: Brain areas that are functionally connected with the right lateral parietal cortex (rLPC) concerning PD group.

MNI coordinates of maximum voxel	*Cluster Size (voxels)*	*Brain areas*	*Size p-FWE*	*Size p-FDR*	*Size p-unc*	*Peak p-FWE*	*Peak p-unc*
[-04, 66, 06]	9295	Superior Frontal Medial Gyrus Left	0.000000	0.000000	0.000000	0.005160	0.000000
[06, -52, 14]	6768	Precuneus Right	0.000000	0.000000	0.000000	0.002127	0.000000
[46, -60, 22]	4319	Middle Temporal Gyrus Right	0.000000	0.000000	0.000000	0.000000	0.000000
[-40, -70, 32]	2944	Middle Occipital Gyrus Left	0.000000	0.000000	0.000000	0.008115	0.000000
[-56, -20, -30]	815	Inferior Temporal Gyrus Left	0.000000	0.000000	0.000000	0.230909	0.000001
[54, -02, -28]	412	Postcentral Gyrus Right	0.000011	0.000005	0.000000	0.875585	0.000023
[66, -36, -10]	351	Middle Temporal Gyrus Right	0.000051	0.000018	0.000002	0.533846	0.000006
[28, -32, -18]	308	Fusiform Gyrus Right	0.000153	0.000048	0.000006	0.184688	0.000001
[08, 12, -10]	257	Caudate Nucleus Right	0.000603	0.000168	0.000022	0.666477	0.000009
[-02, 00, 68]	241	Supplementary Motor Area Left	0.000944	0.000237	0.000035	0.983325	0.000059
[44, 16, -34]	175	Temporal Pole Middle Right	0.006766	0.001547	0.000250	0.886422	0.000024
[-54, 24, 34]	141	Inferior Frontal Gyrus Operculum Left	0.020436	0.004314	0.000761	0.188570	0.000001
[-06, -50, -50]	129	Cerebellum 9 Left	0.030736	0.006021	0.001151	0.754529	0.000013
[34, 38, -10]	122	Inferior Frontal Gyrus Orbital Right	0.039180	0.007158	0.001474	0.732440	0.000012
[54, 12, 00]	107	Rolandic Operculum Right	0.066674	0.011533	0.002544	0.902822	0.000027
[26, -22, 76]	91	Precentral Gyrus	0.119422	0.019928	0.004689	0.020545	0.000000

		Right					
[-62, -52, 02]	90	Middle Temporal Gyrus Left	0.259696	0.044346	0.011086	0.997486	0.000103

Table 7. 3: Brain areas that are functionally connected with the posterior cingulate cortex (PCC) concerning PD group.

MNI coordinates of maximum voxel	*Cluster Size (voxels)*	*Brain areas*	*Size p-FWE*	*Size p-FDR*	*Size p-unc*	*Peak p-FWE*	*Peak p-unc*
[00, -68, 48]	20026	Precuneus Left	0.000000	0.000000	0.000000	0.000000	0.000000
[12, 50, -14]	3808	Orbital Superior Frontal Gyrus Right	0.000000	0.000000	0.000000	0.030009	0.000000
[26, 26, 40]	960	Middle Frontal Gyrus Right	0.000000	0.000000	0.000000	0.015087	0.000000
[-24, 30, 42]	926	Middle Frontal Gyrus Left	0.000000	0.000000	0.000000	0.321283	0.000002
[04, -54, -38]	533	Vermis 9	0.000001	0.000000	0.000000	0.335579	0.000002
[62, -02, -18]	365	Middle Temporal Gyrus Right	0.000040	0.000018	0.000001	0.031671	0.000000
[52, 12, -02]	345	Superior Temporal Pole Right	0.000065	0.000025	0.000002	0.797966	0.000016
[08, 16, -10]	285	Caudate Right	0.000307	0.000103	0.000011	0.739710	0.000013
[-64, -04, -20]	226	Middle Temporal Gyrus Left	0.001565	0.000468	0.000058	0.986849	0.000066
[14, -36, -52]	207	Cerebellum 8 Right	0.002722	0.000733	0.000102	0.724293	0.000012
[-32, -36, -40]	131	Cerebellum 7b Left	0.030090	0.007468	0.001141	0.328555	0.000002
[28, -16, 76]	109	Precentral Gyrus Right	0.064577	0.014957	0.002493	0.003078	0.000000
[46, -08, 62]	103	Precentral Gyrus Right	0.079974	0.017239	0.003113	0.962732	0.000044
[50, 20, -32]	79	Middle Temporal Pole Right	0.191409	0.040803	0.007934	0.944952	0.000037
[-32, -90, -24]	73	Cerebellum Crus1 Left	0.238366	0.048807	0.010168	0.903035	0.000027

Table 7. 4: Brain areas that are functionally connected with the left lateral parietal cortex (lLPC) concerning controls group.

MNI coordinates of maximum voxel	*Cluster Size (voxels)*	*Brain areas*	*Size p-FWE*	*Size p-FDR*	*Size p-unc*	*Peak p-FWE*	*Peak p-unc*
[08, 38, 10]	10488	Anterior Cingulum Right	0.000000	0.000000	0.000000	0.000150	0.000000
[-38, -76, 32]	9418	Middle Occipital Gyrus Left	0.000000	0.000000	0.000000	0.000000	0.000000
[40, -70, 28]	2959	Middle Occipital Gyrus Right	0.000000	0.000000	0.000000	0.000275	0.000000
[26, -40, 56]	867	Postcentral Gyrus Right	0.000000	0.000000	0.000000	0.022749	0.000000
[54, -04, -18]	634	Middle Temporal Gyrus Right	0.000000	0.000000	0.000000	0.396330	0.000003
[64, -28, 26]	603	SupraMarginal Gyrus Right	0.000000	0.000000	0.000000	0.749607	0.000012
[38, 10, 02]	513	Insula Right	0.000001	0.000000	0.000000	0.109982	0.000000
[06, -52, -50]	391	Cerebelum 9 Right	0.000012	0.000004	0.000000	0.610574	0.000007
[-26, -34, -14]	310	Fusiform Gyrus Left	0.000102	0.000028	0.000004	0.217615	0.000001
[16, -02, 74]	282	Superior Frontal Gyrus Right	0.000219	0.000054	0.000008	0.487510	0.000004

[46, -58, -08]	273	Inferior Temporal Gyrus Right	0.000282	0.000063	0.000010	0.558913	0.000006
[-60, -22, -12]	222	Middle Temporal Gyrus Left	0.001243	0.000243	0.000044	0.995353	0.000082
[-40, -82, -24]	221	Cerebellum Crus 1 Left	0.001281	0.000243	0.000045	0.793998	0.000014
[10, -80, -42]	195	Cerebellum Crus 2 Right	0.002852	0.000503	0.000101	0.953114	0.000037
[28, -34, -16]	180	Fusiform Gyrus Right	0.004597	0.000757	0.000162	0.022199	0.000000
[-28, -40, 70]	152	Postcentral Gyrus Left	0.011612	0.001800	0.000411	0.924922	0.000029
[-34, 34, -14]	147	Orbital Inferior Frontal Gyrus Left	0.013775	0.002011	0.000488	0.014812	0.000000
[-30, -72, 08]	127	Middle Occipital Gyrus Left	0.027771	0.003857	0.000992	0.213919	0.000001
[68, -34, -06]	123	Middle Temporal Gyrus Right	0.032066	0.004228	0.001148	0.993264	0.000074
[32, -76, -44]	105	Cerebelum Crus 2 Right	0.062170	0.007911	0.002260	0.999711	0.000151
[28, 32, -12]	87	Orbital Inferior Frontal Gyrus Right	0.123292	0.015446	0.004634	0.167578	0.000001

Table 7. 5: Brain areas that are functionally connected with right lateral parietal cortex (rLPC) concerning controls group.

MNI coordinates of maximum voxel	***Cluster Size (voxels)***	***Brain areas***	***Size p-FWE***	***Size p-FDR***	***Size p-unc***	***Peak p-FWE***	***Peak p-unc***
[-06, 48, -06]	14663	Orbital Medial Frontal Gyrus Left	0.000000	0.000000	0.000000	0.000037	0.000000
[-02, -56, 20]	6969	Precuneus Left	0.000000	0.000000	0.000000	0.000003	0.000000
[48, -66, 28]	4074	Middle Occipital Gyrus Right	0.000000	0.000000	0.000000	0.000000	0.000000
[-46, -62, 28]	3164	Angular Gyrus Left	0.000000	0.000000	0.000000	0.000358	0.000000
[58, -04, -28]	1928	Inferior Temporal Gyrus Right	0.000000	0.000000	0.000000	0.032217	0.000000
[-54, -08, -20]	1396	Middle Temporal Gyrus Left	0.000000	0.000000	0.000000	0.007813	0.000000
[36, -28, 72]	1108	Postcentral Gyrus Right	0.000000	0.000000	0.000000	0.009177	0.000000
[00, -56, -48]	940	Cerebellum 9 Right	0.000000	0.000000	0.000000	0.284212	0.000000
[-16, -88, -44]	700	Cerebellum Crus 2 Left	0.000000	0.000000	0.000000	0.308297	0.000002
[30, -70, -20]	332	Cerebellum 6 Right	0.000060	0.000016	0.000002	0.584110	0.000006
[56, 10, 04]	313	Rolandic Operculum Right	0.000100	0.000024	0.000004	0.855124	0.000019
[56, -28, 28]	228	Supramarginal Gyrus Right	0.001089	0.000238	0.000039	0.613558	0.000007
[34, -80, -38]	173	Cerebelum Crus 2 Right	0.005994	0.001214	0.000213	0.951680	0.000037
[20, -44, 50]	147	Inferior Parietal Gyrus Right	0.014242	0.002599	0.000509	0.776180	0.000014
[-58, 12, -02]	146	Superior Temporal Pole Left	0.014737	0.002599	0.000527	0.989452	0.000065
[-24, -32, -24]	136	Cerebellum 4_5 Left	0.020822	0.003454	0.000747	0.259327	0.000001
[-36, -48, 64]	110	Superior Parietal Lobule Left	0.052937	0.008402	0.001930	0.963866	0.000042
[-50, -36, 52]	94	Inferior Parietal Lobule Left	0.096328	0.014778	0.003595	0.979886	0.000053
[10, -86, -38]	87	Cerebelum Crus 2	0.125779	0.018580	0.004771	0.262577	0.000002

		Right					
[00, -04, 56]	71	Supplementary Motor Area Left	0.232499	0.034747	0.009391	0.596486	0.000007

Table 7. 6: Brain areas that are functionally connected with posterior cingulate cortex (PCC) concerning controls group.

MNI coordinates of maximum voxel	***Cluster Size (voxels)***	***Brain areas***	***Size p-FWE***	***Size p-FDR***	***Size p-unc***	***Peak p-FWE***	***Peak p-unc***
[-06, -62, 34]	22820	Precuneus Left	0.000000	0.000000	0.000000	0.000000	0.000000
[22, 30, 44]	8505	Middle Frontal Gyrus Right	0.000000	0.000000	0.000000	0.000135	0.000000
[-46, 32, 04]	1625	Triangularis Inferior Frontal Gyrus Left	0.000000	0.000000	0.000000	0.023036	0.000000
[-24, 26, 44]	927	Middle Frontal Gyrus Left	0.000000	0.000000	0.000000	0.094606	0.000000
[08, -54, -50]	510	Cerebellum 9 Right	0.000002	0.000001	0.000000	0.408313	0.000003
[60, 18, 04]	444	Operculum Inferior Frontal Gyrus Right	0.000007	0.000002	0.000000	0.926193	0.000032
[-50, -42, -38]	346	Cerebellum Crus 1 Left	0.000070	0.000020	0.000003	0.665179	0.000010
[62, -04, -28]	295	Middle Temporal Gyrus Right	0.000257	0.000064	0.000010	0.850793	0.000021
[-68, -06, -16]	271	Middle Temporal Gyrus Left	0.000485	0.000108	0.000018	0.011764	0.000000
[16, -74, -54]	190	Cerebellum 8 Right	0.004822	0.000969	0.000183	0.641107	0.000009
[-04, 10, 74]	126	Supplementary Motor Area Left	0.037280	0.006921	0.001436	0.066991	0.000000

Table 7. 7: The brain areas that show activation in controls group.

Component	***Maximum Voxel***	***Brain areas***	***z-score***
1	[-50,28,-5]	Orbital Inferior Frontal Gyrus Left	5.6455
2	[-34,-80,-15]	Fusiform Gyrus Left	5.1936
3	[30,-84,-20]	Cerebellum Crus 1 Right	11.1809
4	[-34,-84,-25]	Cerebellum Crus1 Left	7.353
5	[34,12,-20]	Orbital Inferior Frontal Gyrus Right	7.6982
6	[2,-52,20]	Precuneus Right	6.3801
7	[-26,-68,-20]	Cerebellum 6 Left	4.2253
8	[50,16,-5]	Insula Right	6.4867
9	[-2,-28,80]	Paracentral Lobule Left	8.767
10	[30,-68,55]	Superior Parietal Lobule Right	6.4147
11	[-2,20,-10]	Olfactory Sulcus Left	3.6483
12	[6,-28,-50]	Pons	13.1346

Table 7. 8: The brain areas that show activation in the first control subject.

Component	***Maximum Voxel***	***Brain areas***	***z-score***
1	[-42,-64,40]	Angular Gyrus Left	6.0857
2	[14,-88,-15]	Cerebellum Crus1 Right	10.8579
3	[22,-8,-15]	Lingual Gyrus Right	20.9321
4	[2,28,64]	Superior Medial Frontal Gyrus Right	7.2633
5	[2,-44,-30]	Vermis 10	6.8355
6	[2,-48,65]	Precuneus Right	5.5434
7	[-42,-64,-15]	Fusiform Gyrus Left	5.9079
8	[30,-84,-15]	Inferior Occipital Gyrus Right	10.3593
9	[-2,-24,80]	Paracentral Lobule Left	7.7172
10	[34,-68,55]	Inferior Parietal Lobule Right	6.7349
11	[2,-64,5]	Lingual Gyrus Right	4.944
12	[6,-28,-50]	Pons	11.0658

Table 7. 9: The brain areas that show activation in the second control subject.

Component	*Maximum Voxel*	*Brain areas*	*z-score*
1	[2,-28,-50]	Pons	12.484
2	[2,32,60]	Superior Medial Frontal Gyrus Right	6.8094
3	[6,-28,-45]	Pons	4.1712
4	[-46,-80,-10]	Inferior Occipital Gyrus Left	3.8874
5	[14,-56,15]	Precuneus Right	5.4139
6	[46,-56,50]	Inferior Parietal Lobule Right	5.9069
7	[-34,-84,-20]	Cerebellum Crus 1 Left	6.9314
8	[30,12,-20]	Superior Temporal Pole Right	7.6346
9	[42,-76,-15]	Inferior Occipital Gyrus Right	10.7943
10	[-38,-88,10]	Middle Occipital Gyrus Left	6.4816
11	[2,32,60]	Medial Superior Frontal Gyrus Right	6.7136
12	[-34,-84,-20]	Cerebellum Crus1 Left	6.5204

Table 7. 10: The brain areas that show activation in the third control subject.

Component	*Maximum Voxel*	*Brain areas*	*z-score*
1	[-2,-40,75]	Paracentral Lobule Left	13.13
2	[22,-68,60]	Superior Parietal Lobule Right	6.5719
3	[2,-80,45]	Cuneus Right	5.3964
4	[2,-52,15]	Precuneus Right	6.2982
5	[50,20,-5]	Orbital Inferior Frontal Gyrus Right	6.2131
6	[-34,-64,55]	Superior Parietal Lobule Left	6.863
7	[54,-56,-15]	Inferior Temporal Gyrus Right	4.9852
8	[-34,12,-25]	Superior Temporal Pole Left	10.5653
9	[14,-28,-40]	Pons	6.4223
10	[-50,-64,-25]	Cerebellum Crus1 Left	11.8693
11	[2,28,65]	Medial Superior Frontal Right	6.2343
12	[14,-92,-10]	Lingual Gyrus Right	6.7896

Table 7. 11: The brain areas that show activation in the fourth control subject.

Component	*Maximum voxel*	*Brain areas*	*z-score*
3	[2,-16,80]	Supplementary Motor Area Right	5.7107
4	[-38,-80,-15]	Fusiform Gyrus Left	12.9052
5	[-22,56,-5]	Orbital Superior Frontal Gyrus Left	6.5406
6	[34,16,-25]	Superior Temporal Pole Right	12.2051
7	[-6,-32,-50]	Pons	10.9364
9	[-42,40,-15]	Orbital Inferior Frontal Gyrus Left	7.156
10	[-38,-80,-20]	Cerebellum Crus 1 Left	10.7458
12	[-30,64,10]	Superior Frontal Gyrus Left	4.807
1,2,8,11	[30,-88,-15]	Inferior Occipital Gyrus Right	7.8879, 13.6128, 14.7652, 10.7718

Table 7. 12: The brain areas that show activation in the fifth control subject.

Component	*Maximum Voxel*	*Brain areas*	*z-score*
1	[-26,-88,-25]	Cerebellum Crus 1 Left	8.2146
2	[26,52,40]	Superior Frontal Gyrus Right	4.87
3	[-26,-88,-20]	Cerebellum Crus 1 Left	7.0427
4	[-62, -52, -5]	Middle Temporal Gyrus Left	5.3193
5	[-42,-72,30]	Middle Occipital Gyrus Left	8.0297
6	[-10,-88,-20]	Cerebellum Crus 1 Left	9.6162
7	[2,-36,75]	Paracentral Lobule Right	5.9147
8	[46,-68,-40]	Cerebellum Crus 2 Right	5.9925
9	[-38,-80,-30]	Cerebellum Crus 1 Left	7.6974
10	[-10,-28,-45]	Pons	13.6901
11	[-2,-68,60]	Precuneus Left	5.9954
12	[-6,-88,30]	Cuneus Left	7.1656

Table 7. 13: The brain areas that show activation in the sixth control subject.

Component	*Maximum Voxel*	*Brain areas*	*z-score*
1	[2, -80, 45]	Cuneus Right	8.9546
2	[18, -92, -15]	Lingual Gyrus Right	9.4551
3,10,11	[-6, 0, -15]	Amygdala Left	9.9485, 8.0716, 8.1834
4,6	[-22, -92, -15]	Lingual Gyrus Left	10.5072, 10.5165
5	[30, 8, -20]	Superior Temporal Pole Right	13.8152
7	[10, -80, 50]	Superior Parietal Lobule Right	7.5098
8	[2, -88, 35]	Cuneus Left	11.6371
9	[2, -16, 80]	Supplementary Motor Area Right	6.6672
12	[26, -88, -20]	Cerebellum Crus 1 Right	19.2961

Table 7. 14: The brain areas that show activation in the seventh control subject.

Component	*Maximum Voxel*	*Brain areas*	*z-score*
1	[2, -68, 25]	Cuneus Left	6.2332
2	[-2, 52, -15]	Rectus Left	6.3714
3	[-6, -88, -15]	Lingual Gyrus Left	12.3827
4	[-6, -32, -50]	Pons	10.5271
5,7	[-38, -76, -25]	Cerebellum Crus 1 Left	11.041, 9.8098
6	[-34, -44, -40]	Cerebellum 7b Left	6.0203
8	[38, -60, 55]	Superior Parietal Lobule Right	6.848
9	[54, 12, 0]	Rolandic Opercular Right	6.744
10	[-50, 20, 0]	Triangularis Inferior Frontal Gyrus Left	4.8746
11	[2, 52, -15]	Rectus Right	5.5613
12	[42, 12, -15]	Superior Temporal Pole Right	11.4382

Table 7. 15: The brain areas that show activation in the eighth control subject.

Component	Maximum Voxel	Brain areas	z-score
1	[-18, -88, -20]	Cerebellum Crus 1 Left	12.4378
2	[-26, -84, -20]	Cerebellum Crus 1 Left	10.8847
3,8	[-26, -84, -25]	Cerebellum Crus 1 Left	16.0534, 16.3754
4	[-6, -88, -15]	Lingual Gyrus Left	6.2778
5	[-30, -84, -25]	Cerebellum Crus 1 Left	23.3432
6,9	[-50, -64, -20]	Cerebellum Crus 1 Left	14.42, 12.4522
7	[26, -88, -20]	Cerebellum Crus 1 Left	8.3776
10	[-14, -28, -40]	Pons	11.8624
11	[30, -84, -20]	Cerebellum Crus 1 Right	11.6284
12	[-34, -80, -20]	Cerebellum Crus 1 Left	15.7548

*The observed brain areas are similar because the maximum voxels are in nearby coordinates.

Table 7. 16: The brain areas that show activation in the ninth control subject.

Component	*Maximum Voxel*	*Brain areas*	*z-score*
1	[-30, -72, 45]	Inferior Parietal Lobule Left	6.0497
2	[-46, 20, 35]	Opercular Inferior Frontal Gyrus Left	5.8241
3	[22, -28, 75]	Precentral Gyrus Right	7.0765
4	[38, -12, 65]	Precentral Gyrus Right	3.7034
5	[38, -76, -20]	Cerebellum Crus 1 Right	8.045
6	[-34, -72, -45]	Cerebellum Crus 2 Left	5.5662
7	[54, 16, 0]	Opercular Inferior Frontal Gyrus Right	6.0348
8	[-38, -72, 40]	Middle Occipital Gyrus Left	6.6686

9	[6, -28, -50]	Pons	14.9
10	[-30, -88, -15]	Lingual Gyrus Left	8.9033
11	[-30, -88, -20]	Cerebellum Crus 1 Left	12.3408
12	[-6, -96, 0]	Calcarine Cortex Left	9.7576

Table 7. 17: The brain areas that shown activation in the tenth control subject.

Component	***Maximum Voxel***	***Brain areas***	***z-score***
1	[38, 16, -20]	Superior Temporal Pole Right	8.2588
2	[-2, -28, 80]	Paracentral Lobule Left	9.3751
3	[2, -76, 0]	Lingual Gyrus Right	4.9975
4	[38, -80, -20]	Cerebellum Crus 1 Right	14.4844
5	[50, -60, 30]	Angular Gyrus Right	7.1468
6	[30, -84, -25]	Cerebellum Crus 1 Right	10.2988
7	[-42, -76, -25]	Cerebellum Crus 1 Left	7.2689
8	[42, -68, -20]	Cerebellum Crus 1 Right	5.7195
9	[-10, -36, -50]	Cerebellum 9 Left	14.9744
10	[30, -68, 50]	Superior Parietal Lobule Right	7.8565
11	[-38, -80, -25]	Cerebellum Crus 1 Left	6.9109
12	[58, 8, -5]	Superior Temporal Pole Right	8.5864

Table 7. 18: The brain areas that show activation in the eleventh control subject.

Component	***Maximum Voxel***	***Brain areas***	***z-score***
1,3,4,5	[38, -80, -20]	Cerebellum Crus1 Right	8.412, 10.1758, 9.9593, 8.7215
2	[14, -88, -20]	Cerebellum Crus1 Right	13.5994
6	[-6, -52, 65]	Precuneus Left	9.7947
7	[-46, -72, -20]	Cerebellum Crus1 Left	4.0231
8	[-34, -84, -25]	Cerebellum Crus1 Left	13.4967
9	[-2, -24, 80]	Paracentral Lobule Left	7.4252
10	[-6, -52, 65]	Precuneus Left	5.5003
11	[-34, -84, -20]	Cerebellum Crus1 Left	5.9915
12	[-2, 0, 75]	Supplementary Motor Area Left	10.5984

Table 7. 19: The brain areas that shown activation in twelfth control subject.

Component	***Maximum Voxel***	***Brain areas***	***z-score***
1	[2, -28, -50]	Pons	21.2358
2	[26, -88, -25]	Cerebellum Crus 1 Right	12.3434
3	[-18, -88, -20]	Cerebellum Crus 1 Left	5.7887
4	[22, -68, 60]	Superior Parietal Lobule Right	9.0536
5	[2, -52, 15]	Precuneus Right	7.6552
6	[2, -68, 0]	Lingual Gyrus Right	7.058
7	[10, -84, 40]	Cuneus Right	7.4908
8	[2, 40, 55]	Medial Superior Frontal Gyrus Right	9.0917
9	[54, -56, -30]	Cerebellum Crus 1 Right	7.6655
10	[2, -44, 5]	Vermis 4_5	7.5728
11	[2, -76, -5]	Lingual Gyrus Right	6.248
12	[-2, -40, 75]	Paracentral Lobule Left	11.0513

Table 7. 20: The brain areas that show activation in thirteenth control subject.

Component	***Maximum Voxel***	***Brain areas***	***z-score***
1	[6, -28, -50]	Pons	15.0238
2	[54, 8, 0]	Superior Temporal Pole Right	5.0793
3	[18, -28, -20]	Cerebellum 3 Right	5.0199
4	[30, 64, 15]	Superior Frontal Gyrus Right	4.6606
5	[-2, -72, 35]	Cuneus Left	6.1981

6	[10, -16, 80]	Precentral Gyrus Right	7.1482
7	[-38, -76, -25]	Cerebellum Crus 1 Left	9.8994
8	[-6, -88, -15]	Lingual Gyrus Left	6.0158
9	[18, 8, -20]	ParaHippocampal Gyrus Right	8.4571
10	[-54, -56, 30]	Angular Gyrus Left	5.3793
11	[22, -68, 60]	Superior Parietal Lobule Right	7.8948
12	[-30, -84, -25]	Cerebellum Crus 1 Left	4.3646

Table 7. 21: The brain areas that show activation in the fourteenth control subject.

Component	***Maximum Voxel***	***Brain areas***	***z-score***
1	[2, -20, 0]	Thalamus Right	8.6635
2	[-6, -32, -50]	Pons	14.6121
3	[18, -76, 55]	Superior Parietal Lobule Right	10.2975
4	[26, -92, -15]	Lingual Gyrus Right	7.2467
5,8,10	[-14, -32, -45]	Cerebellum 10 Left	8.7392, 10.0838, 6.8709
6	[54, -56, -25]	Inferior Temporal Gyrus Right	5.9593
7	[18, -92, -15]	Lingual Gyrus Right	12.1407
9	[-6, 68, 15]	Medial Superior Frontal Gyrus Left	4.9934
11	[-2, -24, 80]	Paracentral Lobule Left	11.2695
12	[-34, -84, -25]	Cerebellum Crus1 Left	7.4345

Table 7. 22: The brain areas that show activation in PD group.

Component	***Maximum Voxel***	***Brain areas***	***z-score***
1	[2,-72,40]	Precuneus Right	6.3088
2	[34,56,5]	Middle Frontal Gyrus Right	4.1911
3	[-26,-84,-30]	Cerebellum Crus 1 Left	5.6288
4	[-50,-60,30]	Angular Gyrus Left	5.8226
5	[-6,-28,-50]	Pons	11.0831
6	[34,16,-25]	Superior Temporal Pole Right	7.0113
7	[38,-80,-25]	Cerebellum Crus 1 Right	10.2877
8	[-38,-80,-15]	Fusiform Gyrus Left	5.6988
9	[2,-4,75]	Supplementary Motor Area Right	12.9611
10	[-42,-52,55]	Inferior Parietal Lobule Left	6.0779
11	[2,-76,55]	Precuneus Right	4.1397
12	[-62,-20,15]	Rolandic Operculum Left	5.8766

Table 7. 23: The brain areas that show activation in the first PD subject.

Component	***Maximum Voxel***	***Brain areas***	***z-score***
1	[2, -56, 20]	Precuneus Right	10.4482
2	[-42, -76, -15]	Fusiform Gyrus Left	7.2299
3	[14, -24, -40]	Pons	7.3812
4	[14, -92, -10]	Lingual Gyrus Right	6.6352
5	[6, -28, -50]	Pons	12.4861
6	[6, -92, -5]	Lingual Gyrus Right	8.8708
7	[10, -88, -15]	Cerebellum Crus 1 Right	8.9839
8	[22, -92, -10]	Lingual Gyrus Right	8.4199
9	[-2, 0, 75]	Supplementary Motor Area	10.1897
10	[42, -64, 45]	Angular Gyrus Right	5.29
11	[26, -92, -10]	Inferior Occipital Gyrus Right	6.1564
12	[34, 16, -25]	Superior Temporal Pole Right	6.2652

Table 7. 24: The brain areas that show activation in second PD subject.

Component	***Maximum Voxel***	***Brain areas***	***z-score***
1	[-38, -68, 45]	Angular Gyrus Left	5.1487
2	[2, -48, 10]	Precuneus Right	5.1683
3	[2, -48, 10]	Precuneus Right	6.1436
4	[-22, -88, -20]	Cerebellum Crus 1 Left	4.1985

5	[2, -44, -30]	Vermis 10	8.7105
6	[22, -88, -20]	Cerebellum Crus1 Right	15.0921
7	[30, 24, -15]	Insula Right	4.322
8	[10, -88, -15]	Lingual Gyrus Right	6.1206
9	[-34, -76, -15]	Fusiform Gyrus Left	4.7264
10	[10, -32, -50]	Pons	10.3583
11	[-2, -12, 75]	Paracentral Lobule Left	16.3885
12	[14, -88, -15]	Lingual Gyrus Right	9.348

Table 7. 25: The brain areas that show activation in the third PD subject.

Component	Maximum Voxel	Brain areas	z-score
1	[-2, -56, 70]	Precuneus Left	5.1667
2	[-26, -88, -20]	Cerebellum Crus 1 Left	8.4029
3	[26, -88, -20]	Cerebellum Crus 1 Right	5.0299
4	[-50, 28, -5]	Orbital Inferior Frontal Gyrus Left	6.8601
5	[26, -88, -20]	Cerebellum Crus 1 Right	6.6819
6	[-2, 20, 65]	Supplementary Motor Area Left	9.3948
7	[-62, -28, 15]	Superior Temporal Gyrus Left	6.1874
8	[-38, -52, 60]	Superior Parietal Lobule Left	8.6435
9	[26, -88, -20]	Cerebellum Crus 1 Right	7.6504
10	[-2, -56, 70]	Precuneus Left	13.8023
11	[-2, -80, -5]	Calcarine Cortex Left	9.9472
12	[2, -72, 55]	Precuneus Right	7.9859

Table 7. 26: The brain areas that show activation in the fourth PD subject.

Component	***Maximum Voxel***	***Brain areas***	***z-score***
1	[-46, -72, -20]	Cerebellum Crus 1 Left	8.592
2	[-2, -56, 70]	Precuneus Left	12.3591
3	[-50, -44, 50]	Inferior Parietal Lobule Left	5.9747
4	[-30, -84, -25]	Cerebellum Crus 1 Left	9.3791
5	[-62, -24, 15]	Superior Temporal Gyrus Left	5.3951
6	[-30, -88, 10]	Middle Occipital Gyrus Left	6.2742
7	[34, -84, -20]	Cerebellum Crus 1 Right	6.3327
8	[26, 60, -5]	Orbital Superior Frontal GyrusRight	4.445
9	[-54, -60, 35]	Angular Gyrus Left	6.772
10	[46, -72, -20]	Cerebellum Crus 1 Right	6.0617
11	[34, -84, -20]	Cerebellum Crus1 Right	13.478
12	[62, -44, 40]	SupraMarginal Gyrus Right	4.9512

Table 7. 27: The brain areas that show activation in the fifth PD subject.

Component	***Maximum Voxel***	***Brain areas***	***z-score***
1	[14, -88, -20]	Cerebellum Crus 1 Right	6.8927
2	[2, -68, 35]	Precuneus Right	7.0149
3	[-2, -44, -35]	Vermis 10	8.4784
4	[42, 4, -15]	Superior Temporal Pole Right	8.2265
5	[54, 12, -5]	Superior Temporal Pole Right	7.2198
6	[-6, -84, -20]	Cerebellum Crus 2 Left	11.5302
7	[2, -80, 50]	Superior Parietal Lobule Right	6.0666
8	[-38, -64, 55]	Superior Parietal Lobule Left	7.2604
9	[54, -48, 45]	Inferior Parietal Lobule Right	4.9892
10	[42, -56, 55]	Angular Gyrus Right	5.4232
11	[-10, -36, -50]	Cerebellum 9 Left	14.0362
12	[-2, -12, 75]	Paracentral Lobule Left	10.126

Table 7. 28: The brain areas that show activation in the sixth PD subject.

Component	***Maximum Voxel***	***Brain areas***	***z-score***
1	[-14, -68, 60]	Precuneus Left	7.5351
2	[-30, -64, 55]	Superior Parietal Lobule Left	6.2057
3	[2, -52, 20]	Precuneus Right	6.9003
4	[-58, -4, 10]	Rolandic Operculum Left	5.6974

5	[-46, -72, -20]	Cerebellum Crus 1 Left	5.8182
6	[2, -44, -30]	Vermis 10	5.4328
7	[-6, -28, -50]	Pons	8.3058
8	[-18, -44, 75]	Superior Parietal Lobule Left	6.262
9	[6, 68, 10]	Medial Superior Frontal Gyrus Right	6.1567
10	[2, -24, 75]	Paracentral Lobule Right	14.933
11	[-26, -88, -20]	Cerebellum Crus 1 Left	13.3288
12	[-6, -92, -10]	Calcarine Cortex Left	10.3211

Table 7. 29: The brain areas that show activation in the seventh PD subject.

Component	***Maximum Voxel***	***Brain areas***	***z-score***
1,4	[-34, -68, 55]	Superior Parietal Lobule Left	8.1176, 6.2591
2	[-50, -60, -25]	Angular Gyrus Left	6.3768
3	[-42, -60, 50]	Angular Gyrus Left	6.3845
5	[-2, -80, -15]	Cerebellum 6 Left	11.1267
6	[54, -52, 30]	Angular Gyrus Right	4.1331
7	[-2, -24, 75]	Paracentral Lobule Left	7.0831
8	[-34, -84, -15]	Lingual Left	10.379
9	[2, -4, 75]	Supplementary Motor Area Right	15.1426
10,12	[-30, -68, 55]	Superior Parietal Lobule Left	10.1474, 9.7156
11	[-6, -28, -50]	Superior Parietal Lobule Left	11.1716

Table 7. 30: The brain areas that show activation in the eighth PD subject.

Component	***Maximum Voxel***	***Brain areas***	***z-score***
1	[14, -32, -50]	Cerebellum 9 Right	14.463
2,9	[2, 4, 70]	Supplementary Motor Area Right	5.5716, 19.627
3	[-42, -76, -30]	Cerebellum Crus 1 Left	8.3314
4	[2, 40, 55]	Medial Superior Frontal Gyrus Right	5.6767
5	[-42, -76, -25]	Cerebellum Crus 1 Left	13.1362
6	[-14, -88, -25]	Cerebellum Crus 2 Left	7.1634
7	[-34, 12, -25]	Superior Temporal Pole Left	10.0126
8	[-54, -36, 50]	Inferior Parietal Lobule Left	6.3245
10	[2, -52, 15]	Precuneus Right	7.1332
11	[-6, -88, -20]	Cerebellum Crus 1 Left	13.6774
12	[-10, 32, 60]	Medial Superior Frontal Gyrus Left	5.067

Table 7. 31: The brain areas that show activation in the ninth PD subject.

Component	***Maximum Voxel***	***Brain areas***	***z-score***
1,4,9	[26, -92, -10]	Inferior Occipital Gyrus Right	11.2952, 10.0192, 6.4914
2	[34, 16, -20]	Orbital Inferior Frontal Gyrus Right	7.945
3	[-34, -84, -20]	Cerebellum Crus 1 Left	7.9991
5	[34, -84, -20]	Cerebellum Crus 1 Right	14.9537
6,12	[14, -28, -45]	Cerebelum 9 Right	6.0098, 6.2064
7	[-6, -28, -50]	Pons	11.6688
8	[38, 56, -5]	Orbital Middle Frontal Gyrus Right	4.9343
10	[10, -4, 75]	Supplementary Motor Area Right	15.0393
11	[-46, -64, 25]	Angular Gyrus Left	5.9592

Table 7. 32: The brain areas that show activation in the tenth PD subject.

Component	***Maximum Voxel***	***Brain areas***	***z-score***
1	[10, -32, -50]	Cerebelum 9 Right	12.9976
2	[-62, -52, 5]	Middle Temporal GyrusLeft	5.3021
3,6	[-42, -56, 55]	Inferior Parietal Lobule Left	6.1378,

			5.5182
4	[18, -88, -25]	Cerebellum Crus 1 Right	7.8154
5,7	[50, -68, -25]	Cerebellum Crus1 Right	9.4539, 11.7782
8	[2, -56, 65]	Precuneus Right	5.366
9	[22, -88, -20]	Cerebellum Crus 1 Right	11.8017
10	[50, 16, -5]	Superior Temporal Pole Right	5.0382
11	[50, -64, -20]	Cerebellum Crus 1 Right	7.1926
12	[14, -32, -50]	Cerebelum 9 Right	6.356

Table 7. 33: The brain areas that show activation in the eleventh PD subject.

Component	***Maximum Voxel***	***Brain areas***	***z-score***
1,7,11	[-34, -84, -20]	Cerebellum Crus 1 Left	4.942, 12.9389, 19.219
2	[2, -52, 65]	Precuneus Right	5.526
3,6	[-46, -72, -20]	Cerebellum Crus1 Left	10.1912, 12.6028
4	[-30, -88, -15]	Lingual Gyrus Left	16.3879
5	[10, -32, -50]	Pons	8.2963
8	[-22, -92, -15]	Lingual Gyrus Left	7.5554
9	[18, -92, -10]	Lingual Gyrus Right	5.8685
10	[-22, -92, -15]	Lingual Gyrus Left	5.8076
12	[6, -92, 5]	Calcarine Cortex Right	13.0484

Table 7. 34: The brain areas that show activation in the twelfth PD subject.

Component	***Maximum Voxel***	***Brain areas***	***z-score***
1	[-42, -72, -25]	Cerebellum Crus1 Left	6.0897
2	[-10, -76, 50]	Precuneus Left	6.3166
3	[10, -88, -10]	Lingual Gyrus Right	13.4364
4	[-2, 40, 55]	Medial Superior Frontal Gyrus Left	9.1099
5	[10, -32, -50]	Pons	9.8303
6	[6, -88, 0]	Calcarine Cortex Right	8.9704
7	[-2, -16, 75]	Paracentral Lobule Left	6.6426
8	[2, -72, 35]	Cuneus Left	6.8667
9	[26, -88, -15]	Lingual Gyrus Right	8.1845
10	[34, -76, 30]	Middle Occipital Gyrus Right	5.665
11	[-54, -56, 30]	Angular Gyrus Left	5.4014
12	[26, -88, -15]	Lingual Gyrus Right	7.3175

Table 7. 35: The brain areas that show activation in the thirteenth PD subject.

Component	***Maximum Voxel***	***Brain areas***	***z-score***
1	[-42, -48, 55]	Inferior Parietal Lobule Left	7.4235
2	[2, -8, 75]	Supplementary Motor Area Right	11.8076
3	[2, 44, 50]	Medial Superior Frontal Gyrus Left	6.9096
4	[38, -80, -25]	Cerebellum Crus1 Right	17.5022
5	[-42, -76, -20]	Cerebelum Crus1 Left	10.6029
6	[-38, -80, -20]	Cerebellum Crus 1 Left	5.6061
7	[2, -72, 35]	Cuneus Left	5.9264
8,9	[-42, -76, -20]	Cerebellum Crus1 Right	12.5048, 12.2672
10	[-22, -84, -25]	Cerebellum Crus 1 Left	9.4221
11	[-42, -76, -20]	Cerebellum Crus 1 Left	7.7751
12	[2, -80, -10]	Lingual Gyrus Right	9.1658

Table 7. 36: The brain areas that show activation in the fourteenth PD subject.

Component	***Maximum Voxel***	***Brain areas***	***z-score***
1	[34, 12, -20]	Superior Temporal Pole Right	4.1448
2	[38, -48, 55]	Inferior Parietal Lobule Right	6.5379
3	[-42, -56, 55]	Inferior Parietal Lobule Left	5.2939

4	[-38, -80, 30]	Middle Occipital Gyrus Left	4.3041
5	[-6, -28, -50]	Pons	9.3715
6	[10, -32, -50]	Pons	5.4793
7	[10, -24, 80]	Paracentral Lobule Right	7.2388
8,12	[46, 16, 10]	Opercular Inferior Frontal Gyrus Right	6.0604, 5.6975
9	[-50, -64, -25]	Cerebellum Crus 1 Left	4.6371
10	[46, -72, -25]	Cerebellum Crus1 Right	12.3531
11	[2, -64, 55]	Precuneus Right	7.8411

Table 7. 37: Effective connectivity parameters of the first control subject.

	MPFC	***lLPC***	***rLPC***	***PCC***
MPFC	0.0131	0.1729	-0.3609	0.1935
lLPC	0.1944	0.5994	0.0559	0.1050
rLPC	0.3945	0.0030	0.5921	0.1123
PCC	0.2271	0.2228	-0.0258	0.5240

Table 7. 38: Effective connectivity parameters of the second control subject.

	MPFC	***lLPC***	***rLPC***	***PCC***
MPFC	0.3409	-0.0095	0.0287	0.3760
lLPC	0.2225	-0.0663	-0.1892	0.1131
rLPC	0.0649	0.4457	0.2602	-0.0840
PCC	-0.0807	-0.1214	0.4663	0.2411

Table 7. 39: Effective connectivity parameters of the third control subject.

	MPFC	***lLPC***	***rLPC***	***PCC***
MPFC	0.6117	-0.0369	0.2816	0.2229
lLPC	-0.0546	0.4855	-0.1303	0.6263
rLPC	-0.3334	0.3397	0.5930	0.5210
PCC	-0.1049	0.0369	-0.0536	-0.4543

Table 7. 40: Effective connectivity parameters of the fourth control subject.

	MPFC	***lLPC***	***rLPC***	***PCC***
MPFC	0.4194	-0.0475	0.3882	-0.0950
lLPC	-0.2142	0.5035	0.3916	-0.2322
rLPC	-0.4512	-0.4391	-0.5133	-0.2383
PCC	-0.3199	-0.1647	0.5808	0.4402

Table 7. 41: Effective connectivity parameters of the fifth control subject.

	MPFC	***lLPC***	***rLPC***	***PCC***
MPFC	0.6729	0.1377	0.0553	0.4224
lLPC	-0.1940	-0.1770	-0.1849	0.4380
rLPC	-0.4472	0.5938	0.6267	0.2989
PCC	-0.8348	0.5770	0.0535	-0.1177

Table 7. 42: Effective connectivity parameters of the sixth control subject.

	MPFC	***lLPC***	***rLPC***	***PCC***
MPFC	0.4842	0.4467	-0.1681	-0.0220
lLPC	0.1200	0.2641	0.0000	0.1131
rLPC	0.0991	0.1272	0.6863	0.1613
PCC	0.3270	0.1163	-0.0097	0.4175

Table 7. 43: Effective connectivity parameters of the seventh control subject.

	MPFC	***lLPC***	***rLPC***	***PCC***
MPFC	0.0391	-0.2867	0.6001	0.0402
lLPC	0.4096	0.5521	0.1534	0.3647
rLPC	0.4408	-0.6923	-0.7068	-0.0060
PCC	0.4027	-0.1843	0.2199	-0.3658

Table 7. 44: Effective connectivity parameters of the eighth control subject.

	MPFC	*lLPC*	*rLPC*	*PCC*
MPFC	0.2556	0.2622	0.1941	0.3579
lLPC	-0.2610	0.0468	0.1456	0.1605
rLPC	-0.2605	0.1463	0.2897	0.2752
PCC	-0.3177	0.0118	0.3014	-0.0008

Table 7. 45: Effective connectivity parameters of the ninth control subject.

	MPFC	*lLPC*	*rLPC*	*PCC*
MPFC	0.2506	-0.0470	-0.2217	0.4359
lLPC	0.0631	0.3956	0.2300	0.0713
rLPC	0.2096	-0.0338	0.3874	0.1403
PCC	-0.1158	0.3901	0.1173	0.2457

Table 7. 46: Effective connectivity parameters of the tenth control subject.

	MPFC	*lLPC*	*rLPC*	*PCC*
MPFC	0.7435	0.0736	-0.0558	0.5092
lLPC	-0.1576	0.2787	-0.1396	0.1478
rLPC	-0.1550	0.5888	0.8250	0.7199
PCC	-0.2029	0.1685	-0.2094	-0.1367

Table 7. 47: Effective connectivity parameters of the eleventh control subject.

	MPFC	*lLPC*	*rLPC*	*PCC*
MPFC	0.5846	-0.1811	-0.0335	0.3711
lLPC	0.0223	0.8152	-0.0815	0.3541
rLPC	0.0276	0.0058	0.8925	0.3808
PCC	-0.0467	0.0249	-0.0645	-0.6374

Table 7. 48: Effective connectivity parameters of the twelfth control subject.

	MPFC	*lLPC*	*rLPC*	*PCC*
MPFC	0.5616	0.1339	0.0411	0.2949
lLPC	-0.0685	0.7182	0.2263	0.4427
rLPC	-0.1601	0.1592	0.5939	0.4540
PCC	-0.1506	-0.0757	-0.0513	-0.8184

Table 7. 49: Effective connectivity parameters of the thirteenth control subject.

	MPFC	*lLPC*	*rLPC*	*PCC*
MPFC	0.4306	0.0024	0.3613	0.3446
lLPC	-0.2100	0.0355	0.3396	-0.0206
rLPC	-1.0472	-0.0643	-0.3000	0.3540
PCC	-0.4998	-0.1265	0.4724	-0.5394

Table 7. 50: Effective connectivity parameters of the fourteenth control subject.

	MPFC	*lLPC*	*rLPC*	*PCC*
MPFC	0.2465	0.0681	0.0701	0.3364
lLPC	0.1121	0.2454	-0.0887	0.4601
rLPC	0.1628	0.2460	0.1911	-0.1658
PCC	-0.0868	-0.0344	0.3178	0.0635

Table 7. 51: Effective connectivity parameters of the second PD subject.

	MPFC	*lLPC*	*rLPC*	*PCC*
MPFC	-0.6322	0.3110	-0.0398	-0.2094
lLPC	-0.4643	0.1316	0.1278	0.2784
rLPC	0.0680	-0.0238	0.3576	0.1441
PCC	0.4280	-0.4581	0.5122	0.0344

Table 7. 52: Effective connectivity parameters of the third PD subject.

	MPFC	*lLPC*	*rLPC*	*PCC*
MPFC	0.4675	0.3794	0.0284	0.1087

lLPC	-0.0200	0.2241	0.1388	0.2638
rLPC	0.0083	0.1686	0.5896	0.2390
PCC	0.1838	0.3978	-0.0781	0.4249

Table 7. 53: Effective connectivity parameters of the fourth PD subject.

	MPFC	***lLPC***	***rLPC***	***PCC***
MPFC	0.0763	0.1434	-0.0062	0.3200
lLPC	-0.1241	0.0605	0.3132	0.1250
rLPC	0.1699	-0.1590	0.0176	-0.0102
PCC	-0.0155	0.2847	-0.1399	0.1113

Table 7. 54: Effective connectivity parameters of the fifth PD subject.

	MPFC	***lLPC***	***rLPC***	***PCC***
MPFC	-0.3359	-0.2866	0.2099	-0.7475
lLPC	0.3962	0.1932	0.0358	-0.0496
rLPC	0.2299	0.4094	-0.0043	-0.7405
PCC	0.0495	0.3043	0.5294	-0.3430

Effective connectivity parameters of the sixth PD subject were not acquired because of an error.

Table 7. 55: Effective connectivity parameters of the seventh PD subject.

	MPFC	***lLPC***	***rLPC***	***PCC***
MPFC	-0.2670	-0.2563	-0.4601	0.5708
lLPC	-0.4704	-0.3848	0.6135	-0.0690
rLPC	0.0366	-1.1487	-0.7340	0.1846
PCC	-0.4508	-0.4098	0.0917	-0.8893

Table 7. 56: Effective connectivity parameters of the eighth PD subject.

	MPFC	***lLPC***	***rLPC***	***PCC***
MPFC	0.4148	-0.0565	0.0935	-0.1237
lLPC	-0.1748	0.5732	0.4150	-0.2105
rLPC	0.0350	0.0432	0.2588	-0.0311
PCC	-0.2695	-0.0521	0.3483	0.6081

Table 7. 57: Effective connectivity parameters of the ninth PD subject.

	MPFC	***lLPC***	***rLPC***	***PCC***
MPFC	-0.0819	0.6927	-0.1885	0.7225
lLPC	-0.5264	-0.7069	-0.1476	0.0532
rLPC	0.1241	0.5070	0.4875	-0.2572
PCC	-0.1896	0.6535	0.1747	-0.3789

Table 7. 58: Effective connectivity parameters of the tenth PD subject.

	MPFC	***lLPC***	***rLPC***	***PCC***
MPFC	-0.1084	0.6960	-0.9831	0.1389
lLPC	-0.1560	-0.5742	0.0263	-0.0052
rLPC	0.5452	-0.0690	-0.1498	-0.3125
PCC	0.2095	0.3442	0.1495	0.3638

Table 7. 59: Effective connectivity parameters of the eleventh PD subject.

	MPFC	***lLPC***	***rLPC***	***PCC***
MPFC	0.6253	-0.0501	0.0948	0.1418
lLPC	-0.0562	0.7169	-0.2091	0.4637
rLPC	0.0579	0.2405	0.8900	0.2648
PCC	0.4230	-0.0783	-0.3468	-0.3692

Table 7. 60: Effective connectivity parameters of the twelfth PD subject.

	MPFC	***lLPC***	***rLPC***	***PCC***
MPFC	0.4178	-0.1301	-0.1345	0.3827

lLPC	0.2611	0.0039	-0.3343	0.1426
rLPC	0.0485	0.7358	0.8632	0.0364
PCC	-0.7914	-0.2009	0.1081	-1.0468

Table 7. 61: Effective connectivity parameters of the thirteenth PD subject.

	MPFC	***lLPC***	***rLPC***	***PCC***
MPFC	0.0200	0.1930	0.0019	0.1916
lLPC	0.3106	0.0171	0.4912	-0.0532
rLPC	0.0215	0.1330	0.1907	0.3171
PCC	0.1212	-0.6437	0.4787	-0.8774

Table 7. 62: Effective connectivity parameters of the fourteenth PD subject.

	MPFC	***lLPC***	***rLPC***	***PCC***
MPFC	-0.1886	0.0719	0.2209	-0.1399
lLPC	-0.0856	-0.6587	0.4273	-1.1175
rLPC	0.1183	0.2609	-0.0210	-0.4782
PCC	0.1336	-0.0178	0.3283	0.2923